2006

DYNAMICS OF ACTION POTENTIAL DURATION: EFFECTS ON RESTITUTION AND REPOLARIZATION ALTERNANS

Runze Wu
University of Kentucky, wurunze@yahoo.com

ABSTRACT OF DISSERTATION

Runze Wu

The Graduate School

University of Kentucky

2005

DYNAMICS OF ACTION POTENTIAL DURATION: EFFECTS ON RESTITUTION AND REPOLARIZATION ALTERNANS

ABSTRACT OF DISSERTATION

A dissertation submitted in partial fulfillment of the requirements for the degree of Doctor of Philosophy in the Graduate School at the University of Kentucky

By

Runze Wu

Lexington, Kentucky

Director: Dr. Abhijit Patwardhan, Associate Professor
Center for Biomedical Engineering

Lexington, Kentucky

2005

ABSTRACT OF DISSERTATION

DYNAMICS OF ACTION POTENTIAL DURATION: EFFECTS ON RESTITUTION AND REPOLARIZATION ALTERNANS

The presented studies investigate dynamics of action potential duration (APD) to better understand the underlying mechanism for repolarization alternans.

We recorded trans-membrane potentials (TMP) in canine endocardial muscle tissue using standard glass microelectrode under the control of an explicit diastolic interval (DI) control pacing protocol, i.e. feedback protocol. During sequential sinusoidal DI activation, the trajectory of APD dynamics has multiple values of APD correspondent to the same DI, i.e. restitution is a bi-modal relationship. Our results indicate that: 1) there is a delay, similar to hysteresis, of change in APD responding to change in DI, 2) and the time course of the delay is asymmetric for fast or slow pacing history. The alternans was observed during constant DI pacing, i.e. the DI preceding each APD was invariant or changed within a limited range. This finding suggests that alternans of APD do not need the oscillation of preceding DI, i.e. DI dependent restitution is not a necessary condition for the alternans. This result implies that DI independent component exists in the mechanism of the alternans. Nonetheless, the amplitude of alternans was statistically

larger during constant pacing cycle length (PCL) pacing than that during constant DI pacing, even though both PCL and DI pacing trials used similar average activation rate. These results also demonstrate the ability of the feedback protocol to analyze the memory effects and dissect different components in the mechanism of alternans.

Two computational models, Luo-Rudy dynamics (LRD) and cardiac ventricle model (CVM) were used to study the hysteresis in restitution. By perturbing membrane current: L-type calcium current, rapid and slow potassium rectifier, and intracellular calcium transfer rate in sarcoplasmic reticulum (SR) and using sinusoidal DI pacing sequence, we showed that the asymmetric calcium current across the membrane and its interaction with calcium buffer in SR during increasing and decreasing DI phase plays an important role in the hysteresis. CVM was used to study the alternans during constant DI pacing. However CVM failed to replicate the alternans that occurred in the experiments. This result implies that CVM lacks the electrophysiological kinetics related to alternans that was shown in our experiment.

KEYWORDS: Arrhythmia, Restitution, Repolarization Alternans, Action Potential Duration, Cardiac Memory.

Runze Wu

December, 2005

DYNAMICS OF ACTION POTENTIAL DURATION: EFFECTS ON RESTITUTION AND REPOLARIZATION ALTERNANS

By

Runze Wu

Abhijit Patwardhan

Director of Dissertation

Abhijit Patwardhan

Director of Graduate Studies

December, 2005

RULE FOR THE USE OF DISSERTATIONS

Unpublished dissertations submitted for the Doctor's degree and deposited in the University of Kentucky Library are as a rule open for inspection, but are to be used only with due regard to the rights of the authors. Bibliographical references may be noted, but quotations or summaries of parts may be published only with the permission of the author, and with the usual scholarly acknowledgments.

Extensive copying or publication of dissertation in whole or in part also requires the consent of the Dean of the Graduate School of the University of Kentucky.

A library that borrows this dissertation for use by its patron is expected to secure the signature of each user.

Name	Date

DISSERTATION

Runze Wu

The Graduate School

University of Kentucky

2005

DYNAMICS OF ACTION POTENTIAL DURATION: EFFECTS ON RESTITUTION AND REPOLARIZATION ALTERNANS

DISSERTATION

A dissertation submitted in partial fulfillment of the requirements for the degree of Doctor of Philosophy in the Graduate School at the University of Kentucky

By
Runze Wu

Lexington, Kentucky

Director: Dr. Abhijit Patwardhan, Associate Professor
Center for Biomedical Engineering

Lexington, Kentucky

2005

To my wife Xiaoyan, my daughter Zhixuan,
and my parents Weiyu and Shiwei.

ACKNOWLEDGMENTS

The mission of finishing this dissertation would have been impossible without the encouragement and support from several persons. I would like to thank my advisor, Dr. Abhijit Patwardhan, for providing invaluable insight, timely and instructive comments through all stages of the dissertation process. His endeavor and enthusiasm of science exemplified the high quality scholarship, which will continue to benefit my future study and work. I would also like to thank the members of my Dissertation Committee: Dr. Knapp, Dr. Randall, and Dr. Satin. They are not only advisors for my graduate research, but also mentors and friends. I would like also thank Dr Osborn who graciously accepted to serve as the outside examiner.

In additional, I also want to thank my family. It is their love and supports that allow me to pursue the Ph.D. degree in the past several years.

Table of Contents

List of Figures VI

List of Tables VIII

Chapter 1 Background 1

1.1 Antiarrhythmic therapies 2

1.2 Mechanisms of arrhythmia 5

Chapter 2 Introduction 10

2.1 Restitution Hypothesis 10

2.2 Pacing protocols 15

2.3 Two components of alternans and hysteresis in restitution 16

Chapter 3 Methods 18

3.1 Experimental preparation 18

3.2 Pacing protocol used in the experiment 19

3.3 Data analysis 21

3.4 Simulation model 21

3.5 Simulation protocol 27

Chapter 4 Results 32

4.1 Feedback protocol 32

4.2 Hysteresis in restitution of action potential duration 34

4.3 APD alternans exists during constant DI activation 50

4.4 Calcium dynamics and potassium current influence in hysteresis: Simulation results using LRD 66

4.5 Hysteresis and alternans: Simulation using CVM 80

Chapter 5 Discussion 82

5.1 Hysteresis in restitution of APD 82

5.2 Two components in the mechanism of alternans 88

Chapter 6 Summary 92

Reference 98

Vita 117

List of Figures

Figure 2.1 Graphic explanation of restitution hypothesis.....12

Figure 3.1 Schematic diagram of LRD model.....26

Figure 3.2 Schematic diagram of CVM.....27

Figure 3.3 The parameters used in quantification of the hysteresis.....30

Figure 4.1 Demonstration of DI control and cycle length control pacing protocol.....33

Figure 4.2 Hysteresis in restitution of APD in sinusoidal oscillation DI activation.....35

Figure 4.3 Hysteresis loop with period = 100 and 200 beats sinusoidal oscillation.....38

Figure 4.4 Hysteresis in restitution of APD in phase shifted sinusoidal oscillation DI....39

Figure 4.5 Average hysteresis loop from four animals. 41

Figure 4.6 Oscillatory APD with DI activation in the range of 20 to 150 msec.....43

Figure 4.7 Linear DI activation and comparison with standard and dynamic restitution .47

Figure 4.8 Random DI oscillation and comparison with linear DI oscillation. 49

Figure 4.9 APD alternans with relatively constant DI 52

Figure 4.10 Two types of alternans under constant DI and PCL.....54

Figure 4.11 Histogram of instant slope for constant DI and PCL.....57

Figure 4.12 ΔDI vs. ΔAPD plot for constant DI and PCL and their linear regression.....58

Figure 4.13 Constant DI activation with four initial conditions in one animal 60

Figure 4.14 Result of constant DI pacing from four animals with same initial condition 61

Figure 4.15 Result of APD during constant DI before and after random DI perturbation 63

Figure 4.16 Two-level constant DI sequence 65

Figure 4.17 Factors affected hysteresis in restitution.....69

Figure 4.18 MaxDelay and Thickness for membrane current perturbation.....71

Figure 4.19 MaxDelay and Thickness for *Iupbar* and *Tautr* perturbation. 73

Figure 4.20 Intracellular Ca dynamics during sinusoidal DI in LRD model.....77

Figure 5.1 Hysteresis as a mechanism for buffering alternans. 83

Figure 6.1 The summary of the present studies. 94

List of Tables

Table 3.1 Definition of symbols using in the simulation 21

Table 4.1 Results of MaxDelay and Thickness of hysteresis loop 79

Table 4.2 Hysteresis characteristics and alternans threshold in CVM.....81

List of Files

Runze_diss.pdf	661KB

Chapter 1 Background

The last two decades have witnessed the significant enrichment of knowledge and improvement of therapy in treating the heart diseases. However, the cardiovascular disease remains the primary cause of death[1]. Among these causes of death, the sudden cardiac death (SCD) is one of the most serious public health threats. Clinically, SCD is defined as the unexpected natural death from a cardiac cause within a short time period[2]. The death can generally occur less than one hour from onset of symptoms. Such a rapid death can happen to a person without auras, which makes SCD even more dangerous. Because the death certification usually does not include the information of when the SCD symptoms start, it may be difficult to know the duration of the symptoms and apply the above definition of SCD in practice. As an alternative, the SCD can be described as any cardiac death occurring out of hospital, in emergence room, or on the way to the emergence room[3]. Based on this alternative definition, there were 456,076 incidences of SCD among United States residents aged greater than 35 in 1998[4], which account for about 63% of all cardiac deaths at that year. It is believed that the overwhelming number of SCD in coronary disease (about 335,000 deaths per year) is from cardiac arrhythmia or ventricular fibrillation (VF)[1]. During VF, the heart loses the sinus rhythm and cannot work efficiently as a blood pump. Without a propeller of blood, the circulatory system fails to continuously provide oxygen to major organs. The consequence of depriving oxygen especially to the brain is catastrophe.

1.1 Antiarrhythmic therapies

Because of the magnitude of the arrhythmia problems, it becomes a pressing need to develop efficient antiarrhythmic therapies. Theoretically, an effective therapy could be antiarrhythmic agents or non-pharmaceutical methods to prevent the life-threatening arrhythmia. The Vaughan Williams (VW) classification is one of the most widely used classification schemes for antiarrhythmic agents. In the VW classification, the antiarrhythmic agents are classified based on what portion of the action potential that they directly affect[5]. There are five classes: Class I, II, III, IV and V. Class I agents, including sub-class Ia, Ib, and Ic, block sodium (Na) channel. Class Ia depresses phase 0 depolarization and prolongs action potential duration (APD). Class Ib agents shorten APD and reduce refractoriness. Class Ic agents remarkably depress phase 0 depolarization, decrease conductivity, but have minimal effects on APD. Class II agents are conventional beta blockers that slow conduction through the AV node. Class III agents block potassium (K) channels. They prolong APD and increase refractoriness without decreasing conduction velocity. Class IV agents are calcium (Ca) channel blockers. Class V agents work though the other or unknown mechanism to affect the action potential.

Although after decades of intensive studies, the antiarrhythmic drugs clinical trials have shown limited overall success, and some of them even resulted in increased mortality. The Cardiac Arrhythmia Suppression Trial (CAST) was set up by National Heart Lung and Blood Instituted (NHLBI) and its results CAST I and CAST II were published in 1989 and 1992[6]. Encainide and flecainide in CAST I, and moricizine in CAST II were used to treat patients. All of these drugs are Class Ic agents that were

thought to prevent premature ventricular contraction and hence protect patients from arrhythmia. However, results of CAST I showed a 3.6-fold risk of arrhythmic death compared with placebo-treated patients[7]. CAST II was terminated early by the CAST investigators after the first 14-day exposure period, because of the high lethal rate in the treatment group versus the placebo group (17 vs. 3)[8]. In 1996, Survival With Oral D-sotalol (SWORD) trial [9] investigator published their results. They found d-sotalol, a Class III pure K channel blocker, increased the arrhythmic mortality. The results of Amiodarone for Resuscitation after out-of-hospital cardiac arrest (ARREST) trial[10] show that the patients treated with amiodarone have higher rate of survival to hospital admission due to ventricular arrhythmia compared to placebo group. But this study is underpowered to detect the difference between groups of survival to hospital discharge. Another trial, European Myocardial Infarct Amiodarone Trial (EMIAT)[11] assessed the effects of amiodarone in patients with previous myocardial infarction (MI). The results show the amiodarone may decrease arrhythmic death, but have no effects on overall cardiac mortality. It is worthy to notice that although amiodarone is classified as a Class III agent, it blocks many types of ionic channels that give amiodarone features of from Class I to IV agents[12]. The Danish Investigations of Arrhythmia and Mortality on Dofetilide (DIAMOND) trial investigates dofetilide (Class III agent) on mortality among patients with congestive heart failure (DIAMOND-CHF)[13] and prior myocardial infarction (DIAMOND-MI)[14]. Both DIAMOND-CHF and DIAMOND-MI failed to find differences of all-cause survival between the dofetilide group and the placebo group. Nonetheless, dofetilide successfully reduced the risk of hospitalization for patients with heart failure. Treatment of dofetilide also helped in converting atrial fibrillation (AF) into

sinus rhythm and maintaining sinus rhythm once it was restored. The Amiodarone versus Lidocaine in Pre-hospital Ventricular Fibrillation Evaluation (ALIVE)[15] trial compared the amiodarone and lidocaine (Class Ib agent) in patients of out-of-hospital cardiac arrest. The results of ALIVE trial indicated treatment with amiodarone significantly increased survival rate of patients to hospital admission than that with lidocaine. The beta-blocker as an antiarrhythmic agent showed a larger likelihood in reducing cardiac mortality[16], yet under some debate[17]. The Beta-Blocker Heart Attack Trial (BHAT)[18] showed propranolol significantly reduced all-cause mortality by 26%. In some other trials, decrease of mortality was also associated with administration of beta-blocker[16]. In one comparison trial, Antiarrhythmics Versus Implantable Defibrillators (AVID)[19] trial also showed that beta-blocker independently improved survival rate.

In the last two decades, most of antiarrhythmic agent, except beta-blocker and amiodarone, trials showed unsuccessful results. In the view of these disappointing results, the interest in non-pharmaceutical therapy, such as implantable cardioverter-defibrillator (ICD), is growing. The ICD therapy has shown superior benefits on survival compared with drug therapy[2]. The AVID[19] trial investigator concluded that ICD give higher survival rate than drug therapy (predominantly amiodarone) in the patients with lower left ventricular ejection faction (LVEF). Another trial, Defibrillator versus Beta-blockers for Unexplained Death in Thailand (DEBUT)[20] compare the mortality of patients with treatment of beta-blockers versus ICD. During the 3-year follow-up, there were 7 deaths in the beta-blocker group. No death occurred in the defibrillator group, although 12 defibrillator patients received shocks due to recurrent VF. In Multicenter Automatic Defibrillator Implantation Trial (MADIT I)[21], ICD improved survival in patients with

coronary disease, reduced left ventricular ejection fraction, and previous MI. MADIT I did not find evidence that support beta-blocker or amiodarone decrease mortality rate in its included patients. MADIT II[22] used ICD as prophylactic therapy in patients with a prior MI and advanced left ventricular dysfunction. The results show prophylactic ICD therapy improves survival compared with the conventional therapy.

The ICD therapy reduces the mortality in patients with high risk of ventricular arrhythmia. But the success of electrical therapy does not mean we have won the war against the arrhythmia. The cost of ICD implantation is still expensive, which prohibits its usage to many people in the world. These implanted devices also have psychological and lifestyle negatives[12]. A majority of SCD occur outside of hospital without medical attention[23]. It is very important to identify those patients before the mishap happens. However, the results from antiarrhythmic agent trials indicate how inadequate our knowledge of the mechanism of arrhythmia is[12], and because of that, an efficient method has not been found to accurate identify the patients at a high risk of SCD[24], which will allow physicians to prevent the cardiac catastrophe. Therefore, it is still critical to study the fundamental mechanism of arrhythmia. Until we reach the level of systematic understanding arrhythmia, we will not be able to accurately screen out the patients at high risk, and prevent VF with a cost-effective treatment.

1.2 Mechanisms of arrhythmia

The exploration of the mechanisms responsible for arrhythmia can be largely divided into three parts: the substrate of arrhythmia, the triggering events, and their interactions [24]. The triggering events are transient incidents that initiate an episode of deadly arrhythmia,

such as nervous regulation[25], ischemia[26], stress[27] and sleep[2]. One of the triggering events is the autonomic nervous system (ANS) that influences the cardiac properties[25] via sympathetic and parasympathetic innervations[27, 28]. The heterogeneity of sympathetic response to cardiac injury is repeatedly connected with high arrhythmogenesis[29, 30]. Because of the transient and variable features of the trigger events, it is not easy to characterize them. Comparing these evanescent triggering events, the substrate of arrhythmia is easier to study and thereafter we can find a way to control it.

By using integrative and deductive approaches[31], the study of VF can be divided into several levels: organ, tissue, cell, and sub-cellular level. The arrhythmia could rise from different levels[32,33, 34]. Our study was primarily focused on cellular/membrane level in the experiment study and slightly down to cell/sub-cellular level in the computational study.

Cardiac function is established on a finely balanced system. The rhythm problems are highly complicated and there may be more than one mechanism that can produce fibrillation[35-41]. It is specially meaningful, because, as the results of CAST trials[7, 8] pointed out, the efforts of trying to suppress one mechanism to fibrillation might raise another one. Reentry is the current textbook mechanism of VF[42]. The normal propagation of electrical wave starts from the sinus node, meanders through the atria, passes the AV node, goes through the bundles of His, and excites the ventricles from endocardium to epicardium. During the propagation through the ventricles, the impulses travel only in the forward direction, i.e. excited cells will not excite the exciting cells. However, under some conditions, the antegrade impulses are blocked by a unidirectional block. In the classical description of reentry mechanism[43], if the conduction velocity and pathway are suitable, the retrograde impulse can travel back into the previously blocked area. And if

that segment of tissue has become excitable, the retrograde impulse is able to travel through the block area and returns to the previous passed area. Such re-entry completes a circuit. This reentry circuit has self-sustained manner that provides the substrate for fibrillation.

A prevalent[44] hypothesis for mechanism of reentry wave break up is single or multiple spiral wavelet(s) hypothesis. It was hypothesized that during fibrillation, there are one[45-48] or more[49-54] 3-dimensional spiral wavelets of electrical activation present. These wavelets continuously stimulate the reentry circuit. In the multiple wavelet case, the wavelets also crash on each other. The collisions annihilate the mother spirals and at the same time initiate more daughter spirals. These spiral waves become rotors that drive the ventricular muscle cells at a much faster rate than the sinus rhythm into a highly spatiotemporal disorder state, i.e. VF. Therefore, the study of spiral wave break up and evolution can provide valuable information for developing therapies to prevent the onset of fibrillation and terminate VF.

The current experimental techniques provide powerful tools to investigate the spiral wave dynamics. Besides the standard glass micropipette techniques, the plunge needles[55] and epicardial recording sock electrode array[56], allow us to observe the electrical wave activities across the ventricular wall and heart surface. The optical mapping techniques[57, 58] can visualize the surface potentials at a higher resolution. In spite of the advantage of these techniques, the transmural information remains largely hidden[44]. The mathematical modeling and simulation presents a promising way to further explore the experimental data and bring insightful ideas back to the experiment studies. Early computational study by Wiener and Rosenblueth provided a theoretical explanation of the obstacle causing

reentry waves[44]. After that, because of the dramatic increase of computation capability, the investigation for mechanisms of spiral wave break up has been extended to 2-dimensional[33, 59-61], 3-dimensional[62, 63], and 3-dimensional model with realistic structures[64].

A number of mechanisms of spiral wave break up have been proposed[44]. It is believed that the instability of action potential duration (APD) plays a critical role to the initiation and maintain of fibrillation[65]. As the heart rate increases to a threshold level, APDs may show an oscillating pattern. It usually manifests as long and short alternative change of APD, i.e. alternans[66]. Under some conditions, for instance, further increasing heart rate, the alternans would go into a high order periodic oscillation and eventually fall into chaotic fibrillation[67]. Although the break up can occur in a homogeneous tissue[68, 69], the spatial heterogeneity[55, 70-74], conduction velocity[33, 34], and their interaction[75, 76] may also provide substrate for fibrillation.

Although the general pattern of spiral wave break up has been characterized, the underlying mechanisms responsible for the onset and the perpetuation of alternans have not been elucidated[38, 44]. The present dissertation explored the cardiac electrical restitution relationship, which is believed to be a key issue in identifying the mechanisms of fibrillation. Our researches are focused on the temporal characteristics including: 1) the delay response of change in APD to the change of DI in the restitution of APD, 2) two components of mechanism responsible for the APD alternans, 3) ionic dynamics underlying the hysteresis and alternans by using computational models. The rest of the dissertation is organized as follows. Chapter 2 is the introduction section that reviewed current advance in research of alternans and restitution. Chapter 3 describes the methods

used in our experimental and theoretical studies. Chapter 4 presents the results of our experiment and simulation. In chapter 5, we discuss the experiment and simulation results. At the end of the dissertation, chapter 6 provides a short summary of the present studies.

Chapter 2 Introduction

Repolarization alternans is a periodic change in the electrocardiogram T wave or the action potential[32]. Usually, the time course of repolarization is manifested as a beat by beat change that repeats once every other beat. The beat by beat change of T-wave amplitude, named T-wave alternans (TWA), is associated with SCD under different pathologic conditions[77-79] and therefore can be used as a marker to arrhythmia[80-84]. Therefore, the origin of fibrillation has been closely related to repolarization alternans or APD alternans[32, 85].

2.1 Restitution Hypothesis

A putative mechanism of alternans and spiral wave break up is the restitution hypothesis. The restitution can be described by the relationship that associates APDs to its preceding diastolic intervals (DIs). It is hypothesized that a steep slope of restitution relationship is proarrhythmic, and a flat slope therefore is antiarrhythmic[86]. As shown in Figure 2.1, the restitution relationship is defined by the APD at the n beat (APD_n) and its preceding DI (DI_n). For clarity, this relationship was simplified as a straight line. Because the slope of restitution in Figure 2.1A is larger than 1, a perturbation from old cycle length to a new cycle length results in the functional block. When the activation rate switched to new cycle length after the n-1 beat of APD (APD_{n-1}), the rest time left for the next beat (DI_n) was decided by the intersection point of restitution curve and new cycle length line. As shown in Figure 2.1A, the APD_{n-1} is calculated at point 'A', and DI_n is

computed at point ‘B’ by subtracting APD_{n-1} from cycle length (CL). According to the restitution, the APD_n following DI_n is the ordinate of point ‘C’. The reiteration of above process demonstrates an oscillation of APD. When the DI reached point ‘X’, the cell was in the refractory period, which caused a functional block. On the contrary, if slope of restitution is less than 1, the perturbation of cycle length change will not lead to block as Figure 2.1B showed.

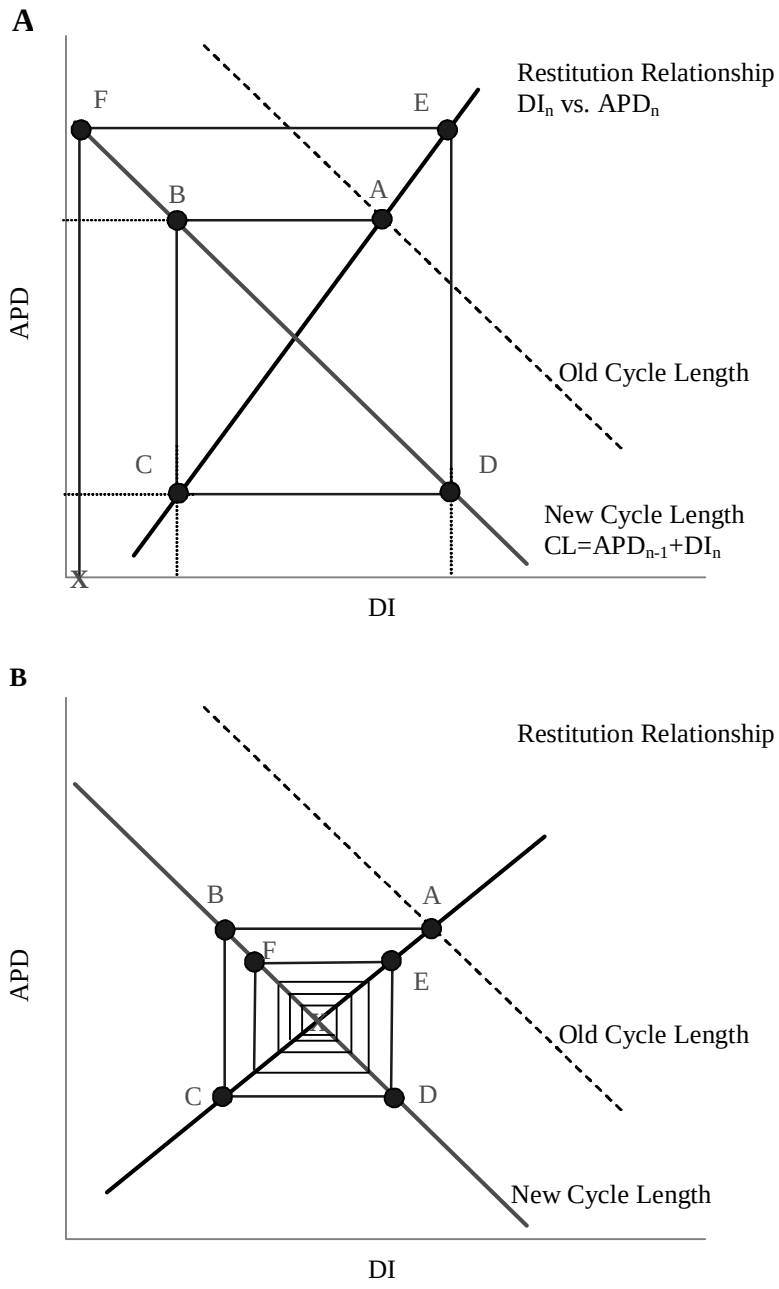

Figure 2.1 Graphic explanation of restitution hypothesis. These cartoons depict that the APD evolution when the cycle length is shortened from old cycle length to new cycle length. The original working point was point ‘A’, i.e. the intersection of ‘Old Cycle Length’ line and the ‘Restitution Relationship’. When the cycle length switched to the ‘New cycle length’ line, the DI for the next beat

was decided by point 'B'. Then the following APD was resulted by point 'C'. Similarly, the DIs and APDs for the following beats can be obtained at point D, E, and F. In panel A, the slope of restitution relationship is larger than one. The shortening of cycle length leads to a functional block that is shown at point 'X'. On the contrary, in panel B, a flattened restitution relationship a convergent APD evolution to the point 'X', i.e. the intersection of the 'New cycle length' line and restitution relationship.

Several experimental results[56, 87-89] provide evidence supporting the hypothesis that steepness of restitution plays a determinant role in arrhythmogenesis. Theoretical studies[59, 68, 90] indicate that the spiral wave can break up in the homogeneous tissues with a steeper slope of restitution, i.e. the dynamic spatiotemporal heterogeneity is sufficient for alternans and conduction block. The evidence supporting the restitution hypothesis of slope is further strengthened by experimental study in Purkinje fiber[69] and simulation study on realistic three-dimensional computer model of cardiac anatomy[64]. Therefore, flattening the slope of restitution[91, 92] may become a novel approach[66] in developing therapy to treat patients at high risk of VF. The traditional restitution relationship is a one dimensional map that only includes the immediately preceding DI's contribution to the current APD. But the effects on APD from previous activation history, i.e. cardiac memory, are also critical in initiation and perpetuation of arrhythmia[93-96]. Because of the presence of cardiac memory, APD may become shorter than that predicted by restitution with a shorter previous APD activation history, and vice versa[97]. Given strong enough

memory, alternans may not happen in spite of a steep restitution relation[93]. New criterions of spiral wave stability with consideration of cardiac memory effects are still developing [98, 99].

Several lines of recent studies[100-104] suggest that the mechanism responsible for electrical alternans root in the intracellular calcium store[105]. Chudin, et al[101] showed the alternans of Ca transient occurred when the membrane potential was identical by using action potential clamp (AP clamp). Pruvot, et al[104] demonstrated a weak correlation between the threshold of alternans and the steepness of the restitution slope in guinea pig model by using a simultaneous membrane potential and calcium (Ca) optical mapping setup. In another fluorescent experiment, Omichi, et al[106] found the results of dominant frequency analysis from intracellular Ca and membrane voltage were similar during ventricular tachycardia (VT), but significantly different during VF in swine ventricle. Lakireddy, et al[107] further indicated the alternans of Ca transient was not necessarily associated with alternans of APD on ischemic guinea pig heart. The results of these studies suggest the role of restitution in alternans, and in wave break, may be equivocal.

The primary evidence used in these studies is the lack of correlation between the slope of restitution and alternans[70, 104]. In most previous studies, alternans and restitution were measured by using different schedules of constant pacing cycle length (PCL) protocols. For example, Walker, et al[100] when quantifying the hysteresis of alternans on guinea pigs, used a decreasing and increasing PCL stepwise pacing protocol beginning with the baseline cycle length of 500 msec. At each step, a constant PCL was maintained for 1 minute, which means at least 120 beats (1min/500msec = 120beats). Then the APDs were measured for the last two consecutive beats. During alternans of APD, their

preceding DI was also oscillating, i.e. the restitution mechanism was always engaged. With the existence of restitution of APD, shortening of DI causes shortening of APD, and vice versa. It is impossible, therefore, when pacing at constant cycle lengths to determine the mechanisms of alternans without the process being complicated by DI dependent restitution. For the studies questioning the role of DI dependent restitution in arrhythmogenesis, the lack of correlation can serve as *indirect* evidence predisposing to factors other than restitution. However, are these alternating DIs the cause or the effect of alternans of APDs? This question was still unanswered by the previous studies. One objective of our studies is providing a conclusion to this question.

2.2 Pacing protocols

The restitution of APD is often measured by using S1S2 or S1S1 pacing schemes. In S1S2 scheme, a stimulus (S2) is delivered after several tens of beats at constant cycle length (S1). This S1S2 stimulus train is repeated and the S2 intervals are shortened in stepwise manner until 2:1 block occurs. The APD resulting from S2 stimulus and its preceding DI are measured. When all pairs of DI and APD have been collected from all S2 stimuli, the DI and APD pairs are plotted in a restitution curve. This protocol is referred to as the standard restitution protocol[87]. Another frequently used scheme, the S1S1 protocol, was proposed recently[87]. Similar to standard restitution protocol, tissue is also first paced for several tens of S1 beats. However, instead of using S2 stimulus, the DI and APD are measured at the end of the S1 stimulus train. Then the sequence of S1 stimuli is repeated at a shorter S1-S1 interval. When the PCL is short enough to generate alternans, the DI and APD were measured twice from the last two consecutive beats. This protocol is referred to as the dynamic restitution protocol[87]. Both standard and dynamic

restitution include several tens of pacing beats before the measurement of DI and APD, which involved steady state effects. However, recent studies[95, 108-110] demonstrate that the stability also depend on the rate-dependent and memory aspects of restitution, which are not measured in either standard or dynamic protocol.

In the present studies, we used a previously developed DI-control based pacing protocol – feedback protocol[111, 112] to explore the characteristics of restitution and alternans. The feedback pacing protocol can explicitly control DI and hence make the DI independent of APD[112]. The motivation for using a feedback based protocol is as follows: 1) Although in restitution hypothesis prediction of the change in APDs is in a beat by beat manner, the restitution relationship is not quantified during sequential changes in DI in currently utilized protocols[111]. 2) Explicitly controlling DI permits a more direct demonstration of effects of memory by varying the rate of change of DIs, which would improve understanding restitution and prediction of APD stability. 3) Furthermore, by applying a specially designed constant DI sequence, the restitution effects, the preceding DI change causes following APD change, are eliminated. Then this research will be able to identify the underlying mechanism of alternans. It also provides a more applicable way to explore the restitution relationship sequentially, which brings insight into the mechanism responsible for restitution.

2.3 Two components of alternans and hysteresis in restitution

The restitution hypothesis proposes the change in DI leads to the change in APD. Therefore, the restitution or DI restitution serves as one of the fundamental contributors to the alternans and fibrillation. However, results from recent experiments suggest the

role of DI restitution is equivocal. We hypothesized that DI restitution is not a necessary condition for alternans of APD to exist. To test this hypothesis, the feedback pacing protocol was applied on endocardial tissue from canines. Unlike the conventional pacing protocols, the DIs preceding each long and short APDs were the same. Alternans of APD was observed even when preceding DIs were invariant. These results provide *direct* evidence that there are two components in the mechanism responsible for alternans: DI restitution dependent and independent components These results provide the explanation for the seemingly contradict results of previous studies[66, 71, 93, 105]. Nonetheless, when DIs were changed in short and long pattern accordingly during constant PCL pacing, the amplitude of alternans was larger than that during constant DI pacing. This result suggests that DI restitution plays an important role in maintaining the alternans.

We investigated restitution relationship during sequential change of DI. During oscillatory DIs, restitution showed bi-modal trajectory similar to hysteresis. For a given DI, there were multiple values of APD. Sequential and explicit control of DI suggests that use of a uni-modal relationship to predict APD when DIs change in sequence may not be appropriate. Because the restitution is strongly affected by activation history, i.e. cardiac memory, the restitution quantified under sequential activation directly evaluates the memory effects. Our results provide a mechanism that explains how cardiac memory buffers the alternans via hysteresis in the restitution.

Chapter 3 Methods

3.1 Experimental preparation

Experimental data were collected from a total of eleven adult mongrel dogs of either sex weighting between 18-25 kg. Six dogs were used to study the hysteresis in the restitution of APD. Five dogs were used in investigating alternans during constant DI activation. All of the studies were approved by the Institutional Animal Care and Use Committee at the University of Kentucky.

The dogs were anesthetized with sodium pentobarbital (40 mg/kg, IV). The hearts were rapidly excised, and a small piece of endocardium approximately the size of 20×10×5 mm was isolated from the free wall of the right ventricle. The tissue was mounted in a Plexiglas chamber and superfused by modified Tyrode's solution. The solution was bubbled with 95% O_2 plus 5% CO_2. Temperature and pH of the solution were maintained at 36° ± 1° C and 7.3±0.05. The composition of Tyrode's solution was: (in mmol/L) 0.5 $MgCl_2$, 0.9 NaH_2PO_4, 2.0 $CaCl_2$, 137.0 NaCl, 24.0 $NaHCO_3$, 4.0 KCl, and 5.5 glucose.

The tissue was equilibrated for at least 60 minutes by pacing it at a constant pacing cycle length. The pacing stimuli were delivered through a bi-polar Platinum-Iridium electrode. The total pulse width for the stimulus was 3 msec. The standard micro electrode technique was used to record transmembrane potential (TMP) by using machine pulled glass capillary microelectrodes filled with 3 mol KCl. Distance between

stimulating and recording electrodes was about 5 mm. Stimulation amplitude was 2 to 4 times diastolic threshold. The TMP were digitalized by a standby computer with a commercial data acquisition system at a rate of 10,000 samples per second.

3.2 Pacing protocol used in the experiment

We used our previously developed feedback based pacing protocol that controls DI explicitly[109, 111, 112]. Briefly, a controller program was written in C programming language. The program was customized to detected APD_{90}, i.e. 90% repolarization of action potential, in real time. Whenever the APD_{90} was reached, a stimulus would be triggered after predetermined waiting period. This waiting period then became the DI for the next APD. Therefore, by assigning a value to the waiting period, the DI was controlled independently from PCL or APD. The standard and dynamic restitution were also measured by using protocols similar to those described by Koller et al[87] for comparison.

The experimental study included two parts – the hysteresis of restitution study and the alternans study. The feedback protocol was implemented by applying different DI sequence patterns in these experiments. In the hysteresis of restitution study, APD dynamics was investigated during variable DI activation, i.e. the DI changed following a designed pattern. Three patterns of DI sequences were designed in the hysteresis study, the sinusoidal oscillatory activation, the random activation, and the linear activation. 1) In the sinusoidal oscillatory activation, DI oscillated following a sine wave between the maximum and the minimum value over a period of N beats. The range of oscillation was 100 to 700 msec and 20 to 150 msec. The period, N was equal to 100 and 200 beats/cycle. 2) In the random activation, DI was randomly picked in the range between 25 to 160

msec. The probability of DI falling into this range was uniformly distributed. 3) In the linear activation, DI changed from a maximum to minimum linearly and vice versa. In addition to these sequences, in two animals, restitution relationships were computed by using the standard and dynamic protocols. For the linear pattern, DI was selected such that they reproduced those that resulted during standard and dynamic protocols.

In the alternans study, the beat to beat APD dynamics during constant DI activation was investigated. We had three patterns for constant DI activation, one-level constant DI sequence, two-level constant DI sequence, and constant DI with random perturbation sequence. 1) In the one-level constant DI sequence, tissue was paced for 100 beats, and each of these activations had a constant value of DI. In the experiment, the DI was held between 40 to 45 msec for different trials. Although there are differences on DI level between the trials, these differences do not affect the conclusion of our study, because the critical point is to control the DI change for successive beats in a limited range in each trial. In some trials, data for one-level constant DI sequence were collected from four different initial conditions. These initial conditions were achieved by pacing the tissue for 10 minutes with PCL = 200, 300, 400, and 600 msec. After a constant DI sequence trial, the average cycle length that resulted during this trial was calculated. Then in the next trial, the tissue was paced for 100 beats at a PCL that was equal to the average cycle length from the immediately preceding constant DI trial. 2) Two-level DI sequence was used in the two-level constant DI trials. The tissue was first paced at constant DI = 60 msec for 30 beats. Then the DI was raised to 215 msec abruptly. After 30 beats with DI = 215 msec, the DI switch back to 60 msec for another 30 beats. 3) There were three phases in the constant DI with random perturbation sequence. Two of these phases had 30 beats

of activation with constant DI = 35 msec. Between these two segments of constant DI activation, there was a 30 beat sequence of random DI perturbation. During the random perturbation, DI changed randomly between 15 and 55 msec with a uniform distribution.

3.3 Data analysis

The TMP were recorded using a stand-alone data acquisition system and analyzed using Matlab (MathWorks) after the experiments. APD was detected by using the threshold of APD_{90}, i.e. 90% repolarization from the amplitude of the action potential. We denote APD and its preceding DI as a pair, for example, APD_n and DI_n were the APD and its preceding DI at the n-th activation. For those trials when DI was more than 30 msec, we assumed that the membrane potential was fully recovered, and the APD_{90} was calculated from the amplitude of each beat. This algorithm avoided the error introduced by base line shift for the long time recording. For the trials with DI < 30 msec and those during dynamic restitution protocol, APD was detected by using a fixed threshold that was computed from the first beat of the trial. Dynamic restitution data points were fit to an exponential function, $APD = a + b\,(1 - \exp(-c \times DI))$ (TableCurve 2D v5.01, SYSTAT Software Inc).

3.4 Simulation model

Table 3.1 Definition of symbols using in the simulation

LRD	Luo-Rudy dynamic model
CVM	cardiac ventricle model
Cm	membrane capacitance
V	membrane potential
I_{ion}	summation of membrane currents
I_{stim}	Stimulus current
I_{Na}	Fast sodium current
I_{Nab}	Background sodium current

I_{NaCa}	Current through sodium calcium exchanger
I_{CaL}	L-type calcium channel current
I_{CaT}	T-type calcium channel current
I_{Ca}	Calcium current through L-type calcium channel (CVM)
I_{CaK}	Potassium current through L-type calcium channel (CVM)
I_{Cab}	Background calcium current
I_{Kr}	Rapid delayed potassium rectifier current
I_{Ks}	Slow delayed potassium rectifier current
I_{K1}	Inward rectifier potassium current
I_{to}	Transient outward potassium current
I_{Kp}	Plateau potassium current
I_{NaK}	Sodium potassium pump current
I_{pCa}	Sarcolemmal calcium pump current
SR	Sarcoplasmic reticulum
I_{up}	Calcium uptake current to sarcoplasmic reticulum
I_{tr}	Calcium transfer current from network to junctional SR
I_{leak}	Current of calcium leakage from network SR
I_{rel}	Current of calcium release from SR
JSR	Junctional sarcoplasmic reticulum
[JSR]	Calcium concentration in JSR
NSR	Network sarcoplasmic reticulum or non-junctional SR
[NSR]	Calcium concentration in NSR
$[Ca]_i$	Intracellular calcium concentration or cytosol Ca concentration
$[Ca]_o$	Extracellular calcium concentration
Tautr	Calcium translocation rate from NSR to JSR
Iupbar	Maximal calcium reuptake rate from cytosol to NSR

All simulations were performed using custom code developed using Fortran90. Two computational models were used to calculate membrane currents. One was the Luo-Rudy dynamic (LRD) model[113], and the other one was the canine ventricle model (CVM)[114]. The action potential was reconstructed using the following differential equation:

$$\frac{\partial V}{\partial t} = -\frac{I_{ion} + I_{stim}}{C_m} \qquad \textbf{Equation 3.1}$$

The Luo-Rudy dynamic model[113, 115-117] is a detailed ionic model including the membrane currents, two-chamber model for sarcoplasmic reticulum, and calcium buffers.

A schematic diagram of LRD was shown in Figure 3.1. In our simulation, the summation of membrane current was described using following equation:

$$I_{ion} = I_{Na} + I_{CaL} + I_{CaT} + I_{Kr} + I_{Ks} + I_{K1} + I_{Kp} + I_{NaCa} + I_{NaK} + I_{pCa} + I_{Cab} + I_{Nab} \quad \textbf{Equation 3.2}$$

The meanings of symbols used in the equation and figures were listed in Table 3.1. Especially, in LRD, the stimulus current was added to the potassium current to preserve conservation condition[118].

The L-type calcium current (I_{CaL}) is calculated by the equation:

$$I_{CaL} = d \cdot f \cdot f_{Ca} \cdot (\bar{I}_{Ca,Ca} + \bar{I}_{Ca,K} + \bar{I}_{Ca,Na}) \quad \textbf{Equation 3.3}$$

Where d and f are activation and voltage dependent inactivation gate respectively. The f_{Ca} is Ca dependent inactivation gate. $\bar{I}_{Ca,Ca}$, $\bar{I}_{Ca,K}$ and $\bar{I}_{Ca,Na}$ are Ca, K and Na currents through L-type Ca channel. The f_{Ca}, $\bar{I}_{Ca,Ca}$, $\bar{I}_{Ca,K}$ and $\bar{I}_{Ca,Na}$ were calculated by:

$$f_{Ca} = 1/(1 + ([Ca]_i / K_{m,Ca})^2)$$
$$\bar{I}_{Ca,s} = z_s^2 P_s \cdot \frac{VF^2}{RT} \cdot \frac{r_{si}[s]_i \cdot \exp(z_s VF / RT) - r_{so}[s]_o}{\exp(z_s VF / RT) - 1} \quad \textbf{Equation 3.4}$$

Where $[Ca]_i$ is intracellular or cytosol Ca concentration. $K_{m,Ca}$ = 0.6 umol/L, F = 96,485.0 coulombs/mol, R = 1.987 calories/mol/Kelvin, T = 310 Kelvin. In the equation, 's' is substituted by ion name of Ca, K, and Na when $\bar{I}_{Ca,Ca}$, $\bar{I}_{Ca,K}$ and $\bar{I}_{Ca,Na}$ is computing. Z_s is the valence for ion 's', i.e. Z_s equals to 2, 1, 1 when s is substituted by Ca, K, and Na. Similarly, P_s equals to 5.4×10^{-4}, 6.75×10^{-7}, and 1.93×10^{-7} cm/sec for Ca, Na, and K. $[s]_i$ and $[s]_o$ are intracellular and extracellular concentration for ion s. r_{si} and r_{so} are the

activation coefficients for ion s at intracellular and extracellular space. V is membrane potential.

The rapid potassium rectifier current, i.e. I_{kr} was calculated by Equation 3.5.

$$I_{kr} = G_{kr} \cdot X_r \cdot R \cdot (V - E_{kr}) \qquad \textbf{Equation 3.5}$$

Where G_{kr} is the maximal conductance of I_{kr}, E_{kr} is the reversal equilibrium potential, X_r and R are parameters for voltage gate activation and inactivation, and V is membrane potential.

The slow potassium rectifier current, i.e. I_{ks} was computed by Equation 3.6.

$$I_{ks} = G_{ks} \cdot X_{s1} \cdot X_{s2} \cdot (V - E_{ks}) \qquad \textbf{Equation 3.6}$$

Where G_{ks} is the maximal conductance, E_{ks} is the reversal potential, and X_{s1} & X_{s2} are parameter for the voltage activation gate. V is membrane potential.

The current of the channel that pumps calcium from cytosol to network sarcoplasmic reticulum is denoted by I_{up} and calculated by Equation 3.7.

$$I_{up} = Iupbar \frac{[Ca]_i}{[Ca]_i + K_{m,up}} \qquad \textbf{Equation 3.7}$$

Where *Iupbar* is the maximal current of Ca uptake from myoplasm to NSR, $[Ca]_i$ is the cytosol Ca concentration, and $K_{m,up}$ is half-saturation concentration of I_{up} channel.

The translocation current of Ca from NSR to JSR is represented by I_{tr}. The equation of I_{tr} is showed in Equation 3.8.

$$I_{tr} = \frac{[NSR] - [JSR]}{Tautr}$$ **Equation 3.8**

Where the [NSR] and [JSR] are Ca concentration in NSR and JSR. *Tautr* is the time constant of Ca transferring from NSR to JSR, which is reciprocal to the translocation rate.

Because the LRD model cannot reproduce stable alternans[114], CVM was used to explore the alternans. The schematic diagram of CVM was shown in Figure 3.2. The CVM modeled L-type Ca channel, I_{Ca}, with special Ca inhibitory kinetics, and also added I_{to} into the model. The CVM contains following membrane currents:

$$I_{ion} = I_{Na} + I_{K1} + I_{Kr} + I_{Ks} + I_{to} + I_{Kp} + I_{NaK} + I_{NaCa} + I_{Nab} + I_{Cab} + I_{pCa} + I_{Ca} + I_{CaK}$$ **Equation 3.9**

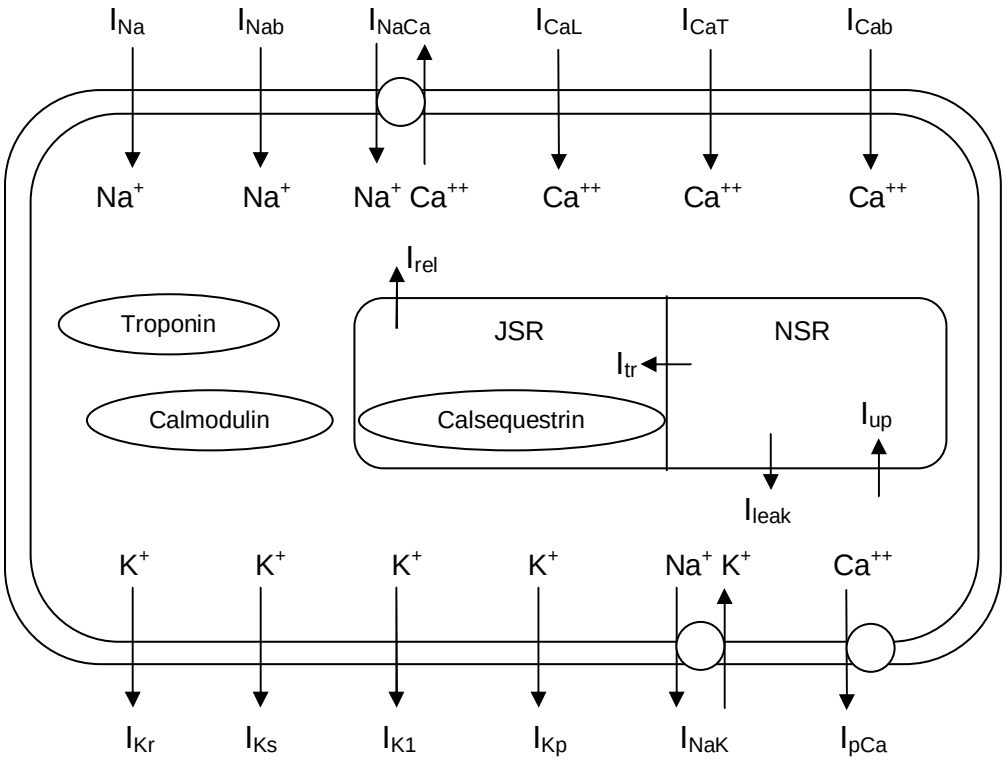

Figure 3.1 Schematic diagram of LRD model

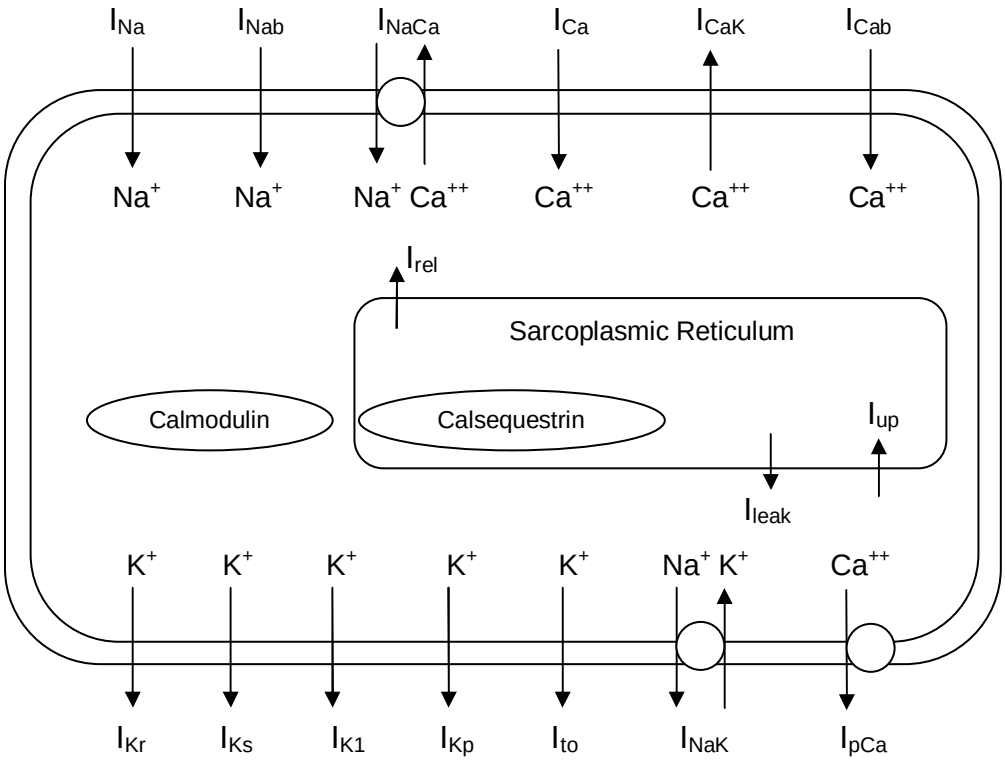

Figure 3.2 Schematic diagram of CVM

3.5 Simulation protocol

The major study of hysteresis was performed in LRD model. Two sinusoidal DI sequences were used to simulate the hysteresis phenomenon. One sinusoidal DI sequence had a mean DI value of 400 msec with a ± 300 msec change around this mean with a period of 100 beats. By using this DI sequence, the range of activation rate was about from 70 to 300 beats per minute. The other sinusoidal DI sequence had 150 msec as mean, ±140 msec changing range from this mean, and a period of 100 beats. We refer to these sequences as those with center DI of 400 and 150 msec. An example of a sinusoidal DI sequence and the resulting APDs is shown in Figure 3.3A.

The potassium currents, I_{Kr} and I_{Ks}, and the L type calcium current, I_{CaL} were perturbed to investigate the factors that affect the characteristic of the hysteresis. The equations that were used to calculate I_{CaL}, I_{kr} and I_{ks} are given in Equation 3.3, 3.5, and 3.6. During each simulation step, these currents were multiplied by the scale factors of 0.2, 0.5, 1, and 1.5. These scale factors simulated antagonist and agonist effects on these ion channels, i.e. when the current was multiplied by a scale factor of 0.2, the current was decreased 80%. If the current was multiplied by 1.5, the current was increased 50%.

We also perturbed the model parameters *Tautr* and *Iupbar*. In the LRD model, the SR is modeled as two chambers, NSR and JSR. I_{tr} is the current that transfer calcium from NSR to JSR as shown in Figure 3.1. The equation of computing I_{tr} is shown in Equation 3.8. The translocation rate of I_{tr} is inversely proportional to *Tautr*, i.e. an increase in the value of *Tautr* leads to a decrease in the rate of calcium transfer. The nominal value of *Tautr* in LRD is 180. During the simulation, the value of 20, 100, 180 and 360 was used for *Tautr* respectively. Another current, I_{up} pumps Ca from cytosol to NSR. The maximal calcium re-uptake rate was governed by the parameter *Iupbar* as shown in Equation 3.7. The nominal value of *Iupbar* in LRD is 0.00875. During the simulation, the value of 0.004375, 0.00875, 0.0175, and 0.02625 was used for *Iupbar* respectively.

The reasons that above currents and parameters were chosen in this study are based on following: these currents/parameters are important for the repolarization and restitution. Recent studies suggest that blocking Ca/K currents[88, 91, 119] or augmenting I_{kr} [120, 121] may be potentially useful to treat arrhythmia. It is concluded in many studies that the Ca cycling in SR plays a key role in the mechanism of alternans[103, 104].

To quantify the characteristics of the hysteresis, we defined the following parameters: MaxDelay, MinDelay, and Thickness of loop. MaxDelay was the delay of the beats when APD and DI reached the maximum values during the sinusoidal sequence. MinDelay was the delay when APD and DI reached their minimum values. Both MaxDelay and MinDelay were measured in units of beats. Figure 3.3A shows how the MaxDelay and MinDelay were measure in an example of a simulation trial. Thickness of loop described the difference between APDs that occurred during ascending and descending trajectories of DI at the central value of DI, i.e. at DI = 400. In Figure 3.3B, the arrows indicate the direction of trajectory evolution, and Thickness of the hysteresis loop.

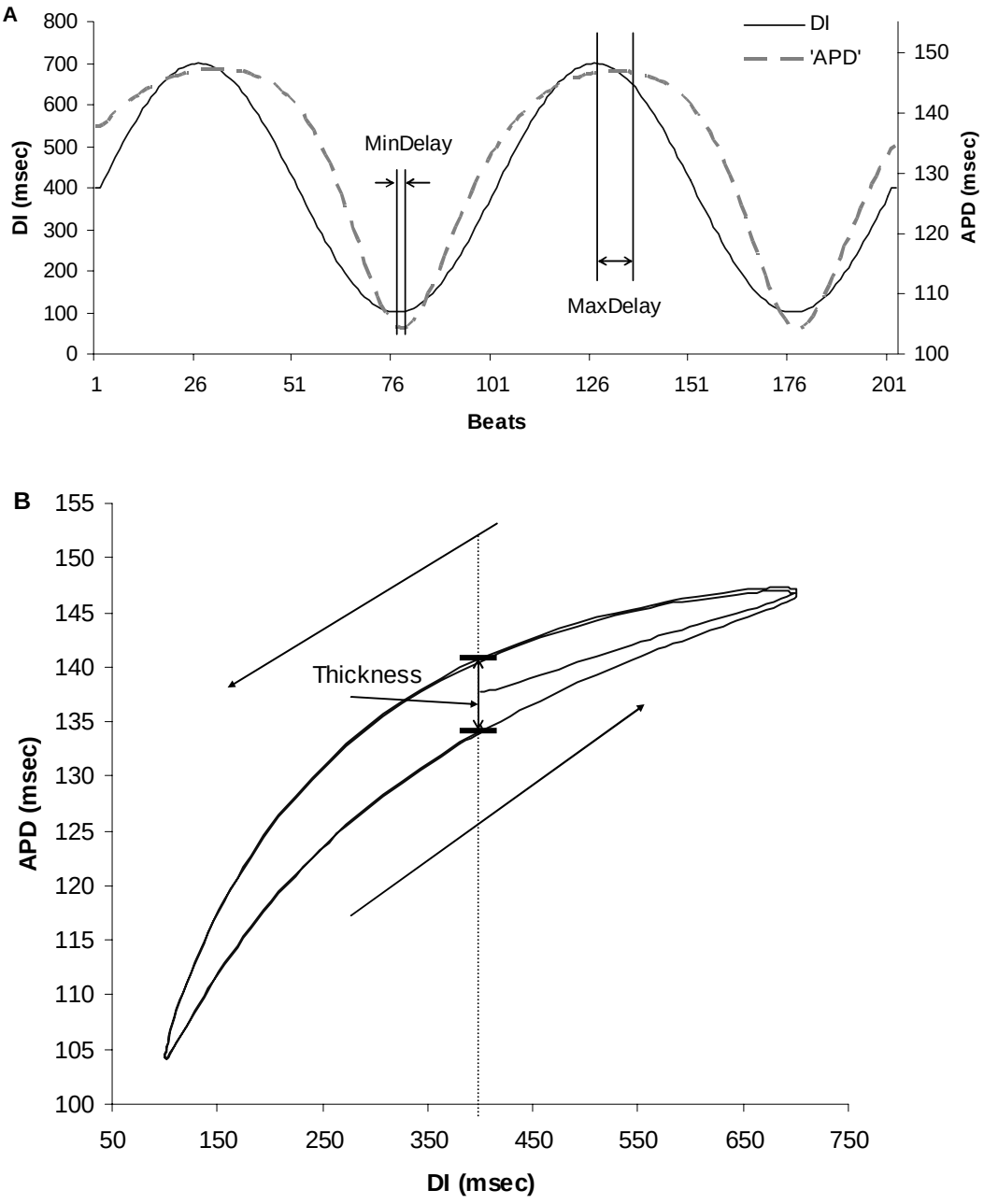

Figure 3.3 The parameters used in quantification of the hysteresis. This is simulation results using the LRD model. The results reproduced the hysteresis phenomenon that was observed in our experiments. The panel A shows the DI sequence and the resulting APDs. Note that two Y-axes were used to present DI and APD value respectively. The places were marked where the parameters of

MaxDelay and MinDelay were measured in panel A. The panel B shows the same DIs and APDs data as in panel A, but in the restitution figure. The arrows point out the changing direction of DI&APD. The parameter, i.e. Thickness of the hysteresis loop, was measured at DI = 400 msec.

Because LRD model's limitation in studying alternans[114], the CVM was used to investigate the alternans and hysteresis. Similar sinusoidal DI sequence as Figure 3.3 showed was used to measure hysteresis characteristic parameters. The alternans threshold was detected by using a stepwise pacing protocol. At this protocol, the pacing cycle length was started at 400 msec, and decreased at 5 msec decrement. At each step, the same cycle length was paced for 50 beats. If the alternans did not happen, or the amplitude of alternans decreased dramatically in 50 beats, that cycle length would continue decreasing, until at some cycle length, the alternans of APD could not be paced away for 50 beats, i.e. the amplitude of alternans did not decrease. This cycle length was saved as the alternans threshold. We also used the constant DI sequence to investigate APD alternans. The CVM model did not replicate the experimental results, i.e. none of the APD alternans was produced during constant DI pacing, which was demonstrated in our experiment.

Chapter 4 Results

4.1 Feedback protocol

Figure 4.1 demonstrates two trials of trans-membrane potential data recorded from the feedback and conventional pacing protocol experiments. A segment of data from a constant DI trial was plotted in panel A. The arrows indicated the points where APD_{90} threshold was reached. After these points, the next stimuli would come after a pre-determined period of time. The gray lines in Figure 4.1 marked the controlled time duration. This result shows the feedback protocol can hold DI at the pre-determined value and following APD changes accordingly. Each of the DIs became the variable independent of PCL or APD. In most of the other conventional pacing protocols, the cycle length was the controlled variable as shown in Figure 4.1. That is, the primary difference between DI and PCL control pacing protocol is the independent variable. The feedback based protocol is a DI control pacing protocol that brings insight into the investigation of alternans and unveils the mechanism concealed in the interaction between DI and APD introduced by PCL control protocols.

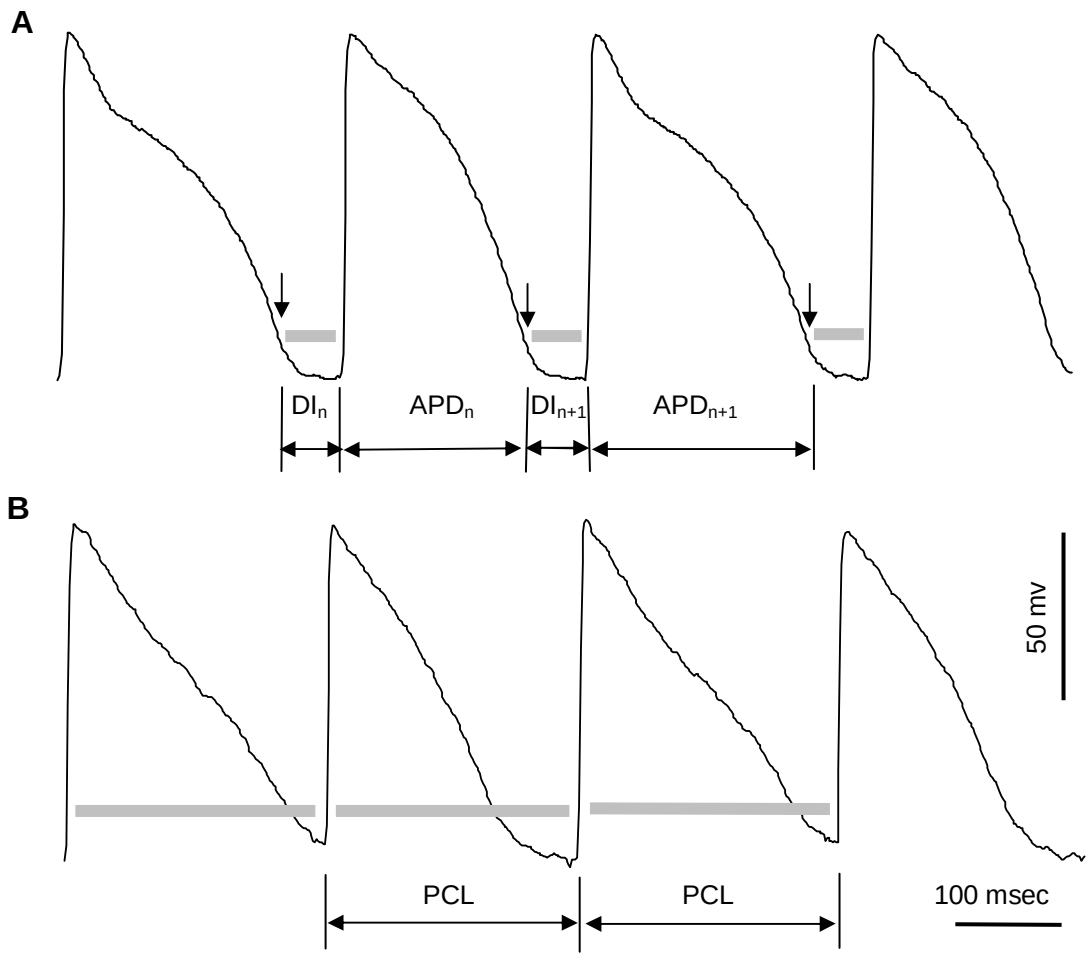

Figure 4.1 Demonstration of DI control and cycle length control pacing protocol. A) An example of trans-membrane potentials that was recorded during an experiment by using constant DI pacing. The arrows and gray bars indicate the DIs preceding each action potential are constant, while APDs show the alternans. B) An example of trans-membrane potentials using constant PCL. The gray bars indicate the PCL for each beat is constant. The alternans of APD is companied with alternans of DI during constant PCL pacing.

4.2 Hysteresis in restitution of action potential duration

The restitution of APD demonstrates hysteresis phenomenon during sequential DI control activation. Figure 4.2 shows results from an experimental trial with sinusoidal oscillation in DI. The tissue was first paced for 20 beats at the constant DI = 400 msec, which was also the mean DI for the following oscillation DI part. Then the DI oscillated between 100 and 700 msec following a sine wave with a period of 100 beats. In each trial, tissue was stimulated for two periods of oscillatory DI. The sequential change of DIs and resulting APDs are shown in Figure 4.2A. Their restitution relationship was plotted in Figure 4.2B. The restitution trajectory is a counter-clockwise rotation loop for successive beats. It shows that APD can be different for the same preceding DI. This discrepancy depends on prior activation history. Given the same DI, APD tend to be shorter with increasing DI activation than with decreasing DI activation. The restitution relationship for accelerating and decelerating activation history demonstrates a hysteresis phenomenon.

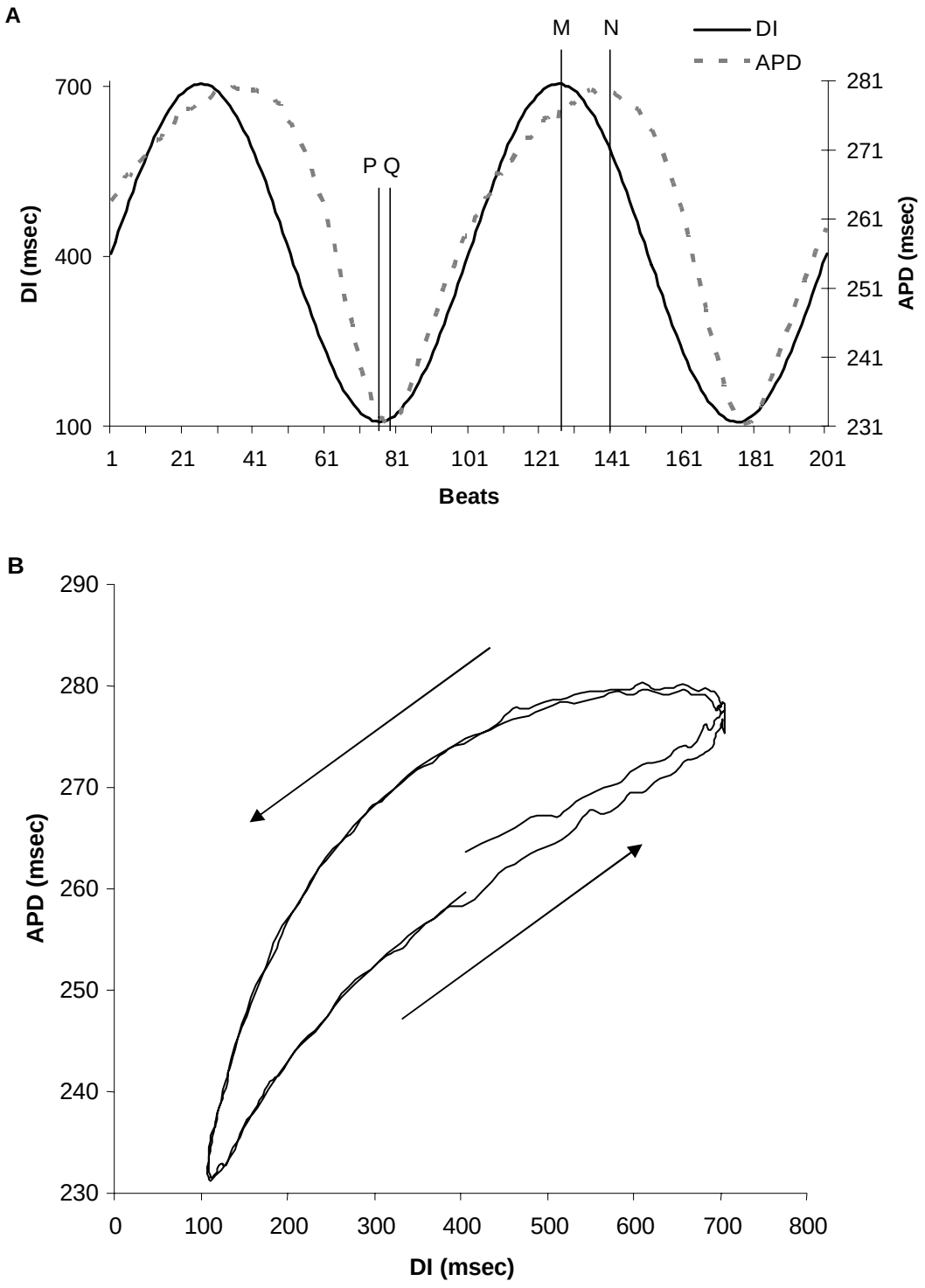

Figure 4.2 Hysteresis in restitution of APD in sinusoidal oscillation DI activation. The panel A shows DIs and their following APDs. The change in APD is a delayed change to oscillatory DI. The delay between maximal APD and

maximal DI was measured at line M and N. The delay between minimal DI and APD was measured at line P and Q. The panel A shows that there are 13 beats of delay between M and N, and 3 beats of delay between P and Q. It is worthy to note that two Y axes were used in the panel A to display the values of DI and APD respectively. In the panel B, DI and APD data were plotted in a restitution figure. The arrows point out the changing direction of DI-APD pairs. This figure shows that multiple APDs are corresponding to the same DI. The 20 beats of constant DI = 400 msec activation before oscillation were not shown in both panel A and B.

During sequential activation, the change in APDs responding to the change in DIs demonstrates a phenomenon of delayed response. As shown in Figure 4.2A, vertical lines M and N marked the points where DI and APD reached their peak value. It showed that APD kept increasing for about 13 beats after the DI maximum and then started decreasing. The delay was not symmetrical for accelerating and decelerating activation history. After the DI passed the nadir, the APD reached the minimum in 3 beats, as depicted in Figure 4.2A by lines P and Q. These results indicated that the APD increase following increasing DI with fast activation history was relatively less than the APD decrease following decreasing DI with slow activation history.

Figure 4.3 and Figure 4.4 also show the hysteresis behavior. In order to determine whether the period of change in DI affected restitution relationship, we used oscillatory DI sequences with different periods. Figure 4.3 shows the hysteresis obtained during two

different trials in which 100 and 200 beats were used to complete one cycle of sinusoidal oscillation. In both trials, mean and range of DI were same. Although longer period of sinusoidal oscillation demonstrated relatively more prominent hysteresis, the basic hysteresis type morphology pattern was similar. Figure 4.4 is an example of the trials in which the period of oscillation, mean value and the range of DIs were same as those in Figure 4.2, but the phase of DI change was inverted. As Figure 4.4A showed, in contrast to the DI pattern in Figure 4.2, the DI was first decreased and then increased. These results indicate that whether DI increased or decreased first did not affect the morphology of restitution relationship. Both of them demonstrated bi-modal trajectories, i.e. hysteresis.

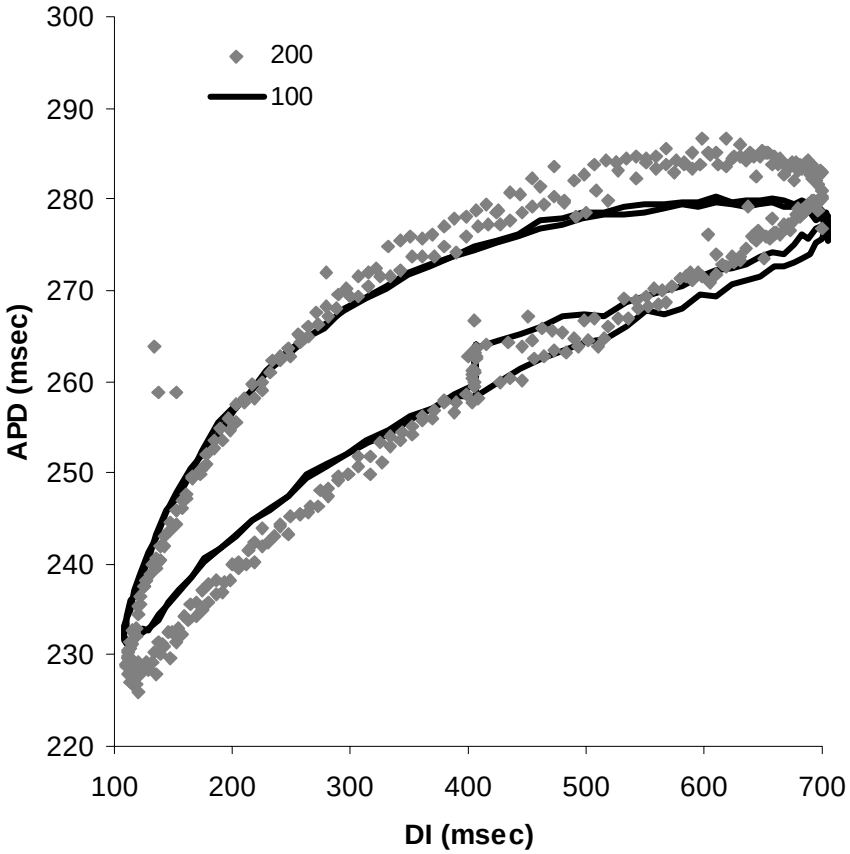

Figure 4.3 Hysteresis loop with period = 100 and 200 beats sinusoidal oscillation. The oscillatory DI was tested using two periods, i.e. the DI sequence used 100 or 200 beats to finish one sine cycle. As shown in the figure, the general characteristic of the hysteresis loops is the same during period = 100 (solid line) and period = 200 (diamond dot).

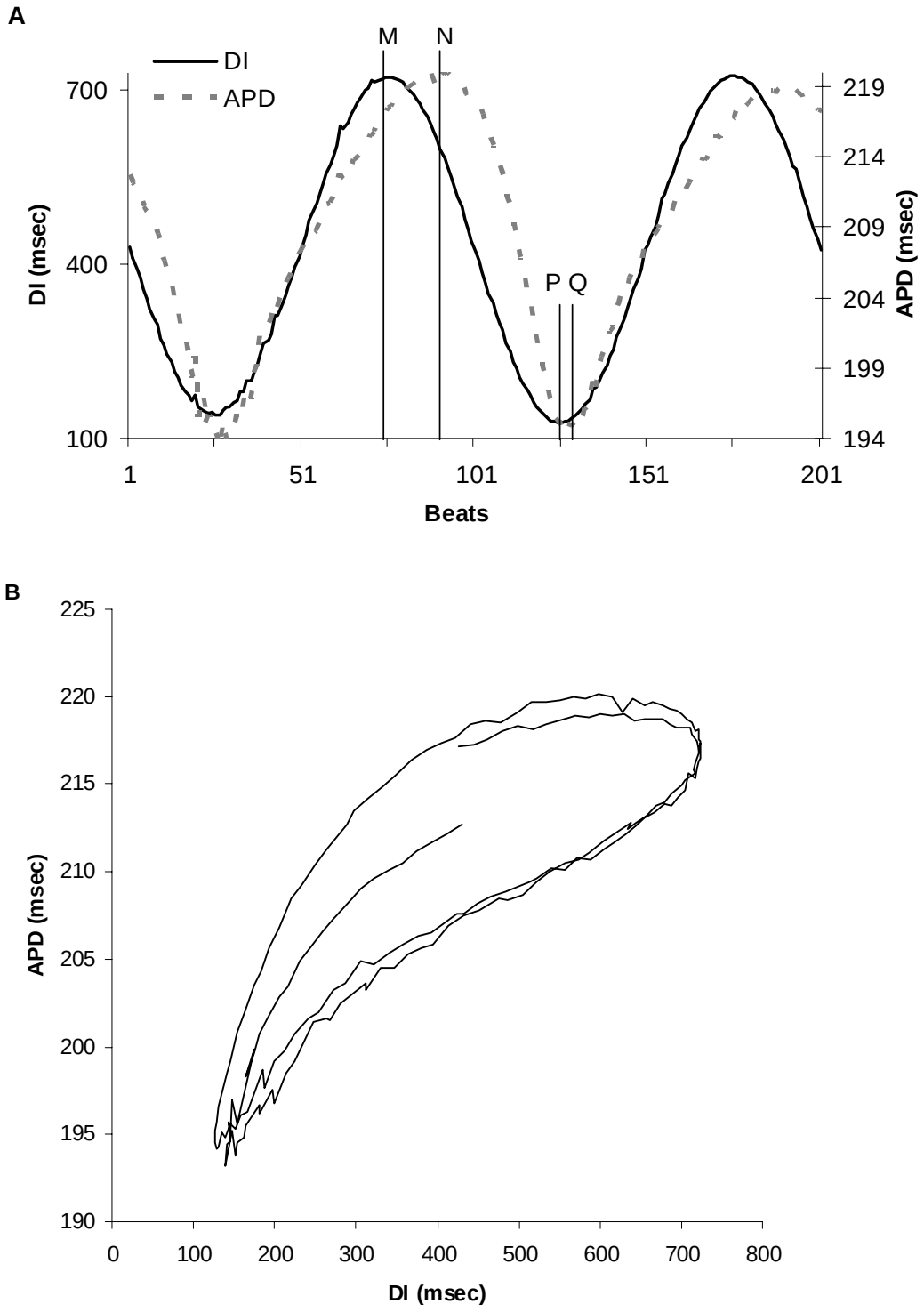

Figure 4.4 Hysteresis in restitution of APD in phase shifted sinusoidal oscillation DI. Similar hysteresis is demonstrated as shown in **Figure 4.2**, except that the initial phase of oscillatory DI was inversed.

The hysteresis in the restitution was a reproducible phenomenon. We verified the reproducibility by repeating the oscillatory DI trials in four animals. All of these trials had the same sinusoidal oscillation pattern; a mean DI of 400 msec, a period of 100 beats and a range of DI between 100-700 msec. The average of the restitution relationships is shown in Figure 4.5. In the figure, the mean of APD values was subtracted and the amplitude of APD was normalized within each animal with respect to the maximum and minimum APD recorded in each trial. In order to address variances among animals, standard error was calculated for normalized APD and represented by vertical bars. Figure 4.5 shows a hysteresis pattern of restitution relationship, which is similar to Figure 4.2 and Figure 4.4.

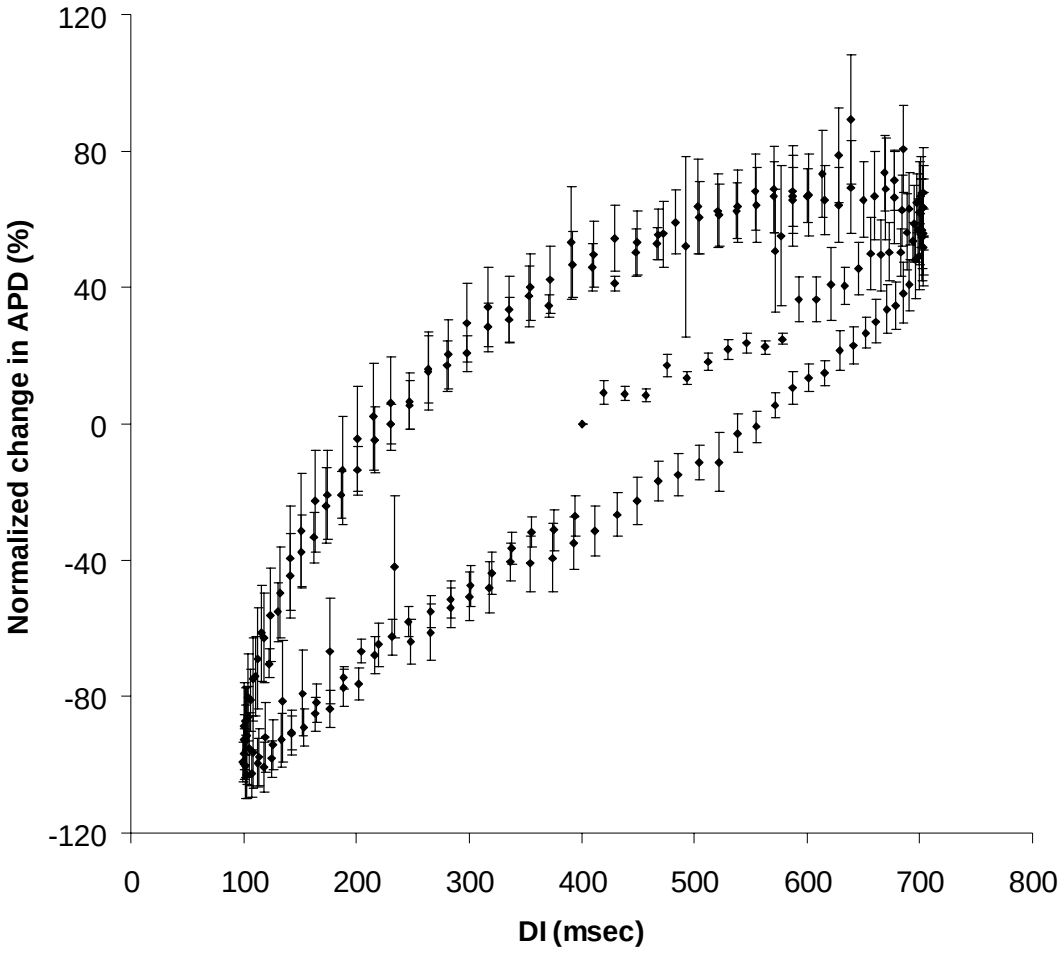

Figure 4.5 Average hysteresis loop from four animals. The change in APD was normalized and presented as change in percentage. The variance from different animals was plotted as standard error bar. The figure shows the dynamics of APD has multi-modal behavior during sequential DI changes.

The oscillatory DI sequence explored above fell into the range of 100 to 700 msec. It resulted in the activation rate from 60 to 180 beats per minute. To test the hysteresis at a higher activation rate range, an oscillatory DI sequence was conducted at the mean of 80 msec and the range of 20-150 msec. An example result of this DI sequence is shown in Figure 4.6. Similar to the 400 msec mean DI sequence, 20 beats of constant DI=80 msec were paced before DIs changed into the oscillatory pattern. Figure 4.6A shows the DI sequence followed with a sinusoidal pattern with a period of 200 beats. The resulting APD is plotted in Figure 4.6B, which showed an oscillatory pattern added on a decreasing monotonic baseline. Due to the monotonic decrease of APD, the restitution relationship displayed a spiral trajectory with continuously downward displacement. To remove the effects of monotonic decrease in APD, a linear function was fitted to the nadirs of the APD curve, as the dash line shown in Figure 4.6B. After subtracting the linear function, APD was plotted versus DI in Figure 4.6C. It demonstrated hysteresis type behavior, similar to that observed during oscillatory DI with longer means. As the DI oscillated between 20 to 150 msec, the tissue was activated at considerably faster rates, ranging from 160 to 350 activations per minute.

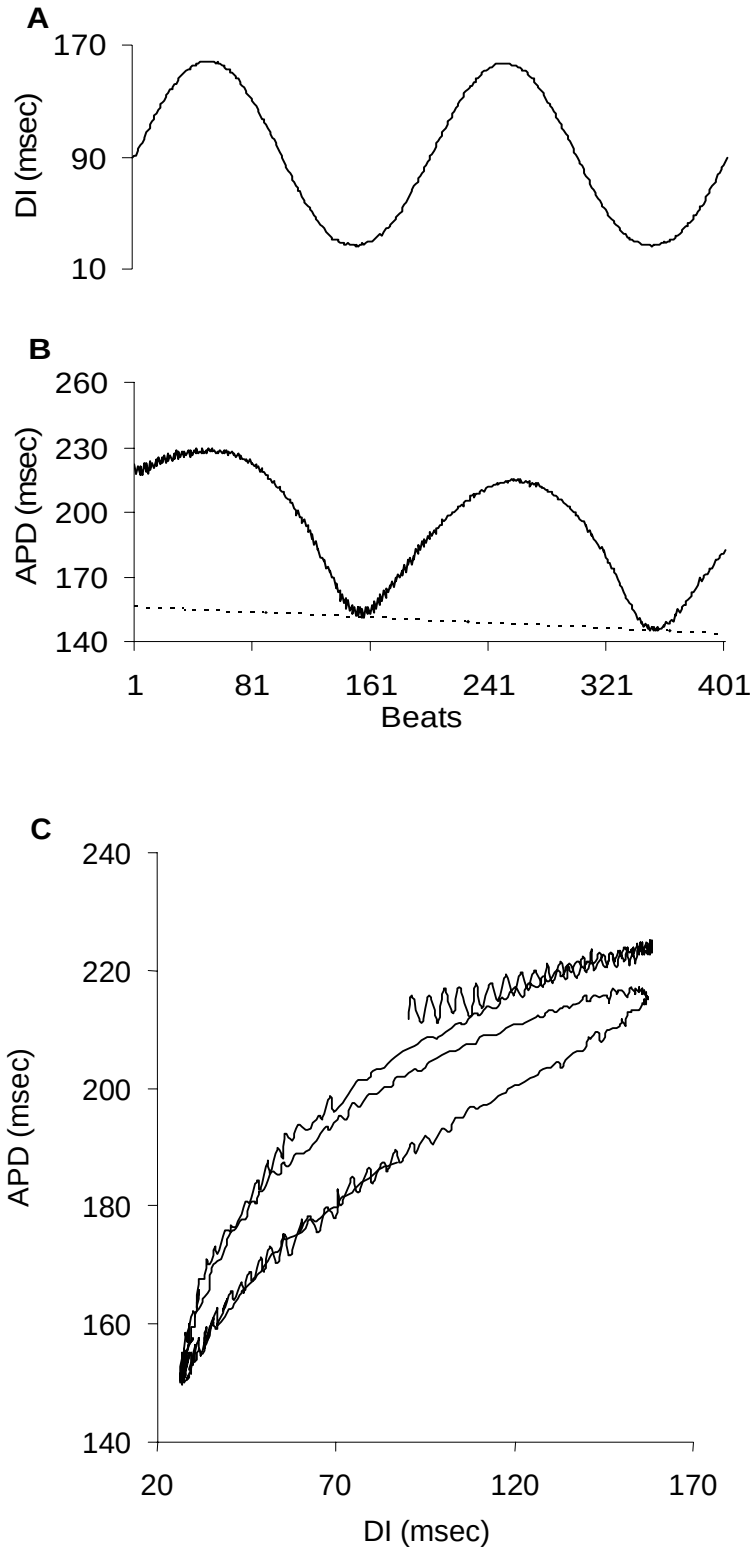

Figure 4.6 Oscillatory APD with DI activation in the range of 20 to 150 msec.

Panel A and B show the oscillatory DIs and resulting APDs. The dash line in B is

the linear function that was used to remove the decreasing baseline. After the linear function was subtracted from APDs, the restitution relationship was plotted in panel C. This result shows hysteresis at the activation rate between 160 to 350 beats/minute (20 beats of constant DI = 80 msec activation before the oscillation were not plotted in the figure)

Standard and dynamic restitution relationship were computed in two animals by using pacing protocols similar to those described by Koller et al[87]. The DI values that were computed for the standard and dynamic restitution relationship were saved for the first animal trial. In the next animal trial, the saved DI values were used for the linear DI sequence to determine restitution relationship. Because the linear DI activation sequence changed DI at every successive activation, the restitution trajectory measured by the linear DI sequence traversed across the DI axis (abscissa of Figure 4.7C) sequentially in time. The linear DI sequence, unlike the standard or dynamic protocol, does not pace the tissue for several tens of beats at a constant cycle length between the beats where the DI and APD were measured. As shown in Figure 4.7A, the tissue was initially paced at a constant DI=140 msec for 20 beats. Then the DI was changed by using the DI data recorded from the standard restitution relationship. The sequence of using DI was from the highest to the lowest value. In Figure 4.7A, the lowest DI was about 20 msec. Once the smallest value of DI was obtained, the DIs were increased from the smallest to the largest value, following the converse sequence of the DI decrease phase, until the initial value of the longest DI was reached. The resulting APD was shown in Figure 4.7B. The

APD value at the last beat returned to a lower value than that at the beginning of linear sequence. Although the first 20 beats and last beat of APD had the same value of preceding DI, they showed a monotonous declining drift of APD. When the DI was changed linearly, the APDs first decreased and then increased corresponding to the DI change. But there is a monotonous decreasing tread of APD level for similar DI level. Figure 4.7B also shows presence of APD alternans during the first 20 beats when the DIs were constant.

The restitution relationships from the linear sequential DI sequence, standard and dynamic pacing protocol, are shown in Figure 4.7C. The solid lines in Figure 4.7C show that the APD during sequential activation was longer than that during either standard or dynamic protocols. Especially, slopes of two trajectories of restitution curves were shallower than the slope of the standard restitution. And dynamic restitution had a steeper slope than standard restitution as expected from previous results of Koller et al[87]. The unit slope line (dash line) indicated the slope of dynamic restitution was markedly steeper than 1 for DI shorter than 50 msec, while in sequential pacing the slope was never larger than 1.

The memory effect is an important factor for the relationship between an APD and preceding activation. As described in previous studies, memory effects can be modeled as accumulative and dissipative, during activated and recovered phases of transmembrane potential. In order to explore the memory effects, the tissue was paced in a sequence such that DIs were randomly distributed between 25 to 160 msec with a mean of 80 msec. The DIs were designed to approach a uniform distribution. The trials were started with 50 beats of constant DI (80 msec) pacing. With uniform random distribution, the DI

preceding any activation had an equal probability of being short or long, which may minimize the cumulative effects of memory. During random activation, the tissue was paced at rates between 160 and 300 activations per minute. Random DI and resulting APD from a trial were shown in Figure 4.8A and B. Figure 4.8A is rotated by 90 degrees, which make the DI axis in panel A and C parallel. The restitution, in Figure 4.8C, shows that the relationship is a cluster of DI-APD points, instead of a well-defined trajectory. In the same figure, the result of linear DI activation and unit slope line were plotted. During random DI activation, the plot of APD versus preceding DI largely filled the range of the results from the linear activation. Similar to linear activation, the overall tilt of the cluster from random DI activation was much less than 1. Figure 4.8C shows that the range of DI change is approximately 100 msec, and the resulting change in APD distributes in a range of between 180 to 200 msec.

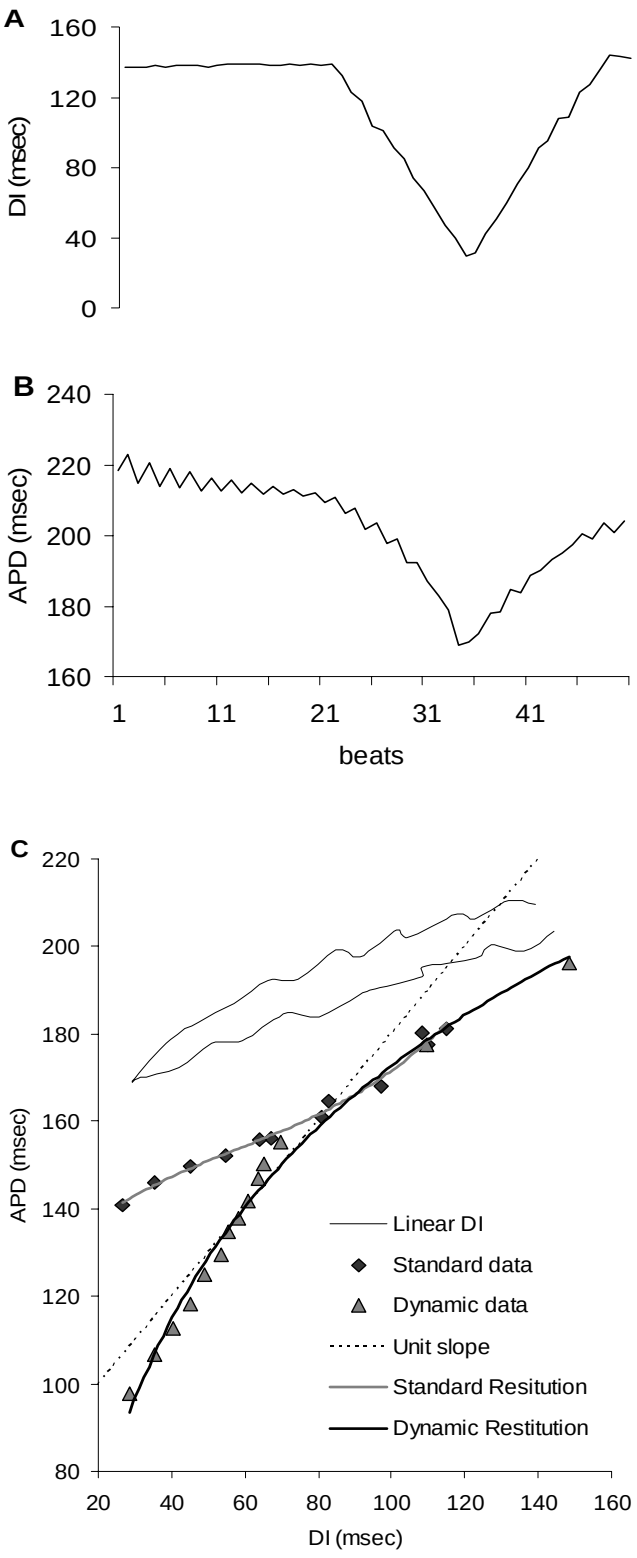

Figure 4.7 Linear DI activation and comparison with standard and dynamic restitution. The DIs were changed linearly as shown in the panel A. The

resulting APDs were shown in the panel B. The descending and ascending DIs and their following APDs were plotted in panel C. The standard and dynamic restitution were also plotted for comparison. The diamond and triangle dots are the data measured for standard and dynamic restitution and these data points were fitted to the exponent curves as shown in the figure. A straight line with unit slope was also included in the figure. These results show that the restitution relationship during linear sequential DI activation is flatter than the prediction of standard and dynamic restitution.

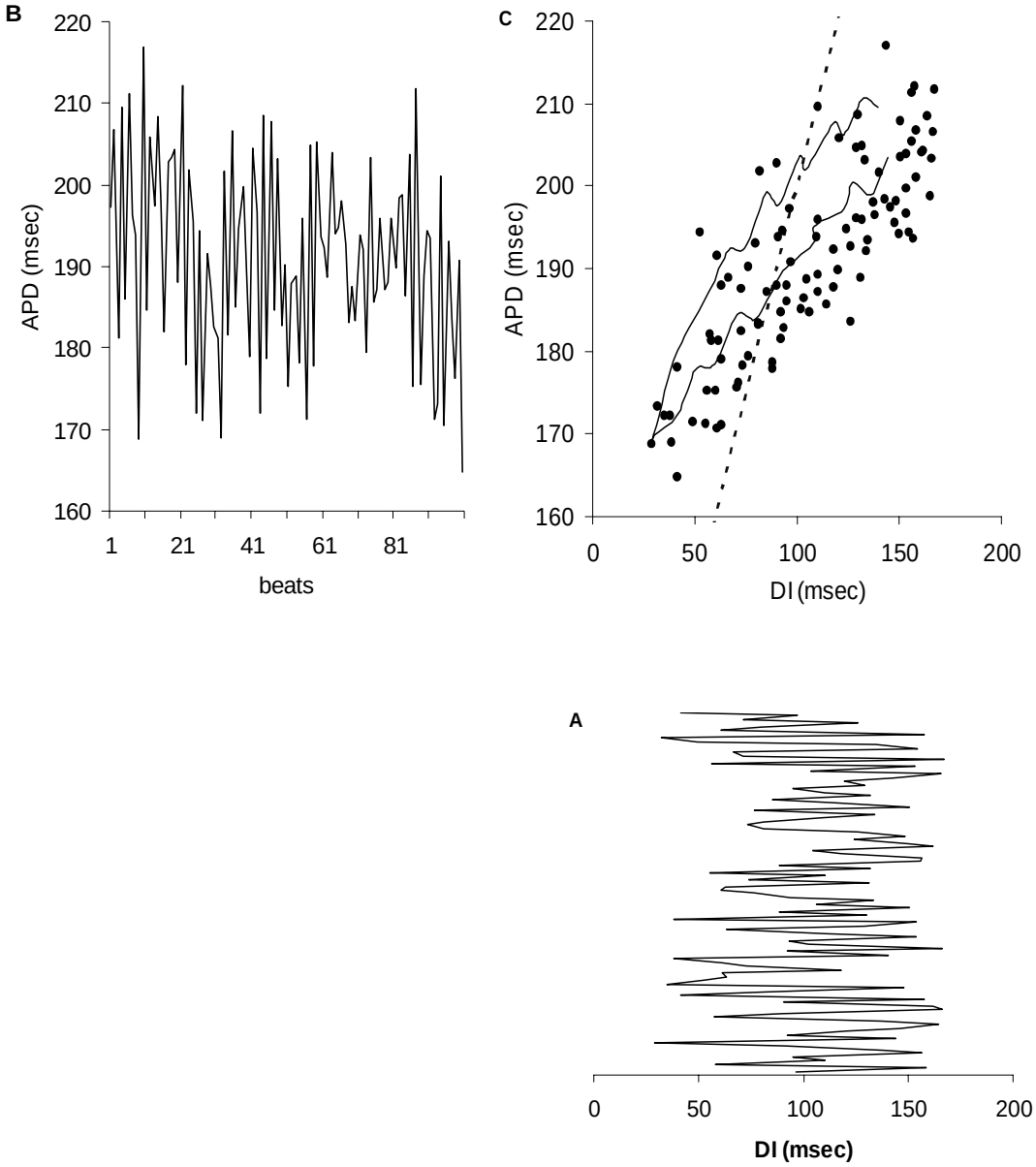

Figure 4.8 Random DI oscillation and comparison with linear DI oscillation. Panel A and B shows the random DIs and the resulting APDs. Panel A is rotated 90 degree, which make the DI axis is parallel to that in panel C. Panel C shows the restitution relationship during random DI (dot) and linear DI sequence (line). For comparison, the dash line was plotted for slope of unit. The results of random

DI gave a cluster of dots, which did not show a single modal restitution relationship. The ranges of DI and APD are largely the same for random DI and linear DI activations.

4.3 APD alternans exists during constant DI activation

When activation rate increases to some threshold, APD start the beat by beat alternative change. This phenomenon is called APD alternans or alternans in short. A typical pattern of alternans is, at a given constant PCL, a short DI after a long APD triggered a short APD, and then left a long DI for the next beat. Figure 4.1B shows four beats of TMP obtained when the tissue was paced at a constant cycle length equal to 174 msec. In such kind of alternans, APD alternative change was usually companied with DI alternative change.

The constant DI sequence resulted in another type of alternans that is shown in Figure 4.1A. This alternans featured long and short APD with same preceding DI. Figure 4.1 illustrates the main result of this part of study as well as an important difference between our and previous related studies. In Figure 4.1, alternans of APD was oscillating between 127 and 153 msec, i.e. alternans amplitude was 26 msec. After adding the DI preceding each of these activations, 42 msec, the cycle length was between 169 msec and 195 msec. This PCL range was close to and included the PCL of 173 msec used in Figure 4.1B. The important difference between Figure 4.1A and B is that DI in panel A does not oscillate, while DI in panel B does. But alternans of APD occurred in both of them. Therefore, the effects of DI dependent restitution to the alternans of APD were eliminated.

Occurrence of alternans of APD with invariant preceding DI was not a transient phenomenon that existed for a few beats. TMP were recorded during a trial for 100 beats where DI was controlled at a constant level. The results of DI and APD from one trial are shown in Figure 4.9. The Figure 4.9A shows that the DI had limited beat by beat variation. The standard deviation of |ΔDI|, i.e. beat by beat variation in DI, was ±1.0 msec. The amplitude of APD alternans |ΔAPD|, i.e. beat by beat variation in APD, however, was considerably larger as shown in Figure 4.9B. The mean ± standard deviation of |ΔAPD| equals to 25.5±2.9 msec. This result demonstrated that for 100 beats, alternans of APD occurred even though the preceding DI had almost no change. Data shown in Figure 4.9 were collected during one-level constant DI sequence activation with initial condition that was achieved by pacing at PCL = 600 msec. On the start of the constant DI sequence, the DI was abruptly shortened. It produced a slow drift of APD level as seen in Figure 4.9B. The drift was more pronounced in the first 20 beats or so.

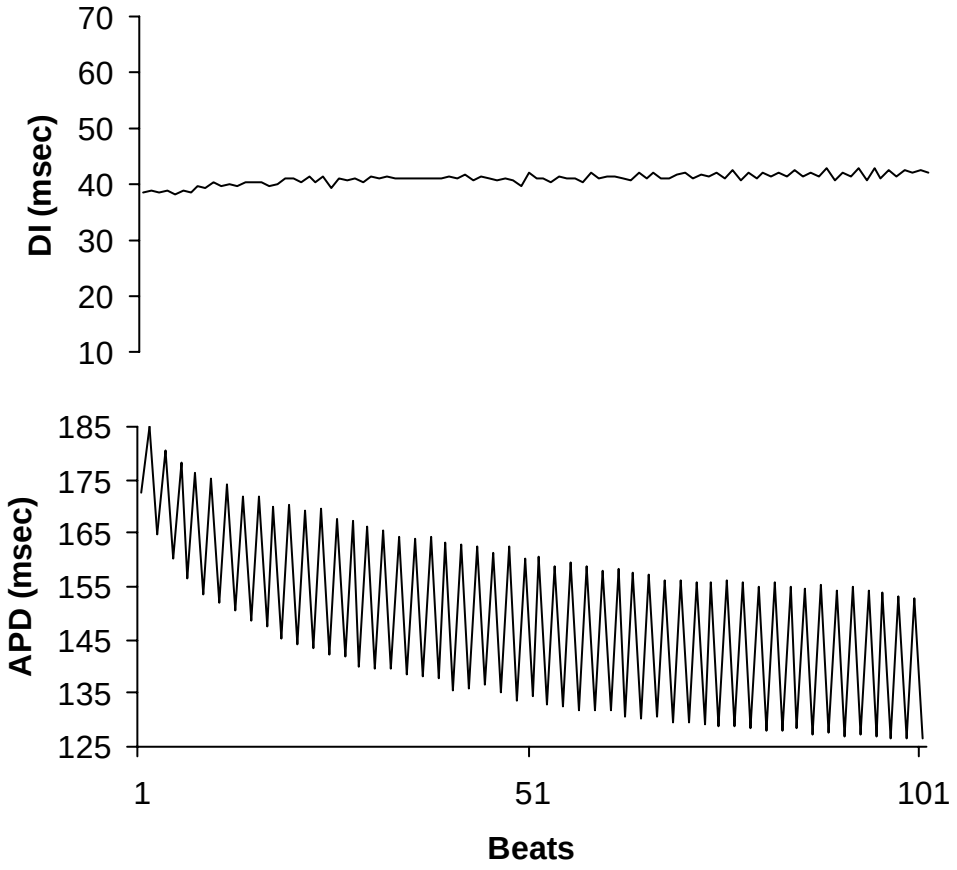

Figure 4.9 APD alternans with relatively constant DI. The DI and APD were measured for an experiment trial during constant DI pacing. The figure shows significant alternans of APD, when DIs are constant or have small variance.

After the data were collected when the tissue was paced by the one-level constant DI sequence, the average activation rate was calculated. In the next trial, this average activation rate was used as a constant PCL to pace the tissue for 100 beats. Both the constant DI pacing trial and its equivalent constant PCL trial resulted in APD alternans. The last 50 beats of DI and APD from both trials are plotted in Figure 4.10. Since the only last 50 beats were plotted, the effects of baseline drift transient had been minimized. The DI and APD relationships in Figure 4.10 demonstrated a clear vision of alternans. For comparison, the fitted dynamic restitution relationship in the same tissue is also shown in the figure. The dynamic restitution was vertically shifted to compromise the differences in baseline APD. The figure shows that during the constant DI pacing, the relationship between APD and DI was almost vertical, two clusters of APD (filled circle) during alternans were vertically aligned. The clusters of APD during constant cycle length pacing (filled diamond) showed two clusters of APD followed the direction of dynamic restitution, and had a slope close to one.

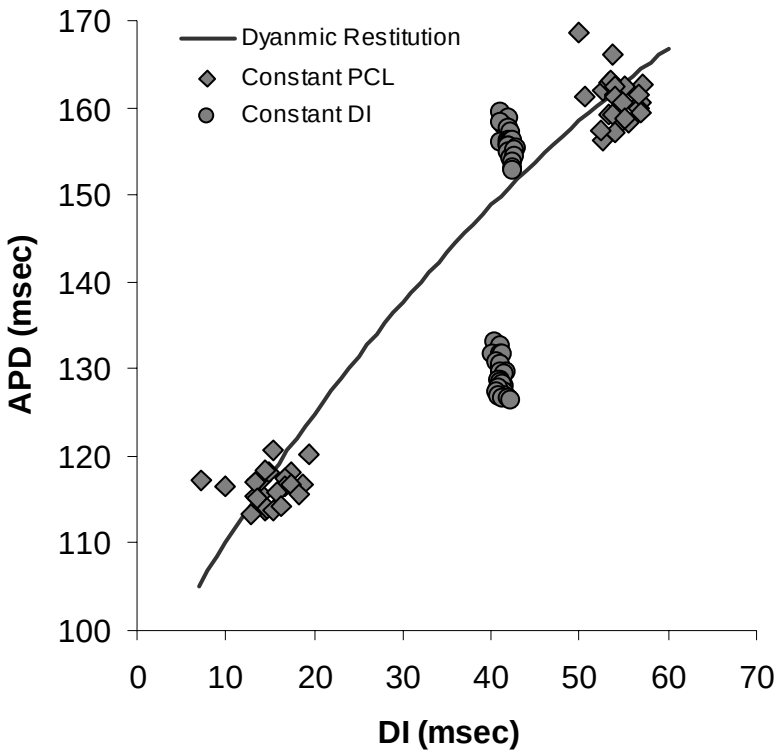

Figure 4.10 Two types of alternans under constant DI and PCL were plotted with dynamic restitution. The results of DI and APD for constant DI and constant PCL trials from same tissue were plotted in the restitution figure. In the figure, the diamond dots represent the result during constant PCL, and round dots represent the result during constant DI. The data for the dynamic restitution was also measured during the experiment and fitted to an exponent curve. The exponent curve was plotted in the same figure. The figure shows that the data for constant PCL trial are following the dynamic restitution relationship. But the alternans of APD during constant DI is unlikely to be explained by the restitution.

A beat by beat relationship between a DI and subsequent APD was computed as instantaneous slopes, equal to $\Delta APD/\Delta DI = (APD_n-APD_{n-1})/(DI_n-DI_{n-1})$. The function of instantaneous slope computed the ratio of the change in DI, $\Delta DI=DI_n-DI_{n-1}$, and the change in subsequent APD, $\Delta APD = APD_n-APD_{n-1}$. The ratio should be equal to the slope in the restitution relationship that was used to predict alternans. Instantaneous slopes for both constant DI and its equivalent constant PCL trials were calculated. As described before, the average activation cycle length during the constant DI pacing trial served as the PCL for the constant PCL trial. These trials resulted in comparable pacing rate. The instantaneous slopes calculated from five animals were pooled and plotted in a histogram form to illustrate the distribution of slopes. The instantaneous slope was computed from trials based on two conditions: i) a reasonable control of DI was achieved. Since the stimulation pulse width used in this experiment was 3 msec, the criterion for a reasonable DI control was set as the absolute beat to beat changes in DI were smaller than 3 msec, i.e. $|\Delta DI| = |DI_n-DI_{n-1}| < 3$ msec. and ii) a significant APD alternans was present. The threshold for a significant alternans was set to 4 msec, i.e. absolute beat to beat changes in APD, $|\Delta APD| = |APD_n-APD_{n-1}| > 4$ msec, which was identical to the threshold used recently by Pruvot et al[104].

Figure 4.11 show the histogram for the instantaneous slopes. The instantaneous slope during constant cycle length pacing concentrated in a narrow distribution with the mean±standard deviation of 1.07±0.4. In contrast, instantaneous slopes during constant DI pacing spread over a much wider range with the mean±standard deviation of 3.35±56.83. When computing the slopes for constant DI pacing trials, we found about 3% of beats have numerical zero change in $|\Delta DI|$. Because the sample rate was 10,000

samples per second, zero meant the DI change was smaller than 0.1 msec. This zero |ΔDI| change made the instantaneous slope infinite. The infinite slope was assigned to the value of maximal positive or negative finite instantaneous slope computed from the constant DI trials depending on the sign of change in APD. The extreme of finite slope was ± 263. That is, the change in APD corresponding to invariant or small range variant DI sequence was considerable larger. A larger maximal instant slope for constant DI trials than that for constant PCL pacing, 3.35 versus 1.07, was also observed in Figure 4.11. To show detail, Figure 4.11 presents the histograms in a range of slopes between -10 and 10.

A linear regression was used to fit a straight line to ΔAPD and ΔDI, i.e. the beat by beat changes in APD and DI. Results of the regression are shown in Figure 4.12. ΔDI and ΔAPD during constant PCL trials were fitted to the relation, $\Delta APD = 1.04 \times \Delta DI - 0.14$, with a r^2 value equal to 0.984. In contrast, the fit for data collected during constant DI pacing, $\Delta APD = 3.15 \times \Delta DI - 0.22$, had a much lower $r^2 = 0.162$. We also observed that 68 percent of data points in constant DI pacing fell in quadrants other than I and III. For the group data shown in Figure 4.12, although the average activation rate were similar between the two groups, the amplitude of alternans of APD was larger during constant cycle length than constant DI pacing, 32.2±12.3 verses 7.5±2.8 msec ($p<0.01$, t test).

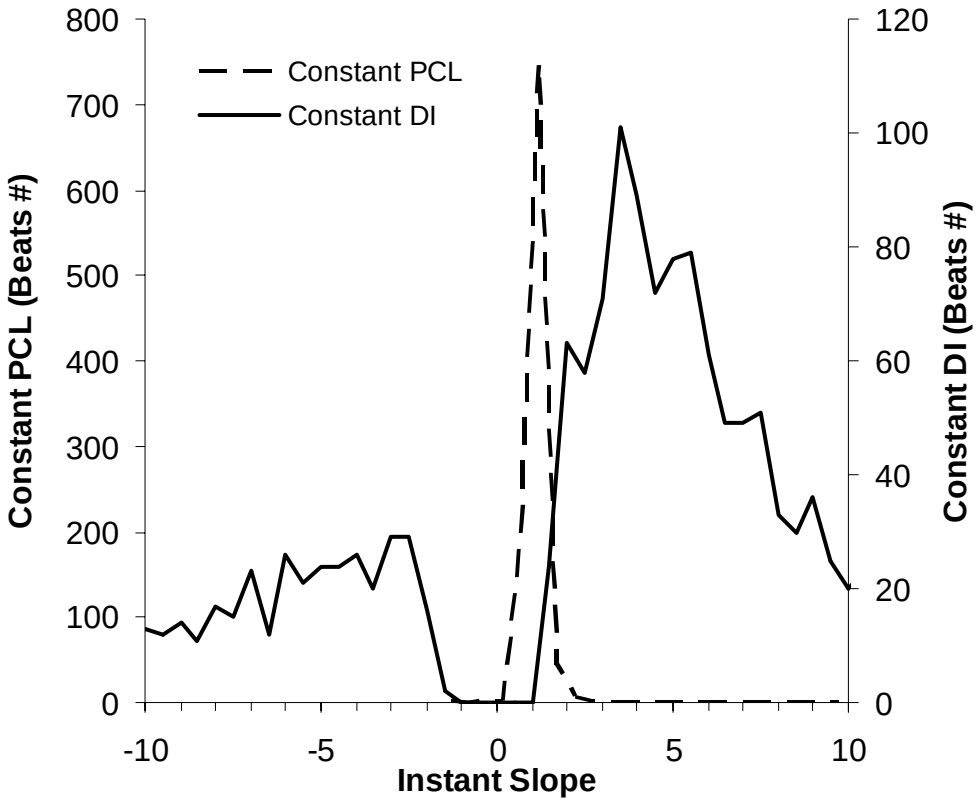

Figure 4.11 The beat counts of instant slope for the constant DI and PCL presented in a frequency distribution histogram. The instant slope that is equal to ΔAPD/ΔDI was computed for the constant DI and PCL trials from all animals. The counts for the instant slope between -10 to +10 are shown in the figure. But the instant slope for the constant DI is distributed to a much wider range (see text for detail). The maximum in the displayed range for the constant DI and PCL trials are at the instant slope of 3.35 and 1.07. Unlike the constant PCL trials, there is a large portion of instant slope for constant DI trials fell into the negative slope side.

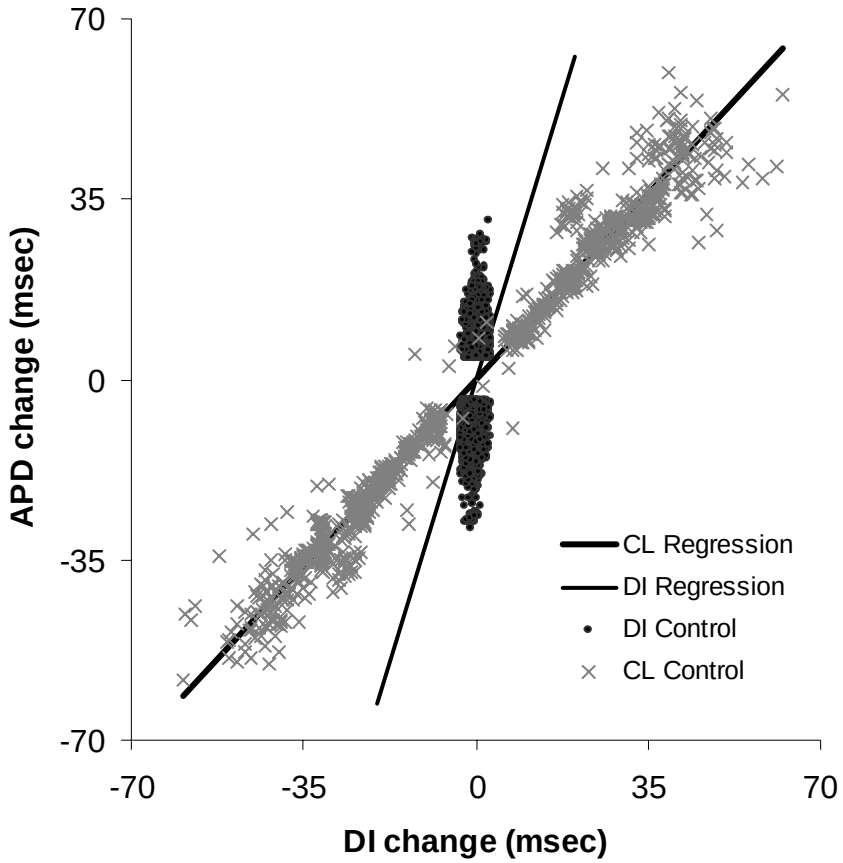

Figure 4.12 ΔDI vs. ΔAPD plot for constant DI and PCL and their linear regression. The beat by beat APD change (ΔAPD) and their preceding DI change (ΔDI) were calculated and plotted as X and Y axis in the figure. The dot represents the result during constant DI and cross represents the result during constant PCL trials. The linear regression was used to fit these data respectively. The fitting results were plotted as thin and thick line for constant PCL and DI pacing.

Beat by beat changes in DI and APD are shown in Figure 4.13 and Figure 4.14. Figure 4.13 show the trials with four different initial steady states in one animal (within animal case), and Figure 4.14 from four animals with same initial steady state (across animal case). In the within animal case, before the DI control protocol was started, the tissue was initially paced at a constant PCL for 10 minutes to achieve a steady state. The PCLs were equal to 200, 300, 400, and 600 msec. For PCL of 200 msec, some alternans may have occurred, but we still consider this as a steady state. At the end of each 10 minute pacing at constant cycle length, a pacing trial with constant DI was initiated. For the across animal case, the initial steady state was achieved by 10 minutes of constant PCL in all four animals at 600 msec. Then constant DI pacing was used in the same way as the within animal case. As Figure 4.13 and Figure 4.14 show, similar alternans behavior was observed within and across animal cases. The mean and standard deviation for the amplitude of APD alternans were 11.6±4.7 msec for the within animal case and 14.1±6.5 msec for the across animal case. There was no significant difference in the alternans for constant DI pacing with four different initial conditions for the within animal case.

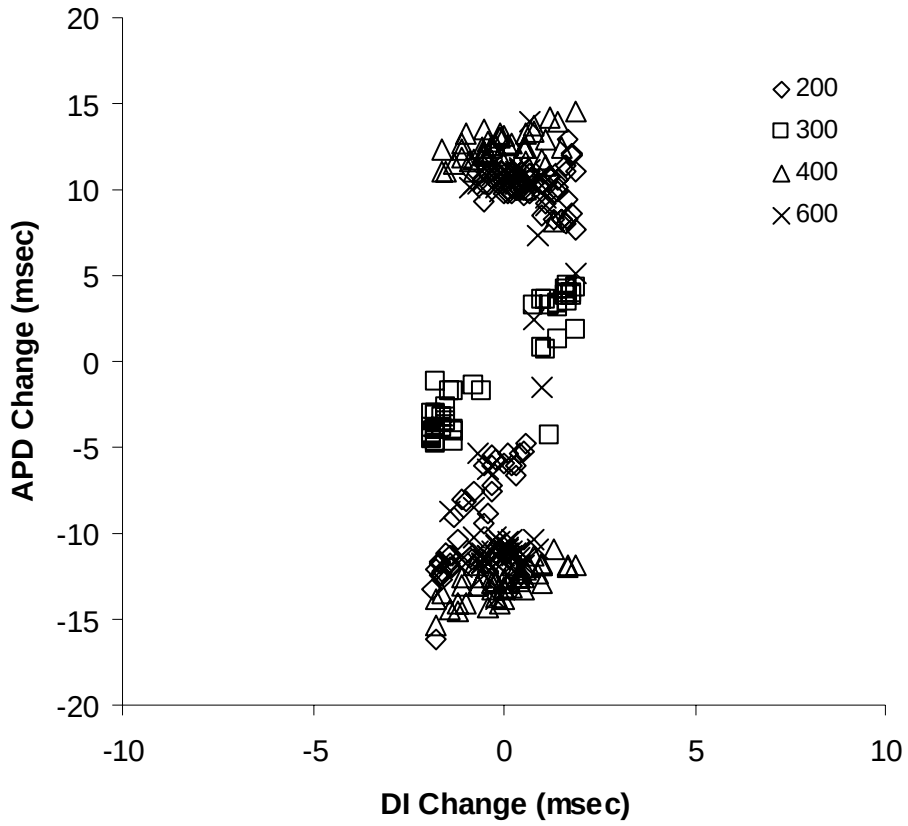

Figure 4.13 Constant DI activation with four initial conditions in one animal (within animal case). The initial steady states were achieved by pacing the tissue for 10 minutes at a PCL of 200, 300, 400, and 600 msec. The marker for this four states was shown in the legend. The numbers in the legend denote the cycle length for initial pacing. The beat by beat change in DIs and their following APDs were calculated and plotted as X and Y axis.

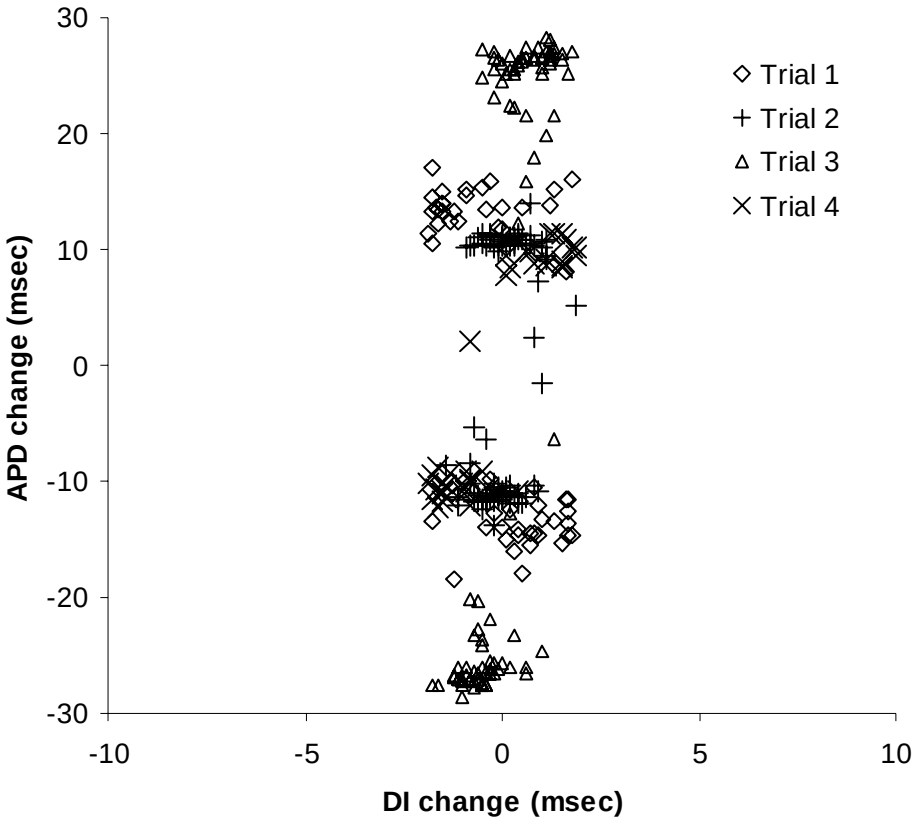

Figure 4.14 The result of constant DI pacing from four animals with same initial condition. The tissue for trial 1 to trial 4 was initialized at PCL = 600 msec. The markers for each trial were shown in the legend. Similar to **Figure 4.13**, the change in APD and its preceding DI were calculated and plotted as X and Y axis.

The constant DI with random perturbation pacing was used in four animals. One example trial is shown in Figure 4.15. The figure shows that DIs for the first and last 30 beats (pre and post random phase) were at the same constant value (33 msec). The designed value of DI in the constant DI phase is slightly different from the DI value achieved during the experiment. However, the target of control is to minimize the beat by beat variation in DI. In these trials, the mean±standard deviation of ΔDI was 0.0±0.7 and 0.0±0.8 msec during the pre and post phases. Although the variances of ΔDI, the beat by beat change in DI, were very small, the alternans of APD during the same phases were significant. The mean±standard deviation of |ΔAPD| during the pre and post random phases were 14.7±4.8 msec, and 10.5±3.4 msec. The mean of |ΔAPD| between pre and post random DI phases was significantly different ($p<0.01$, t test).

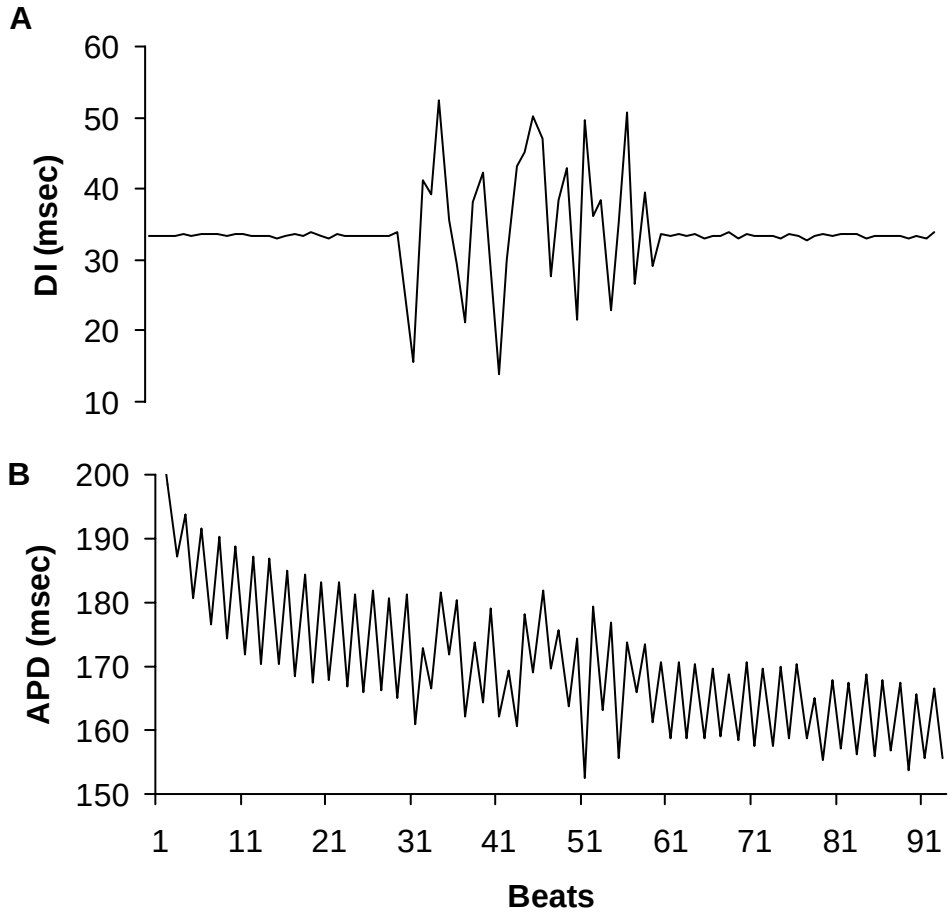

Figure 4.15 The result of APD during constant DI before and after random DI perturbation. As panel A showed, the DI sequence has three phases. In the first and third phase, the DIs are constant. In the second phase, the DIs were randomized to fit a uniform distribution. The resulting APDs were shown in panel B. The amplitude of APD alternans was smaller in the third phase than the first phase.

In two additional animals, the two-level DI sequence was used. As shown in Figure 4.16A, there were two constant DI values; the low DI level was in the range of 60±1 msec, and the high DI level was in 215±1 msec. Figure 4.16B showed the resulting APD. During two phases of lower DI pacing, the beat by beat APD alternans amplitude was clearly larger than 5 msec. In contrast, during the phase of high DI level, after subtracting the baseline drift of APD, |ΔAPD| was less than 2 msec except the overshooting at the first beat.

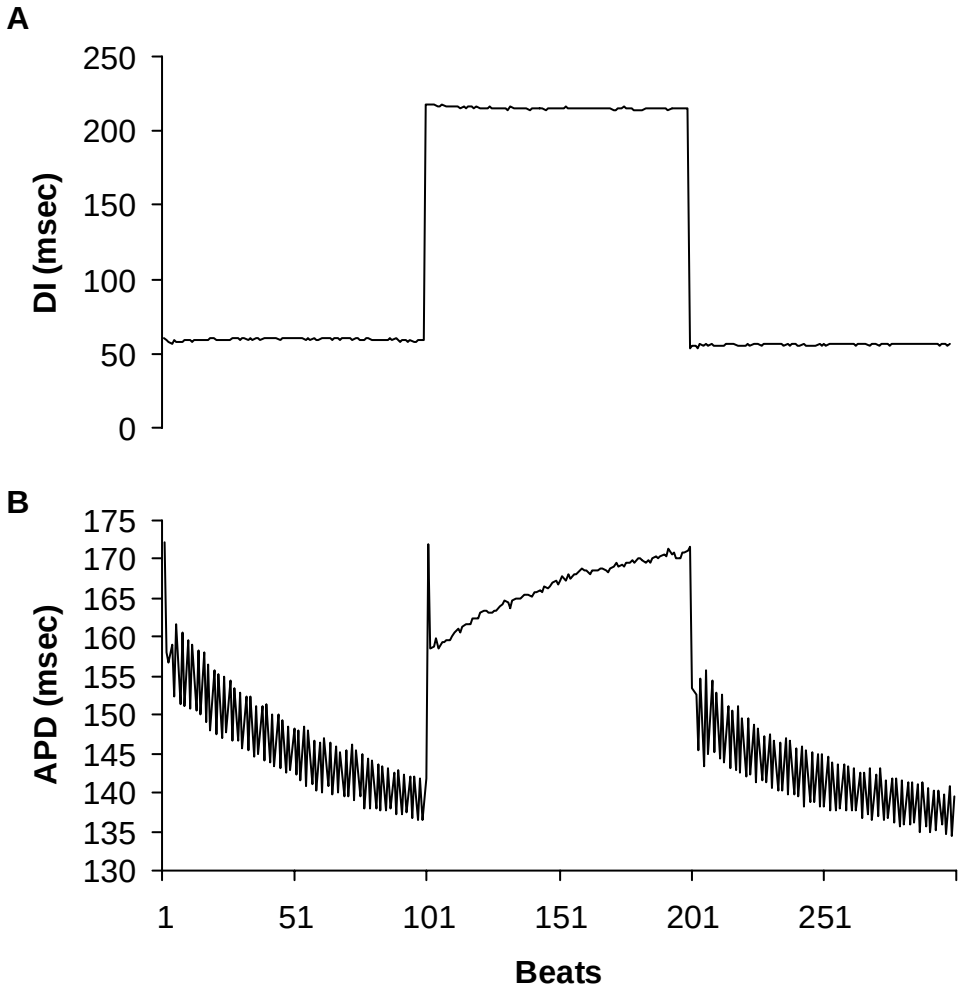

Figure 4.16 Two-level constant DI sequence. A) The DIs were held at a pattern of low-high-low fashion. B) Their following APDs show alternans at low level of DI, but do not have at high level of DI.

4.4 Calcium dynamics and potassium current influence in hysteresis: Simulation results using LRD

To investigate the factors that affect the hysteresis in the restitution of APD, we used computational model LRD to study the calcium and potassium membrane currents and intracellular calcium cycling. Figure 4.17 demonstrates the effects of scaling potassium/calcium currents on hysteresis when the center DI of 400 msec sequence was used. For clarity, restitution curves for the largest and smallest scaling factors are shown in the figure, e.g. the restitution curves for two extreme scaling factors, 0.2 and 1.5 for I_{kr} are represented by the thin and thick line in Figure 4.17A. The perturbation of membrane currents or the other model parameters causes baseline shift of APD at the same DI level. For example, a decrease or increase of I_{kr} resulted in prolongation or shortening of the APD level. To account for this shift, the restitution curves were moved vertically in Figure 4.17. The amount of offset was determined by the difference of APD at the start point of the curve or center DI = 400 msec in the figure. All of curves were aligned with the APD at the center DI that resulted from the nominal value of the model parameters. The numbers in the legend are the offset values. For example, Figure 4.17A shows the restitution curve with blockage of I_{kr} for center DI of 400 msec by the thin line. The APD at the start of the DI sequence was about 20 msec longer than the APD at the start of the sequence when the scale factor for I_{kr} was equal to 1. An offset of -20 msec is noted in the legend. Similarly, when I_{kr} was increased, an offset of +10 msec was added to the initial value of APD to match to the nominal APD. Figure 4.17A and B show that the increase of I_{kr} and I_{ks} decreased the APDs as well as the overall tilt of hysteresis loop, i.e. the loop looks flatter. But I_{kr} and I_{ks} perturbation change loop thickness in different

direction. Increasing I_{kr} led to a larger thickness. On the contrary, increasing I_{ks} decreased the thickness. Blocking I_{CaL} made the loop thin and flat, which is shown in Figure 4.17C. *Iupbar* had minimal effects on hysteresis as shown in Figure 4.17D. The major effect of *Tautr* was on the increasing DI limb. As Figure 4.17E showed, during increasing DI limb, the APDs became relatively larger when the *Tautr* was smaller, i.e. the transfer rate was faster.

Figure 4.18 and Figure 4.19 show the data for the MaxDelay and loop thickness at different membrane current scales and model parameters. The results from center DI =400 msec and 150 msec are presented by using square and triangle mark. Figure 4.18A and B show that with increasing I_{kr} during the center DI = 400 msec, MaxDelay increased from 2 to 7 beats, the thickness of the loop increased from 4.6 to 7.4 msec. The MaxDelay and Thickness of loop increased almost linearly with increasing I_{kr}. Both center DIs of 400 and 150 msec trials showed pronounced change in MaxDelay and Thickness of the hysteresis loop. The change in loop thickness and MaxDelay were very similar for faster changes in DI and slower and faster rates of activation. Figure 4.18C and D show effects of perturbing I_{ks}. In contrast to I_{kr}, increasing I_{ks} decreased MaxDelay and Thickness of loop. Although reduction of I_{ks} increased MaxDelay and Thickness of loop, it also increased the overall tilt of the restitution as shown in Figure 4.17B. The MinDelay was small for all conditions that were explored, it was 0 beats for center DI of 150 msec, and 1 beat for center DI of 400 msec, except for minimal I_{ks} when it was 2 beats. There were no changes in MinDelay as a result of changes in model parameters, and the only change was of 1 beat at the smallest I_{ks}.

Increasing L-type Ca current increased loop thickness during both 400 and 150 msec central DI sequences (Figure 4.18F). However, increasing I_{CaL} decreased MaxDelay during 400 msec central DI, while MaxDelay was unchanged during 150 msec central DI trial (Figure 4.18E). As observed for the potassium currents, I_{CaL} had minimal effects on MinDelay.

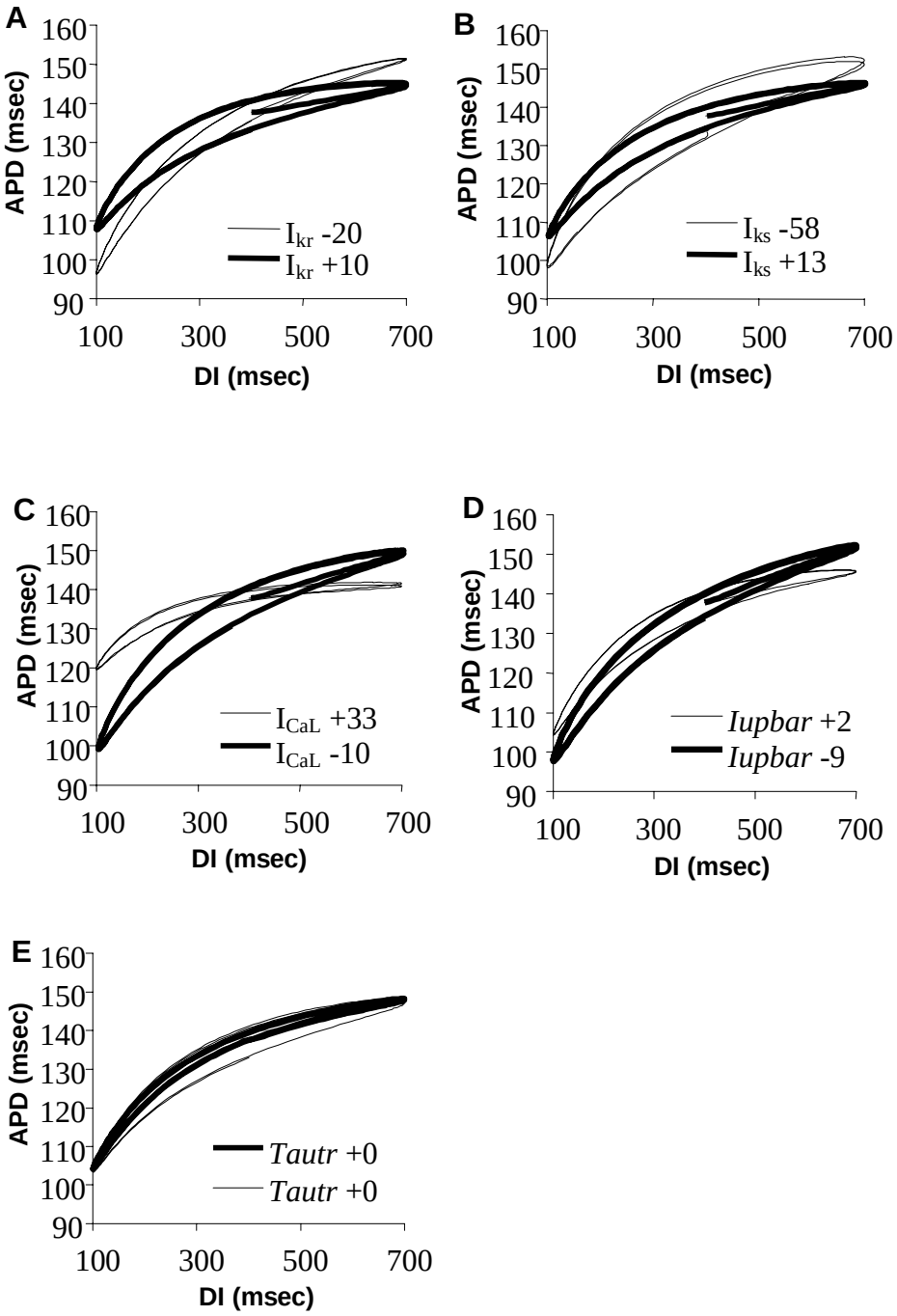

Figure 4.17 Factors affected hysteresis in restitution. This is the simulation result of the hysteresis loops from LRD model. The DIs were oscillated following a sinusoidal function as shown in **Figure 3.3**. The resulting APD and DI were plotted in A, B, C, D, and E for perturbing I_{kr}, I_{ks}, I_{CaL}, *Iupbar* and *Tautr*. For clarity

of presentation, only the results of minimal and maximal scale factors or parameters are shown by using the thin and thick lines. Exceptionally, for *Tautr*, because of the reciprocal relationship to the transfer rate, the thick line represents a smaller *Tautr* value, but a larger transfer rate. The legend indicates the currents or parameters that were perturbed during the simulation trials. In order to compare the hysteresis loop at the same level of APD, the result of APD was add an offset to move the loop up or down to the APD level that resulted from nominal currents and parameters trial, i.e. control trial. The offset value are shown in the legend, e.g. the 'I_{kr} -20' after thin line in the legend of panel A, represents when I_{kr} was multiplied by the scale factor 0.2, 20 milliseconds was subtracted from the APD of every beat, i.e. the hysteresis loop was shifted downward vertically for 20 msec. On the contrary, the 'I_{kr} +10' means the hysteresis loop was move upward for 10 msec when the I_{kr} was multiplied by the factor 1.5. Especially, the loops for the *Tautr* trials were not moved. Therefore, '+0' is displayed in the legend of panel E.

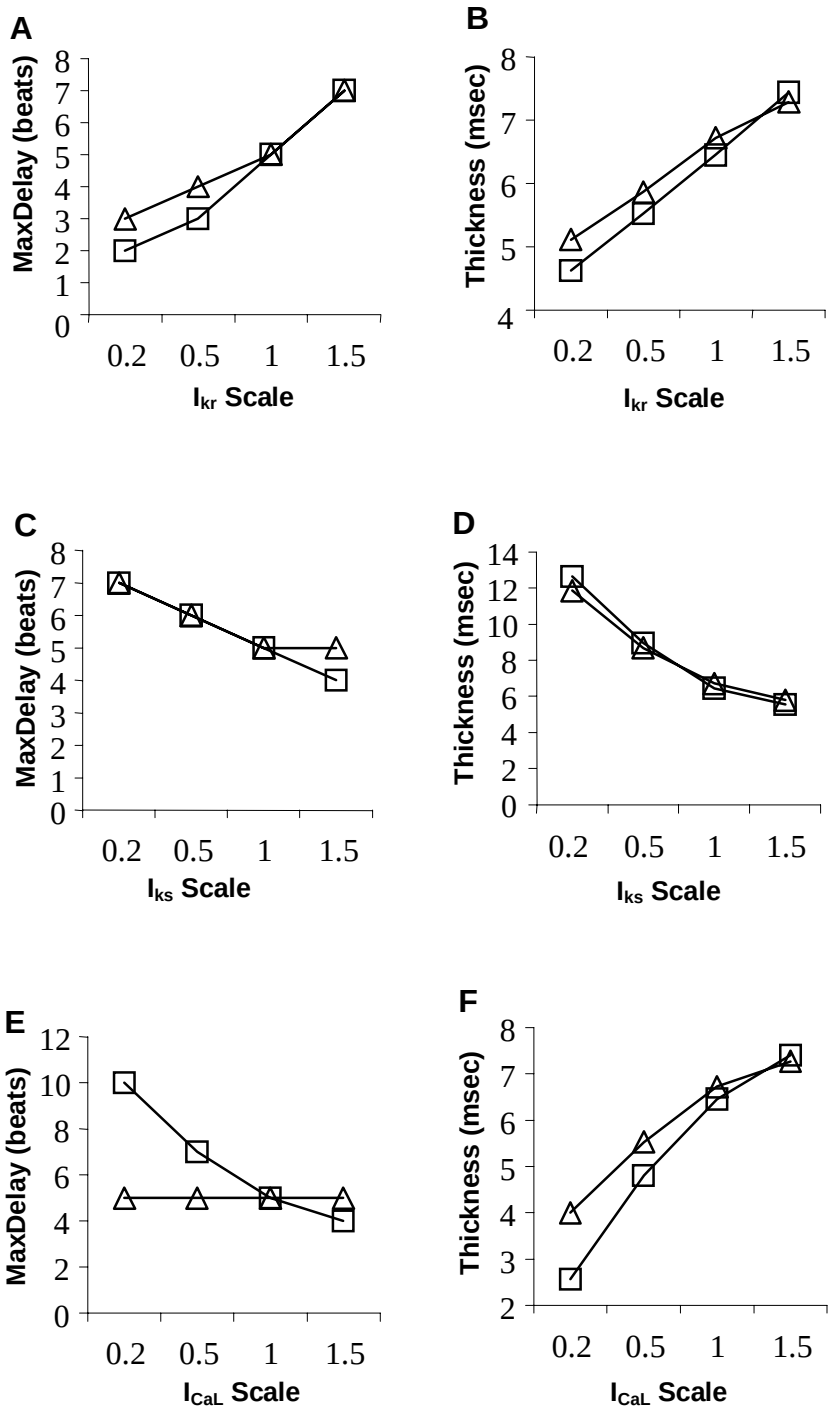

Figure 4.18 MaxDelay and Thickness for membrane current perturbation during simulation using LRD model. The measurement of hysteresis, MaxDelay and Thickness of hysteresis loop are shown for each current at the

scale factors of 0.2, 0.5, 1, and 1.5. The panel A and B present the results for I_{kr}, the C and D show the results for I_{ks}, and the E and F depict the results for I_{CaL}. The square marker represents the results for the oscillatory DI sequence at central DI =400 msec and the triangle marker represents the results for central DI =150 msec.

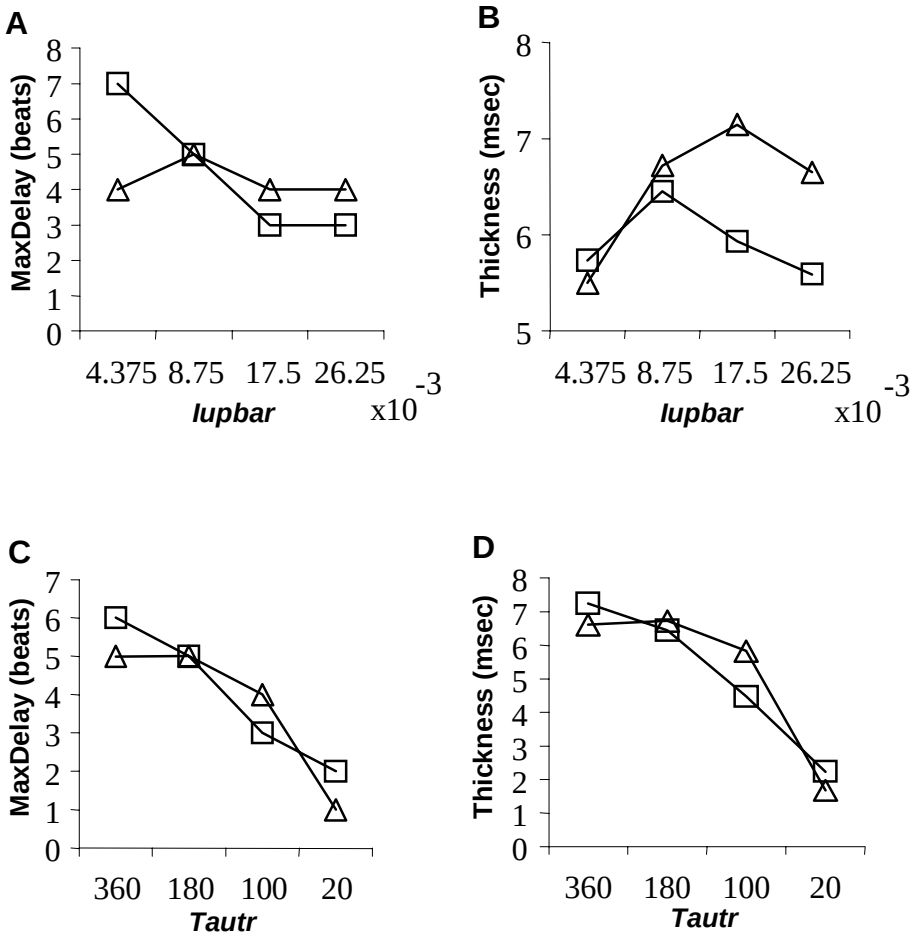

Figure 4.19 MaxDelay and Thickness for *lupbar* and *Tautr* perturbation during simulation using LRD. The measurement of hysteresis parameters, MaxDelay and Thickness of hysteresis loop are shown in the figure with the parameter value used during simulation as the X axis. Similar to **Figure 4.18**, the square and triangle markers represent the result during the simulation using central DI = 400 and 150 msec sequence.

The *Iupbar* was given four values, 0.004375, 0.00875, 0.0175, and 0.02625 to decrease and increase the rate of uptake of calcium into the SR (nominal value in LRD model is 0.00875). Therefore, when *Iupbar* was = 0.02625, the rate of calcium uptake from the cytosol into SR was three times larger than that at the nominal *Iupbar* value. Figure 4.19A and B show that the decrease in *Iupbar* increased MaxDelay for center DI = 400 msec, but had little effect during 150 msec center DI, similar to that observed for I_{CaL}. Increase in *Iupbar* further than 0.0175 had no effect on MaxDelay. The Thickness of loop was largest at the nominal value of *Iupbar* for center DI of 400 msec, and for *Iupbar* of 0.0175 for center DI of 150 msec. The loop thickness decreased for both further decrease and increase in *Iupbar*.

Tautr was varied from its nominal value of 180 to 20, 100, and 360 to determine the effects of calcium transport from NSR to JSR. Because of the reciprocal relationship, an increase in *Tautr* from 180 to 360 indicated that the transfer rate is 0.5 times of the nominal rate in this model. Figure 4.19C and D show that both MaxDelay and Thickness of loop increased as *Tautr* was increased or rate of transfer slowed down.

The intracellular Ca movement was recorded during a trial with center DI = 400 msec and nominal values of currents and rates of transport. The results are shown in Figure 4.20. I_{CaL} was integrated during each activation to estimate Ca ion influx for that action potential. Because of the definition of positive ionic movement direction during the simulation, the integrated I_{CaL} has negative value. More negative integrated I_{CaL} means more positive charge to the membrane. Similarly, the maximal concentrations of Ca in JSR and NSR during each activation were recorded. The result of integrated I_{CaL},

and maximal Ca concentration in JSR and NSR are plotted in Figure 4.20B, C and D. Figure 4.20B shows that, at the same DI level pointed by arrows, Ca influx was larger during DI decreasing phase than that during DI increasing phase. When we increased scale factor to I_{CaL}, a larger calcium transient was observed with augmented asymmetric behavior. The differences of integrated I_{CaL} at DI = 400 msec between increasing and decreasing DI phases were 7.6 for minimal I_{CaL} scale, and 89.36 uA/uF for maximal I_{CaL} scale.

Figure 4.20C and D show that changes of Ca concentration in the JSR and NSR. The changing speed of Ca concentration in JSR and NSR are asymmetric between decreasing and increasing phases of DI. The time when NSR achieved the maximal concentration was slightly later than that when DI achieved the minimal value. The speed of increase of Ca concentration in JSR was faster during increasing DI phase than that during decreasing DI phase. When *Tautr* was decreased from 360 to 20, the Ca transfer rate from NSR to JSR was increased eight fold. It resulted in during the sinusoidal DI sequence the amplitude of NSR change decreased from 1.97 to 0.09 mM. When *Iupbar* increased from 0.004375 to 0.02625, the concentration of Ca in NSR at the longest DI (700msec) increased from 1.7 to 3.55 mM. The difference in the integrated I_{CaL} at the same DI = 400 msec between decreasing and increasing DI phases reached the highest level equal to 65.4. When *Iupbar* was at the nominal value, this difference decreased for both increasing and decreasing *Iupbar*.

The results of simulation are summarized in Table 4.1. At central DI = 400 msec, increasing I_{kr} increased MaxDelay and Thickness of hysteresis loop. On the contrary, increasing I_{ks} decreased MaxDelay and loop Thickness. Augmentation of I_{CaL} made

MaxDelay smaller but thickness of loop larger. Decreasing *Tautr*, i.e. increasing transfer rate, decreased both MaxDelay and thickness. The effects of *Iupbar* were similar to *Tautr* except there was a maximal value of thickness when *Iupbar* was increasing. The results for central DI = 150 msec were similar to that for central DI = 400 msec except that the perturbation of I_{CaL} had minimal effect on MaxDelay.

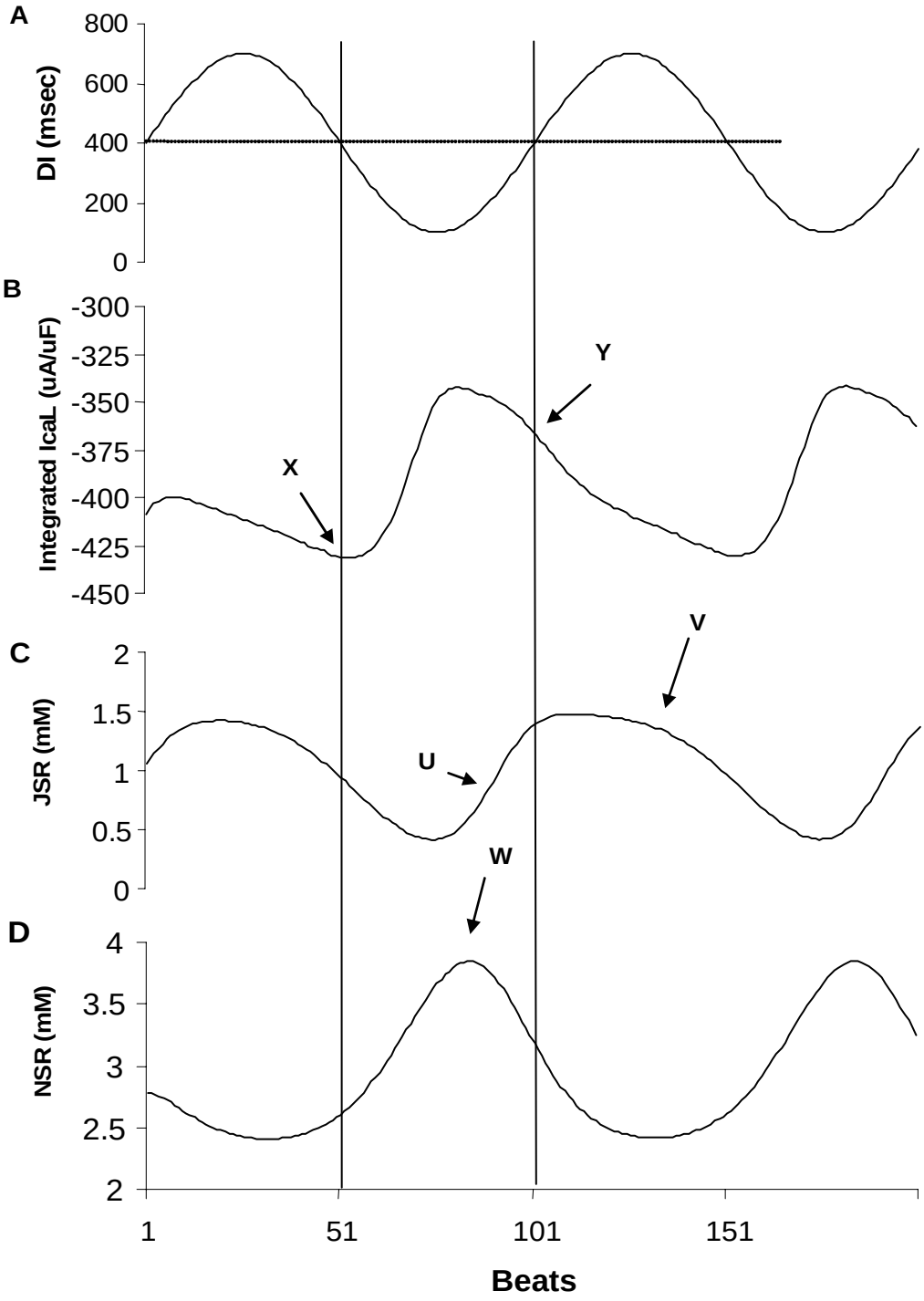

Figure 4.20 Intracellular Ca dynamics during sinusoidal DI in LRD model. The oscillatory DI sequence is shown in the panel A. The I_{CaL} was integrated for

every beat. The result of integrated I_{CaL} is plotted in the panel B and aligned with the DI in panel A. The arrow X and Y indicated the beats where their DIs are the same, but with decreasing and increasing DI activation history. There is more positive charge to the membrane at the position pointed by X than the position pointed by Y. Therefore, APD is longer at X than at Y. The maximal Ca concentration for each beat in JSR and NSR are plotted in the panel C and D and also aligned with the DI. The Ca level increased faster during the phase pointed by arrow U than the phase pointed by V. The arrow W in the panel D indicates a rise of Ca in NSR during the fast pacing phase and then a decline when the DI increased.

Table 4.1 Results of MaxDelay and Thickness of hysteresis loop

	Trials	Parameter	MaxDelay (beats)	Percent change of MaxDelay (%)	Loop Thickness (msec)	Percent change in Thickness (%)
Central DI = 400 msec	I_{kr}	0.2	2	-60	4.62	-28.37
		1.5	7	40	7.44	15.35
	I_{ks}	0.2	7	40	12.63	95.81
		1.5	4	-20	5.54	-14.11
	I_{CaL}	0.2	10	100	2.56	-60.31
		1.5	4	-20	7.40	14.73
	Iupbar	0.004375	7	40	5.73	-11.16
		0.02625	3	-40	5.59	-13.33
	Tautr	360	6	20	7.25	12.40
		20	2	-60	2.24	-65.27
Central DI = 150 msec	I_{kr}	0.2	3	-40	5.11	-23.96
		1.5	7	40	7.29	8.48
	I_{ks}	0.2	7	40	11.85	76.34
		1.5	5	0	5.79	-13.84
	I_{CaL}	0.2	5	0	4.00	-40.48
		1.5	5	0	7.27	8.18
	Iupbar	0.004375	4	-20	5.5	-18.15
		0.02625	4	-20	6.65	-1.04
	Tautr	360	5	0	6.66	-0.89
		20	1	-80	1.67	-75.15

4.5 Hysteresis and alternans: Simulation using CVM model

The CVM is a computational model with special consideration on I_{CaL} to modeling the persistent alternans phenomenon. Similar to the trials in the LRD model, several membrane currents were perturbed to investigate their effects on alternans threshold. The results were listed in Table 4.2. These results showed that increase of I_{kr} decreased hysteresis thickness and delay, and alternans threshold was decreased. Increase of I_{CaL} decreased hysteresis thickness and delay, but alternans threshold was higher. An increase of I_{to} increased hysteresis thickness and delay, but alternans threshold decreased for the increase and decrease of I_{to}. In CVM, I_{ks} has minimal effects on hysteresis and alternans threshold, for it is about 50 times smaller than I_{kr}.

Comparing the results from the LRD model, the I_{ks} in CVM has minimal effect on MaxDelay and Thickness. Interestingly, The I_{kr} has contrast effects on MaxDelay and thickness, compared with that of the LRD model. The results of boosting I_{CaL} decreased the MaxDelay in both LRD and CVM. But thickness decreased for CVM while for LRD thickness increased.

During a constant PCL pacing, the alternans of APD was observed at a short enough PCL. However, the constant DI pacing did not trigger any persistent alternans of APD, which is consistent with the results by Jordan and Christini[122, 123] who used our protocol to control DI to eliminate alternans. However, our experimental results clearly demonstrated that the alternans of APD occurred during constant DI pacing. Therefore, the CVM model does not replicate canine ventricular electrophysiology that relates to alternans behavior.

Table 4.2 Hysteresis characteristics and alternans threshold in CVM

	Scale	Thickness (msec)	Max Delay (beats)	Alternans threshold (msec)
Control		9.71	9	205
Ito	0.5	7.35	8	175
	1.5	28.5	12	<150
Ikr	0.5	10.1	10	220
	1.5	9.51	9	<150
Iks	0.5	9.9	9	205
IcaL	0.5	9.2	12	<150
	1.5	6.3	8	230

Chapter 5 Discussion

5.1 Hysteresis in restitution of APD

During sequential activation by DI control pacing, our results demonstrate that the restitution relationship has multi-modal behavior. We refer this type of behavior as 1:1 hysteresis in the restitution, or hysteresis. The hysteresis provides an antiarrhythmic mechanism that is not necessarily dependent on the slope of restitution. In Figure 5.1, we illustrate this mechanism graphically. When a premature stimulus produces a perturbation to the system, the DI is shortened from operating point of 'X' to point of asterisk as shown in the figure. According to the classical restitution, the dynamics of APD would be predicted by a uni-modal restitution function. If this uni-modal restitution can be presented by 'function 1' in the figure, the iteration of APDs will follow the points marked by 1, 2, 3, 4, and 5 in the figure. It shows that the amplitude of alternans increase when the hysteresis is absent. However, our results indicate that APD dynamics possess hysteresis characteristic, i.e. the APDs are smaller with a shorter DI pacing history than those with a longer DI pacing history. Then with the contribution of hysteresis, the above iteration after point 2 will switch to point A, B, C, and D. Because hysteresis effects contributed from the short APD at point 1 diminished the response of APD at point A, the resulting APD will be smaller than that expected by the restitution relationship - 'function 1'. The iteration of A, B, C, and D show a complex pattern of APD and DI around operation point 'X'. But the amplitudes of these changes became smaller than those without hysteresis. Even with the slope of restitution >1, hysteresis is still able to prevent

evolution of APDs from unstable alternans triggered by one premature perturbation. This interpretation suggests cardiac memory tends to buffer the alternans via a hysteresis mechanism. These results provide a mechanistic explanation for the prediction in a study by Chialvo and colleagues[124], which was one of the first to demonstrate that memory suppressed complex dynamics by flattening restitution. However, our results show how memory can buffer instability independently (to some extent) of slope of restitution.

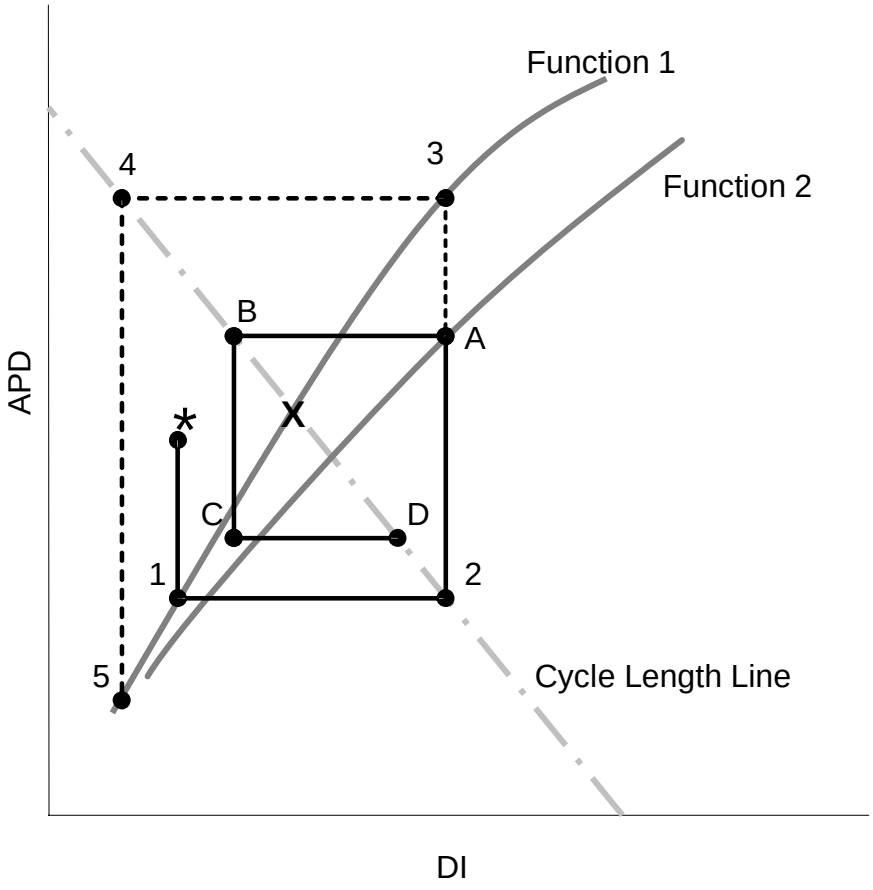

Figure 5.1 Hysteresis as a mechanism for buffering alternans. The function 1 and 2 represent the restitution relationship which gives the APD relating its preceding DI. When a premature contraction (asterisk) occurred, DI was shorter

than the previous beat, which led to APD at 'point 1'. The memory of the premature contraction caused restitution curve flattening that was depicted as 'Function 2'. The 'Function 2' has shorter APDs than 'Function 1' given the same DIs. The amplitude of alternans was dampened.

The transient dynamics of APD possess monotonic and non-monotonic components. Consistent with the observations of Elharrar et al[125] and Watanabe et al[95], results in Figure 4.6 demonstrated a bi-component change in APDs, i.e. a sinusoidal pattern of oscillatory APD change was overlaid on the top of a monotonic decrease in APD. A phenomenon that indirectly is similar to hysteresis in restitution was previously reported by Elharrar et al[125]. They abruptly changed CL between 500 to 1500 msec. When CL increased from 500 to 1500 msec, the APDs increased relatively slowly with more distributed over successive beats, and reached a steady state in about 50 beats. Compared with CL increase trial, the decrease of CL from 1500 to 500 msec made APDs descend more rapidly in the first premature beat, distribute less over successive beats, and reach a steady state in 20 beats. These accommodation phenomena suggest that high order factors, i.e. cardiac memory, are also an important contributor in APD dynamics.

The cardiac memory is considered as contributions from all of previous DIs and APDs to the current APD. A type of memory model computed these factors as accumulation and dissipation during depolarization and repolarization phases[94, 96, 126-128]. According to this type of memory model, an APD following a long APD would be longer than that predicted by preceding DI, and vice versa[71, 125]. We believe that differences in

the rates of change in APD during increasing and decreasing phases of DI are due to the cardiac memory. Beger[129] used an auto-regressive and moving average memory model to demonstrated hysteresis loop, which included the DIs and APDs from several prior beats. If the hysteresis is indeed due to memory, the effect of memory must be very strong that the increase in APD was continual for several beats even after DIs have started decreasing. Because the asymmetric delay (Figure 4.2 line M, N, and P, Q), our results suggest that the memory effect is more pronounced when the DIs and APDs are increasing than when they are decreasing.

We further explored the memory model in a random pacing protocol. In this protocol, the changes in preceding DIs are least correlated with succeeding DIs. Due to the accumulation and dissipation kinetics of the memory model, the resulting restitution relationship should have maximal possible activation history background, which minimizes the effects of special cumulative memory, which was confirmed in study by Choi, et al[58]. Under this assumption, the resulting relationship between DI and APD (Figure 4.8) was a cluster of points with overall slope less than 1. Compared with standard and dynamic restitution, the restitution relationship quantified by using linear and sequential change in DIs (Figure 4.7) also resulted in a shallower curve. It is notable that the cluster from random DI activation and trajectory from linear sequential DI pacing was overlaid on each other.

Hall et al[94], and Yehia et al[130] also demonstrated a hysteresis type of APD dynamics in bullfrog cardiac muscle and isolated rabbit ventricular cells. These studies showed PCL was shorter at the moment when the APD switches from 1:1 to 2:1 response than that at the switch from 2:1 to 1:1 response, which demonstrated hysteresis. Walker, et

al[100] also reported that 2:2 response, occurred at a faster rate, but persisted at a slower rate, i.e. once the alternans is started, we will need a longer PCL to get rid of the alternans than the PCL that started it. In our study, however, the hysteresis in restitution is a phenomenon that delayed change in APDs responds to the change in DIs. We demonstrated the hysteresis completely in 1:1 activation. Yehia et al[130] derived a finite-difference equation to predict stability and 1:1 to 2:1 transition, which was still based on restitution. On the contrary, our results suggest that low dimension restitution dynamics is unlikely to adequately describe activation dynamics during 1:1 and 2:2 response. Banville and Gray[76] further showed that there was no direct link between restitution relationship and activation dynamics in intact perfused hearts. Recently studies by Tolkacheva et al[98, 99] and Kalb et al[108] proposed a restitution portrait as a criterion to assess the dynamics of restitution. However, those studies used the memory models that only included the effects from one prior beat, while our results indicated the memory effects lasted much longer. Then the new criterion proposed in those studies may need to be re-evaluated.

We used the LRD model to investigate the underlying ionic mechanism of hysteresis phenomenon. The dramatic effects of *Tautr* and *Iupbar* on loop thickness suggest that the Ca storage in SR and cytosol plays an important role in the hysteresis behavior. Figure 4.20D indicates that at high activation rate, Ca is retained in NSR. This accumulation in NSR raises the potential energy for diffusing Ca into JSR and resists reuptake of Ca from cytosol. This delay phenomenon could be boosted by slowing down the transfer rate, which made Ca in JSR refill much faster during increasing DI phase. Then there is more Ca in JSR released during calcium induced calcium release. The released Ca is to close the I_{CaL} channel. Therefore, the process of speeding up transfer rate cause less Ca into

JSR during increasing DI phase, which increased APD. The hysteresis loops in Figure 4.17E show that with decreased *Tautr*, the decrease of loop thickness was almost exclusively in the increase of the lower limb during the increasing DI phase. Consistent with this view, the influx through I_{CaL} showed asymmetric throughput during decreasing and increasing DI phase in Figure 4.20B. Changes in *Iupbar* produced non-monotonic, but small changes in loop delay. Increasing *Iupbar* would increase Ca uptake from cytosol to the NSR. When the transfer rate from NSR to JSR was unchanged, increased uptake resulted in accumulation of Ca. Increased *Iupbar* caused a larger accumulation of Ca in NSR, which would increase the driving force for transfer of Ca into the JSR, which was similar to that seen when *Tautr* was decreased. Reducing *Iupbar*, on the other hand, decreased rate of removal of Ca from cytosol. This decreased rate left more intracellular Ca that raised APD for lower limb during increasing DI phase.

On the one hand, the delay or fluctuation of intracellular Ca cycling in SR plays an important role on action potential and hysteresis. On the other hand, the hysteresis can be modified by perturbing the membrane current channels too. For example, Figure 4.18A and B show hysteresis were augmented with increasing I_{kr}, which may be a viable approach to suppressing electrical alternans[121] even though it may have a slight steeper slope of restitution shown in a simulation study[120]. We observed blockage of I_{ks} decreased the influx of potassium, which increased the calcium current and asymmetry of the integrated calcium current. The asymmetric integrated calcium current during decrease and increase of DI phase caused the hysteresis phenomenon. However, our simulation results using two computational models did not generate consistent results when I_{kr} and I_{CaL} were changed. We consider this difference may be caused by the

model's differences and incompletion. The LRD model is based on guinea pig data, while the CVM is based on canine. Furthermore, both of these models failed to replicate the alternans of APD during constant DI pacing that we observed experimentally. It implies that the electrophysiological mechanism responsible for the alternans in experiment is absent in these models.

5.2 Two components in the mechanism of alternans

We hypothesized that the slope of restitution, or DI dependent restitution, is only one of the contributors to the genesis of alternans. Because DIs preceding the long and short APDs were virtually identical in Figure 4.1A, it is unlikely that the slope of restitution is adequate to address this type of alternans. The substrate for this type of alternans provides a explanation for the lack of correlation between slope of restitution and alternans observed in recent studies[70, 97, 104, 131]. Given that APDs are changing (alternans) while preceding DIs are not, it is not surprising that correlation between slope of restitution and alternans is found to be weak.

We proposed that there are two components in the mechanism of alternans: DI dependent and DI independent. A critical question in this situation is whether or not the alternans of DI is causally linked to alternans of APD? The slope of restitution presumes that oscillatory change of DI triggers alternans of APD. Our results, however, show that alternans of APD occurs during constant DI pacing (Figure 4.9). In this scenario, DI dependent restitution is unlikely to contribute to alternans, and the DI independent component plays a major role in the genesis of alternans. The emphasis on DI independent component does not challenge the existence of DI dependent restitution.

Actually, during the constant PCL pacing, our results demonstrated that a change in DI is associated with a parallel change in APD (Figure 4.10). This change in APD is both the result and cause of change in DI. Our works separate the DI independent component from DI dependent restitution. Larger amplitude of alternans was observed during constant PCL pacing, compared with constant DI pacing (Figure 4.12). This observation supports our hypothesis that there are two components in the mechanism of alternans. The difference in the amplitudes of alternans between constant PCL and DI pacing provides an estimate of the relative contributions of DI independent and DI dependent mechanisms.

It is important to control the beat by beat changes in DI in our study, although the exact value of DI that was achieved was not very critical. Ideally, DIs would be identical for all beats. However, numerically identical control of DI for beat after beat is very difficult to achieve in practice. Nonetheless, very small variation in changes in DIs was achieved. In order to determine whether this small beat by beat change in DI could be responsible for alternans of APD during constant DI pacing, the instantaneous slopes were computed (Figure 4.11). If alternans was indeed produced by change in DI via restitution, then slope of restitution relationship near this operating point would be equal to the instantaneous slope. Similar to the slopes observed during VF[97], a large number of negative slopes were observed, i.e. changes in APD and DI were in opposite direction. The negative slope indicates that this alternans could not have been caused by DI dependent restitution. When the slopes were positive, most of them were larger than 3, which was much larger than the restitution slope quantified by the dynamic restitution protocol[87] or any experimental protocol. Especially when these instantaneous slopes were calculated sequentially, slopes of restitution relationship should be much flatter[111].

Therefore, the DI independent component may play a more fundamental role for the alternans during constant DI pacing than the DI dependent restitution.

The finding that alternans occurs independently of DI restitution is consistent with the results by Saitoh et al[132]. Saitoh et al used interpolated beats to make two successive beats to have the same preceding DI. Their results show that alternans could not be suppressed in ventricular tissue with same preceding DI. In our study, the explicit control of DI allows us to demonstrate behavior of APD alternans independent of changes in DIs directly. Action potential (AP) clamp was used in an alternans study by Chudin, et al[101]. In their study, the membrane potentials were driven by an identical AP for every beats. But the intracellular Ca transient showed alternative change, without membrane potential alternans. In our study, the cells decided the time course of repolarization at given controlled resting time interval. Because AP clamp forces an AP on the cell, it is unable to explore the intrinsic electrophysiological mechanism of alternans. Since the non-voltage-gated ion mechanism also influence wavebreak[106], the feedback protocol provided a unique way to investigate intrinsic alternans, which could not be provided by any other contemporary protocols.

It is likely that calcium handling mechanisms[103, 104, 133] are responsible for DI independent component. But once alternans start during constant PCL pacing, effects of restitution dependent and independent mechanisms are not mutually excluded[106, 134]. Recent studies show potassium currents are important contributor to restitution[115, 135, 136] and short-term memory[120, 121]. In our protocol, DI dependent components, such as potassium are minimized. Then contribution from DI independent components, such as SR Ca content fluctuation[103], is manifested. Therefore, the DI control approaches will

help to solve the puzzle brought about by the interaction of DI restitution and DI independent component.

Cardiac memory has been considered an important factor in the mechanism of alternans[58, 94, 96, 99, 131]. As discussed above, memory can be constructed as accumulation and dissipation during depolarization and repolarization states. Our results (Figure 4.9) suggest that it is the memory that causes a short APD after a long APD which results in more accumulation of the memory, given same amount memory is dissipated with same relaxation time (DI). Such memory contributes to alternans in the absence of restitution effects. Random DIs perturb the memory and result in smaller amplitude of alternans (Figure 4.15). Because the DIs before and after random perturbation were the same and different initial conditions do not show a difference in the amplitude of alternans (Figure 4.14), different cardiac memory status may have caused the difference in alternans amplitude. This result supports the idea that cardiac memory plays an important role in the genesis of alternans.

The I_{CaL} channel in CVM was constructed to study alternans[114]. This model can generate persistent alternans during constant PCL pacing. Unfortunately, the CVM failed to reproduce the alternans during constant DI pacing shown in our experiments. This result implies that the alternans via the DI independent component has not been included in these models.

Chapter 6 Summary

What makes reentry spiral wave unstable? This is an important question in the studies of arrhythmogenesis. In the present study, we visualize the answer to this question in a diagram as shown in Figure 6.1. The wave breaks can initiate from functional block or dynamic instability, which lead us to the alternans study. The mechanism of alternans can not be elucidated, until all of the underlying components are identified and evaluated. We demonstrated a type of alternans during constant DI pacing. This result indicates that there are two components in the mechanism of alternans: DI dependent and independent component. Because the real APD dynamics is a high dimension model, we further explore it during sequential DI activation. We found that the APD dynamics showed hysteresis characteristic.

We demonstrated that alternans occurred during constant DI pacing, i.e. the DI preceding each APD was invariant or change within a very limited range. It means that the DI independent component by itself is large enough to maintain the alternans. In this case, the existence of alternans does not necessarily depend on the slope of DI restitution or oscillation of DI preceding APD. Consistent with our results, recent studies[70, 96, 97, 101, 104, 131, 133] found that the correlation between the slope of restitution and onset of alternans is deficient or weak. This discrepancy could be explained by the interaction of DI dependent and independent components during constant PCL pacing. Identifying the effects of these two components could deepen the understanding of the mechanism of alternans. One of our objectives in this study was to delineate the role of DI dependent

restitution of APD in alternans, because the physiological ion mechanisms are different through DI and APD. If so, DI dependent and independent components have significantly different meaning for mechanism of alternans. We used CVM to investigate the possible ionic movement responsible for these two components. CVM produced sustainable alternans during constant PCL pacing, but failed to replicate the alternans during constant DI pacing. This result implies that the kinetics of Ca inhibit L-type Ca channel modeled in CVM is unlikely to be able to explain the DI independent component in the mechanism of alternans.

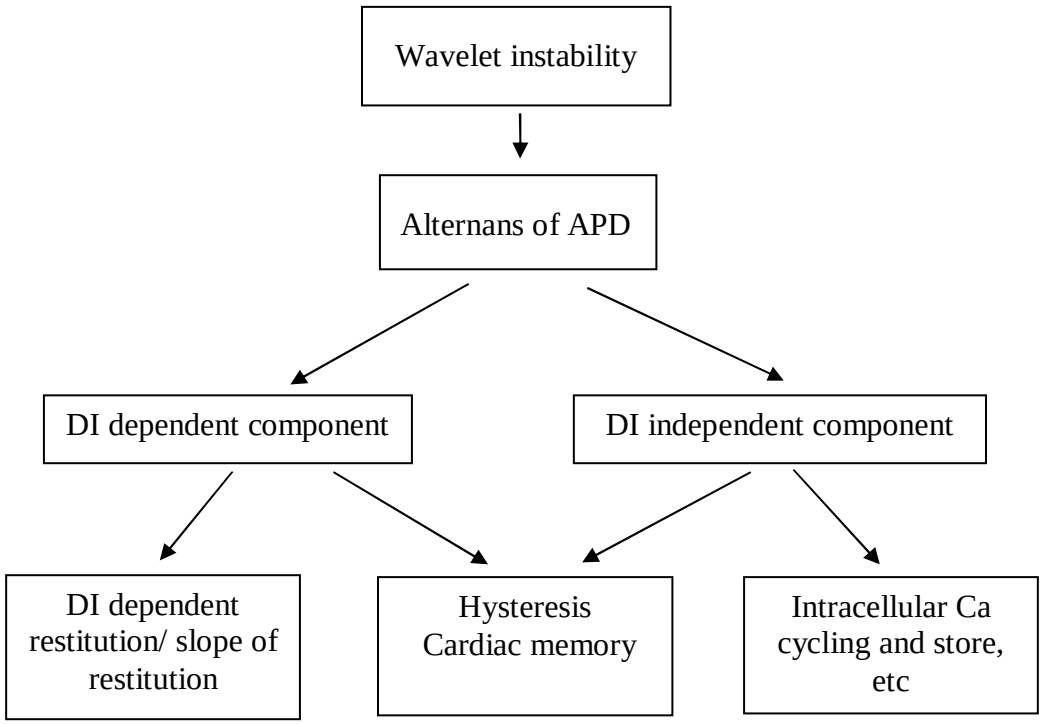

Figure 6.1 The summary of the present studies. The objective of the present studies is to investigate the mechanism of the alternans of APD. The result of the experiment using the feedback protocol and constant DI sequence indicates that there are two components in the mechanism of alternans: DI dependent and independent components. The restitution showed hysteresis like phenomenon during sequential change of DI. The result of the simulation study supports the hypothesis that Ca plays a key role in the hysteresis.

The trajectory of APD dynamics shows the hysteresis phenomenon under sequential activation. We observed multiple values of APD correspondent to a given DI with different activation history. The trajectory of restitution relationship was bi-modal and shallower than that obtained by standard or dynamic restitution protocol. We proposed that alternans of APD could be dampened via hysteresis even though slope of restitution is equal to or larger than 1. Therefore, hysteresis provides a mechanism to develop antiarrhythmic therapy[129]. The computational results showed that the asymmetric Ca dynamics during increasing and decreasing DI phase plays an important role in the hysteresis. Ca ion served as a bridge between intracellular Ca cycling and membrane potential. Our results support the hypothesis that high dimensional dynamics of APD may result from the special role of Ca movement.

Our studies have limitations. We collected data from isolated canine endocardial tissue using superfusion. Although transmembrane potentials recorded from perfused and superfused ventricular tissue in canines are virtually identical[137], it is possible that differences may exist between in vivo and vitro preparations. However, our results are comparable with the large number of studies of alternans conducted using isolated tissue. We also studied the alternans in the view of temporal dynamics. But the alternans may also rise from the spatial factors such as spatial heterogeneity and conduction velocity. The computational models of LRD and CVM have generated inconsistent results, especially, the CVM model which could not replicate the experimental results during constant DI pacing. Although the CVM includes the kinetics of Ca inhibit L-type Ca channel modeled in CVM, the mechanism for DI independent component still remains unclear.

How may we use the new information from the presented studies in the future research of the restitution and arrhythmogenesis? In the study of DI dependent restitution (i.e. restitution hypothesis), there is a propensity to believe that the membrane currents, especially the repolarization currents, are responsible for the restitution. The experiment results of the correlation between intracellular Ca cycling and alternans were therefore used as the evidences to support intracellular Ca cycling as an alternative hypothesis. However, this is problematic. Two questions we may ask: 1) Are the restitution and Ca cycling mutually exclusive or separable? 2) How the restitution should be quantified? The DI dependent restitution related the APD and its preceding DI to form a uni-modal relationship by using 'standard' or 'dynamic' pacing protocols. In this uni-modal relationship, the slope of restitution at relatively short DI range represents the modulation of I_{kr} and I_{ks} responding to the DI change. While our results, i.e. the hysteresis in the restitution and DI independent component in the mechanism of alternans provide convincible evidence that the DIs and APDs in the activation history have a way to project to the current APD, i.e. the value of current APD is affected by all preceding DIs and APDs. It is worthy to notice that the ionic movements during DI and APD are different physiologically. The mechanism such as Ca inhibit L-type Ca channel[114], and baseline I_{kr}[120] were proposed as the pathway that projects preceding APD change to the current APD, i.e. mechanic implication for cardiac memory. Our simulation results further suggest that the Ca storage in SR and cytosol play a key role in the hysteresis in restitution. This result shows the restitution and intracellular Ca cycling are NOT mutually exclusive. It will be more meaningful to identify the DI dependent component and DI independent component in the measurement of APD and DI dynamics. The

constant DI pacing trial provides an example that the effect of I_{kr} and I_{ks} responding to DI change (i.e. DI dependent restitution) is separable in the mechanism of alternans, which help us understanding the ionic mechanism for restitution. Furthermore, the hysteresis provides a promising method to connect a characteristic of restitution to the intracellular Ca storage and cycling. The measurement of the hysteresis provides a way to quantify the restitution under the new view that restitution has a component of intracellular Ca. In summary, the presented results would help to end the discussion between the school of restitution and intracellular Ca cycling, and more importantly open a new view to investigate the controversial restitution hypothesis.

The identification of the mechanism for hysteresis and DI dependent and independent components in the mechanism of alternans is more than theoretical researches. Because the hysteresis may be a potential target for developing anti-arrhythmic therapy, it would be helpful to investigate the strategies to enhance the hysteresis phenomenon. It would also be useful to develop techniques to measure and quantify the hysteresis characteristic, for the hysteresis is a viable way to test the stability of electrical activation in an electrophysiology (EP) laboratory. The results of anti-arrhythmic drug trials manifest the importance of considering overall risk factors when one risk factor is suppressed. It is likely that testing the effects of a combination of drugs on both DI dependent and independent components would generate a safe therapy to prevent the fibrillation.

Reference

1. American Heart Association. Heart and Stroke Statistics - 2005 Update. 2005.

2. Zipes DP, Wellens HJ. Sudden cardiac death. *Circulation.* Nov 24 1998;98(21):2334-2351.

3. Gillum RF. Sudden cardiac death in Hispanic Americans and African Americans. *Am J Public Health.* Sep 1997;87(9):1461-1466.

4. Zheng ZJ, Croft JB, Giles WH, et al. Sudden cardiac death in the United States, 1989 to 1998. *Circulation.* Oct 30 2001;104(18):2158-2163.

5. Vaughan Williams EM. Relevance of cellular to clinical electrophysiology in interpreting antiarrhythmic drug action. *Am J Cardiol.* Dec 5 1989;64(20):5J-9J.

6. Pratt CM, Moye LA. The cardiac arrhythmia suppression trial. Casting suppression in a different light. *Circulation.* Jan 1 1995;91(1):245-247.

7. Preliminary report: effect of encainide and flecainide on mortality in a randomized trial of arrhythmia suppression after myocardial infarction. The Cardiac Arrhythmia Suppression Trial (CAST) Investigators. *N Engl J Med.* Aug 10 1989;321(6):406-412.

8. Effect of the antiarrhythmic agent moricizine on survival after myocardial infarction. The Cardiac Arrhythmia Suppression Trial II Investigators. *N Engl J Med.* Jul 23 1992;327(4):227-233.

9. Waldo AL, Camm AJ, deRuyter H, et al. Effect of d-sotalol on mortality in patients with left ventricular dysfunction after recent and remote myocardial infarction. The SWORD Investigators. Survival With Oral d-Sotalol. *Lancet.* Jul 6 1996;348(9019):7-12.

10. Kudenchuk PJ, Cobb LA, Copass MK, et al. Amiodarone for resuscitation after out-of-hospital cardiac arrest due to ventricular fibrillation. *N Engl J Med.* Sep 16 1999;341(12):871-878.

11. Julian DG, Camm AJ, Frangin G, et al. Randomised trial of effect of amiodarone on mortality in patients with left-ventricular dysfunction after recent myocardial infarction: EMIAT. European Myocardial Infarct Amiodarone Trial Investigators. *Lancet.* Mar 8 1997;349(9053):667-674.

12. Sanguinetti MC, Bennett PB. Antiarrhythmic drug target choices and screening. *Circ Res.* Sep 19 2003;93(6):491-499.

13. Torp-Pedersen C, Moller M, Bloch-Thomsen PE, et al. Dofetilide in patients with congestive heart failure and left ventricular dysfunction. Danish Investigations of Arrhythmia and Mortality on Dofetilide Study Group. *N Engl J Med.* Sep 16 1999;341(12):857-865.

14. Kober L, Bloch Thomsen PE, Moller M, et al. Effect of dofetilide in patients with recent myocardial infarction and left-ventricular dysfunction: a randomised trial. *Lancet.* Dec 16 2000;356(9247):2052-2058.

15. Dorian P, Cass D, Schwartz B, et al. Amiodarone as compared with lidocaine for shock-resistant ventricular fibrillation. *N Engl J Med.* Mar 21 2002;346(12):884-890.

16. Ellison KE, Gandhi G. Optimising the use of beta-adrenoceptor antagonists in coronary artery disease. *Drugs.* 2005;65(6):787-797.

17. Thattassery E, Gheorghiade M. Beta blocker therapy after acute myocardial infarction in patients with heart failure and systolic dysfunction. *Heart Fail Rev.* Apr 2004;9(2):107-113.

18. Goldstein S. Propranolol therapy in patients with acute myocardial infarction: the Beta-Blocker Heart Attack Trial. *Circulation.* Jun 1983;67(6 Pt 2):I53-57.

19. Domanski MJ, Sakseena S, Epstein AE, et al. Relative effectiveness of the implantable cardioverter-defibrillator and antiarrhythmic drugs in patients with varying degrees of left ventricular dysfunction who have survived malignant ventricular arrhythmias. AVID Investigators. Antiarrhythmics Versus Implantable Defibrillators. *J Am Coll Cardiol.* Oct 1999;34(4):1090-1095.

20. Nademanee K, Veerakul G, Mower M, et al. Defibrillator Versus beta-Blockers for Unexplained Death in Thailand (DEBUT): a randomized clinical trial. *Circulation.* May 6 2003;107(17):2221-2226.

21. Moss AJ, Hall WJ, Cannom DS, et al. Improved survival with an implanted defibrillator in patients with coronary disease at high risk for ventricular arrhythmia. Multicenter Automatic Defibrillator Implantation Trial Investigators. *N Engl J Med.* Dec 26 1996;335(26):1933-1940.

22. Moss AJ, Zareba W, Hall WJ, et al. Prophylactic implantation of a defibrillator in patients with myocardial infarction and reduced ejection fraction. *N Engl J Med.* Mar 21 2002;346(12):877-883.

23. Varon J, Sternbach GL, Marik PE, et al. Automatic external defibrillators: lessons from the past, present and future. *Resuscitation.* Aug 1999;41(3):219-223.

24. Zipes DP. *Optical Mapping of Cardiac Excitation and Arrhythmias*: Futura Publishing Co.; 2001.

25. De Jong MM, Randall DC. Heart rate variability analysis in the assessment of autonomic function in heart failure. *J Cardiovasc Nurs.* May-Jun 2005;20(3):186-195.

26. Rodriguez B, Ferrero JM, Jr., Trenor B. Mechanistic investigation of extracellular K+ accumulation during acute myocardial ischemia: a simulation study. *Am J Physiol Heart Circ Physiol.* Sep 2002;283(2):H490-500.

27. Randall DC, Brown DR, Li SG, et al. Ablation of posterior atrial ganglionated plexus potentiates sympathetic tachycardia to behavioral stress. *Am J Physiol.* Sep 1998;275(3 Pt 2):R779-787.

28. Billman GE. Aerobic exercise conditioning: a nonpharmacological antiarrhythmic intervention. *J Appl Physiol.* Feb 2002;92(2):446-454.

29. Verrier RL, Antzelevitch C. Autonomic aspects of arrhythmogenesis: the enduring and the new. *Curr Opin Cardiol.* Jan 2004;19(1):2-11.

30. Chen PS, Chen LS, Cao JM, et al. Sympathetic nerve sprouting, electrical remodeling and the mechanisms of sudden cardiac death. *Cardiovasc Res.* May 2001;50(2):409-416.

31. Winslow RL, Boguski MS. Genome informatics: current status and future prospects. *Circ Res.* May 16 2003;92(9):953-961.

32. Shimizu W, Antzelevitch C. Cellular and ionic basis for T-wave alternans under long-QT conditions. *Circulation.* Mar 23 1999;99(11):1499-1507.

33. Qu Z, Garfinkel A, Chen PS, et al. Mechanisms of discordant alternans and induction of reentry in simulated cardiac tissue. *Circulation.* Oct 3 2000;102(14):1664-1670.

34. Watanabe MA, Fenton FH, Evans SJ, et al. Mechanisms for discordant alternans. *J Cardiovasc Electrophysiol.* Feb 2001;12(2):196-206.

35. Christini DJ, Glass L. Introduction: Mapping and control of complex cardiac arrhythmias. *Chaos.* Sep 2002;12(3):732-739.

36. Karagueuzian HS, Chen PS. Cellular mechanism of reentry induced by a strong electrical stimulus: implications for fibrillation and defibrillation. *Cardiovasc Res.* May 2001;50(2):251-262.

37. Libbus I, Rosenbaum DS. Remodeling of cardiac repolarization: mechanisms and implications of memory. *Card Electrophysiol Rev.* Sep 2002;6(3):302-310.

38. Samie FH, Jalife J. Mechanisms underlying ventricular tachycardia and its transition to ventricular fibrillation in the structurally normal heart. *Cardiovasc Res.* May 2001;50(2):242-250.

39. Gilmour RF, Jr., Chialvo DR. Electrical restitution, critical mass, and the riddle of fibrillation. *J Cardiovasc Electrophysiol.* Aug 1999;10(8):1087-1089.

40. Pogwizd SM, Bers DM. Calcium cycling in heart failure: the arrhythmia connection. *J Cardiovasc Electrophysiol.* Jan 2002;13(1):88-91.

41. Janse MJ. Electrophysiological changes in heart failure and their relationship to arrhythmogenesis. *Cardiovasc Res.* Feb 1 2004;61(2):208-217.

42. Berne R, Levy M. *Princepiles of Physiology*: Mosby Inc.; 1999.

43. Laurita KR, Rosenbaum DS. Restitution, Repolarization, and Alternans as Arrhythmogenic Substrates. In: Zipes DP, Jalife J, eds. *Cardiac electrophysiology: from cell to bedside*. 4th ed: Elsevier Inc.; 2004:232-241.

44. Fenton FH, Cherry EM, Hastings HM, et al. Multiple mechanisms of spiral wave breakup in a model of cardiac electrical activity. *Chaos.* Sep 2002;12(3):852-892.

45. Chen PS, Wu TJ, Ting CT, et al. A tale of two fibrillations. *Circulation.* Nov 11 2003;108(19):2298-2303.

46. Wu TJ, Lin SF, Baher A, et al. Mother rotors and the mechanisms of D600-induced type 2 ventricular fibrillation. *Circulation.* Oct 12 2004;110(15):2110-2118.

47. Wu TJ, Lin SF, Weiss JN, et al. Two types of ventricular fibrillation in isolated rabbit hearts: importance of excitability and action potential duration restitution. *Circulation.* Oct 1 2002;106(14):1859-1866.

48. Jalife J, Berenfeld O, Skanes A, et al. Mechanisms of atrial fibrillation: mother rotors or multiple daughter wavelets, or both? *J Cardiovasc Electrophysiol.* Aug 1998;9(8 Suppl):S2-12.

49. Rogers JM, Huang J, Melnick SB, et al. Sustained reentry in the left ventricle of fibrillating pig hearts. *Circ Res.* Mar 21 2003;92(5):539-545.

50. Patwardhan A, Moghe S, Wang K, et al. Frequency modulation within electrocardiograms during ventricular fibrillation. *Am J Physiol Heart Circ Physiol.* Aug 2000;279(2):H825-835.

51. Witkowski FX, Leon LJ, Penkoske PA, et al. Spatiotemporal evolution of ventricular fibrillation. *Nature.* Mar 5 1998;392(6671):78-82.

52. Gray RA, Pertsov AM, Jalife J. Spatial and temporal organization during cardiac fibrillation. *Nature.* Mar 5 1998;392(6671):75-78.

53. Kim YH, Garfinkel A, Ikeda T, et al. Spatiotemporal complexity of ventricular fibrillation revealed by tissue mass reduction in isolated swine right ventricle. Further evidence for the quasiperiodic route to chaos hypothesis. *J Clin Invest.* Nov 15 1997;100(10):2486-2500.

54. Choi BR, Nho W, Liu T, et al. Life span of ventricular fibrillation frequencies. *Circ Res.* Aug 23 2002;91(4):339-345.

55. Newton JC, Smith WM, Ideker RE. Estimated global transmural distribution of activation rate and conduction block during porcine and canine ventricular fibrillation. *Circ Res.* Apr 2 2004;94(6):836-842.

56. Cao JM, Qu Z, Kim YH, et al. Spatiotemporal heterogeneity in the induction of ventricular fibrillation by rapid pacing: importance of cardiac restitution properties. *Circ Res.* Jun 11 1999;84(11):1318-1331.

57. Rohde GK, Dawant BM, Lin SF. Correction of motion artifact in cardiac optical mapping using image registration. *IEEE Trans Biomed Eng.* Feb 2005;52(2):338-341.

58. Choi BR, Liu T, Salama G. Adaptation of cardiac action potential durations to stimulation history with random diastolic intervals. *J Cardiovasc Electrophysiol.* Oct 2004;15(10):1188-1197.

59. Qu Z, Weiss JN, Garfinkel A. Cardiac electrical restitution properties and stability of reentrant spiral waves: a simulation study. *Am J Physiol.* Jan 1999;276(1 Pt 2):H269-283.

60. Karma A. Electrical alternans and spiral wave breakup in cardiac tissue. *Chaos.* Sep 1994;4(3):461-472.

61. Courtemanche M. Complex spiral wave dynamics in a spatially distributed ionic model of cardiac electrical activity. *Chaos.* Dec 1996;6(4):579-600.

62. Fenton F, Karma A. Vortex dynamics in three-dimensional continuous myocardium with fiber rotation: Filament instability and fibrillation. *Chaos.* Mar 1998;8(1):20-47.

63. Sambelashvili A, Efimov IR. Dynamics of virtual electrode-induced scroll-wave reentry in a 3D bidomain model. *Am J Physiol Heart Circ Physiol.* Oct 2004;287(4):H1570-1581.

64. Xie F, Qu Z, Yang J, et al. A simulation study of the effects of cardiac anatomy in ventricular fibrillation. *J Clin Invest.* Mar 2004;113(5):686-693.

65. Hastings HM, Fenton FH, Evans SJ, et al. Alternans and the onset of ventricular fibrillation. *Phys Rev E Stat Phys Plasmas Fluids Relat Interdiscip Topics.* Sep 2000;62(3 Pt B):4043-4048.

66. Gilmour RF, Jr. A novel approach to identifying antiarrhythmic drug targets. *Drug Discov Today.* Feb 15 2003;8(4):162-167.

67. Weiss JN, Garfinkel A, Karagueuzian HS, et al. Chaos and the transition to ventricular fibrillation: a new approach to antiarrhythmic drug evaluation. *Circulation.* Jun 1 1999;99(21):2819-2826.

68. Xie F, Qu Z, Garfinkel A, et al. Electrophysiological heterogeneity and stability of reentry in simulated cardiac tissue. *Am J Physiol Heart Circ Physiol.* Feb 2001;280(2):H535-545.

69. Fox JJ, Riccio ML, Hua F, et al. Spatiotemporal transition to conduction block in canine ventricle. *Circ Res.* Feb 22 2002;90(3):289-296.

70. Banville I, Chattipakorn N, Gray RA. Restitution dynamics during pacing and arrhythmias in isolated pig hearts. *J Cardiovasc Electrophysiol.* Apr 2004;15(4):455-463.

71. Ideker RE, Rogers JM, Gray RA. Steepness of the restitution curve: a slippery slope? *J Cardiovasc Electrophysiol.* Nov 2002;13(11):1173-1175.

72. Antzelevitch C, Yan GX, Shimizu W. Transmural dispersion of repolarization and arrhythmogenicity: the Brugada syndrome versus the long QT syndrome. *J Electrocardiol.* 1999;32 Suppl:158-165.

73. Obreztchikova MN, Sosunov EA, Anyukhovsky EP, et al. Heterogeneous ventricular repolarization provides a substrate for arrhythmias in a German shepherd model of spontaneous arrhythmic death. *Circulation.* Sep 16 2003;108(11):1389-1394.

74. Zaitsev AV, Berenfeld O, Mironov SF, et al. Distribution of excitation frequencies on the epicardial and endocardial surfaces of fibrillating ventricular wall of the sheep heart. *Circ Res.* Mar 3 2000;86(4):408-417.

75. Derksen R, van Rijen HV, Wilders R, et al. Tissue discontinuities affect conduction velocity restitution: a mechanism by which structural barriers may promote wave break. *Circulation.* Aug 19 2003;108(7):882-888.

76. Banville I, Gray RA. Effect of action potential duration and conduction velocity restitution and their spatial dispersion on alternans and the stability of arrhythmias. *J Cardiovasc Electrophysiol.* Nov 2002;13(11):1141-1149.

77. Pastore JM, Girouard SD, Laurita KR, et al. Mechanism linking T-wave alternans to the genesis of cardiac fibrillation. *Circulation.* Mar 16 1999;99(10):1385-1394.

78. Chinushi M, Restivo M, Caref EB, et al. Electrophysiological basis of arrhythmogenicity of QT/T alternans in the long-QT syndrome: tridimensional analysis of the kinetics of cardiac repolarization. *Circ Res.* Sep 21 1998;83(6):614-628.

79. Huikuri HV, Seppanen T, Koistinen MJ, et al. Abnormalities in beat-to-beat dynamics of heart rate before the spontaneous onset of life-threatening ventricular tachyarrhythmias in patients with prior myocardial infarction. *Circulation.* May 15 1996;93(10):1836-1844.

80. Gold MR, Bloomfield DM, Anderson KP, et al. A comparison of T-wave alternans, signal averaged electrocardiography and programmed ventricular stimulation for arrhythmia risk stratification. *J Am Coll Cardiol.* Dec 2000;36(7):2247-2253.

81. Walker ML, Rosenbaum DS. Repolarization alternans: implications for the mechanism and prevention of sudden cardiac death. *Cardiovasc Res.* Mar 2003;57(3):599-614.

82. Rosenbaum DS, Jackson LE, Smith JM, et al. Electrical alternans and vulnerability to ventricular arrhythmias. *N Engl J Med.* Jan 27 1994;330(4):235-241.

83. Berger RD. Repolarization alternans: toward a unifying theory of reentrant arrhythmia induction. *Circ Res.* Dec 8 2000;87(12):1083-1084.

84. Hohnloser SH, Klingenheben T, Li YG, et al. T wave alternans as a predictor of recurrent ventricular tachyarrhythmias in ICD recipients: prospective comparison with conventional risk markers. *J Cardiovasc Electrophysiol.* Dec 1998;9(12):1258-1268.

85. Surawicz B, Fisch C. Cardiac alternans: diverse mechanisms and clinical manifestations. *J Am Coll Cardiol.* Aug 1992;20(2):483-499.

86. Nolasco JB, Dahlen RW. A graphic method for the study of alternation in cardiac action potentials. *J Appl Physiol.* Aug 1968;25(2):191-196.

87. Koller ML, Riccio ML, Gilmour RF, Jr. Dynamic restitution of action potential duration during electrical alternans and ventricular fibrillation. *Am J Physiol.* Nov 1998;275(5 Pt 2):H1635-1642.

88. Riccio ML, Koller ML, Gilmour RF, Jr. Electrical restitution and spatiotemporal organization during ventricular fibrillation. *Circ Res.* Apr 30 1999;84(8):955-963.

89. Taggart P, Sutton P, Chalabi Z, et al. Effect of adrenergic stimulation on action potential duration restitution in humans. *Circulation.* Jan 21 2003;107(2):285-289.

90. Xie F, Qu Z, Garfinkel A, et al. Electrical refractory period restitution and spiral wave reentry in simulated cardiac tissue. *Am J Physiol Heart Circ Physiol.* Jul 2002;283(1):H448-460.

91. Garfinkel A, Kim YH, Voroshilovsky O, et al. Preventing ventricular fibrillation by flattening cardiac restitution. *Proc Natl Acad Sci U S A.* May 23 2000;97(11):6061-6066.

92. Swissa M, Qu Z, Ohara T, et al. Action potential duration restitution and ventricular fibrillation due to rapid focal excitation. *Am J Physiol Heart Circ Physiol.* May 2002;282(5):H1915-1923.

93. Gilmour RF, Jr. Electrical restitution and ventricular fibrillation: negotiating a slippery slope. *J Cardiovasc Electrophysiol.* Nov 2002;13(11):1150-1151.

94. Hall GM, Bahar S, Gauthier DJ. Prevalence of rate-dependent behaviors in cardiac muscle. *Phys Rev Lett.* April 5 1999;82(14):2995.

95. Watanabe MA, Koller ML. Mathematical analysis of dynamics of cardiac memory and accommodation: theory and experiment. *Am J Physiol Heart Circ Physiol.* Apr 2002;282(4):H1534-1547.

96. Fox JJ, Bodenschatz E, Gilmour RF, Jr. Period-doubling instability and memory in cardiac tissue. *Phys Rev Lett.* Sep 23 2002;89(13):138101.

97. Huang J, Zhou X, Smith WM, et al. Restitution properties during ventricular fibrillation in the in situ swine heart. *Circulation.* Nov 16 2004;110(20):3161-3167.

98. Tolkacheva EG, Schaeffer DG, Gauthier DJ, et al. Condition for alternans and stability of the 1:1 response pattern in a "memory" model of paced cardiac dynamics. *Phys Rev E Stat Nonlin Soft Matter Phys.* Mar 2003;67(3 Pt 1):031904.

99. Tolkacheva EG, Romeo MM, Guerraty M, et al. Condition for alternans and its control in a two-dimensional mapping model of paced cardiac dynamics. *Phys Rev E Stat Nonlin Soft Matter Phys.* Mar 2004;69(3 Pt 1):031904.

100. Walker ML, Wan X, Kirsch GE, et al. Hysteresis effect implicates calcium cycling as a mechanism of repolarization alternans. *Circulation.* Nov 25 2003;108(21):2704-2709.

101. Chudin E, Goldhaber J, Garfinkel A, et al. Intracellular Ca(2+) dynamics and the stability of ventricular tachycardia. *Biophys J.* Dec 1999;77(6):2930-2941.

102. Kameyama M, Hirayama Y, Saitoh H, et al. Possible contribution of the sarcoplasmic reticulum Ca(2+) pump function to electrical and mechanical alternans. *J Electrocardiol.* Apr 2003;36(2):125-135.

103. Diaz ME, O'Neill SC, Eisner DA. Sarcoplasmic reticulum calcium content fluctuation is the key to cardiac alternans. *Circ Res.* Mar 19 2004;94(5):650-656.

104. Pruvot EJ, Katra RP, Rosenbaum DS, et al. Role of calcium cycling versus restitution in the mechanism of repolarization alternans. *Circ Res.* Apr 30 2004;94(8):1083-1090.

105. Sipido KR. Understanding cardiac alternans: the answer lies in the Ca2+ store. *Circ Res.* Mar 19 2004;94(5):570-572.

106. Omichi C, Lamp ST, Lin SF, et al. Intracellular Ca dynamics in ventricular fibrillation. *Am J Physiol Heart Circ Physiol.* May 2004;286(5):H1836-1844.

107. Lakireddy V, Baweja P, Syed A, et al. Contrasting effects of ischemia on the kinetics of membrane voltage and intracellular calcium transient underlie electrical alternans. *Am J Physiol Heart Circ Physiol.* Jan 2005;288(1):H400-407.

108. Kalb SS, Dobrovolny HM, Tolkacheva EG, et al. The restitution portrait: a new method for investigating rate-dependent restitution. *J Cardiovasc Electrophysiol.* Jun 2004;15(6):698-709.

109. Wu R, Patwardhan A. Restitution of action potential duration during sequential activation: A simulation study. *The 25th Annual Conference of the IEEE Engineering in Medicine and Biology Society.* 2003.

110. Wu R, Patwardhan A. Asymmetry in dynamics of action potential duration transition between steady states: A simulation study. Paper presented at: 26th

Annual International Conference of the IEEE Engineering in Medicine and Biology Society, EMBC 2004, 2004.

111. Wu R, Patwardhan A. Restitution of action potential duration during sequential changes in diastolic intervals shows multimodal behavior. *Circ Res.* Mar 19 2004;94(5):634-641.

112. Patwardhan A, Moghe S. Novel feedback based stimulation protocol shows hysteresis in cardiac action potential duration restitution. *Biomed Sci Instrum.* 2001;37:505-510.

113. Luo CH, Rudy Y. A dynamic model of the cardiac ventricular action potential. I. Simulations of ionic currents and concentration changes. *Circ Res.* Jun 1994;74(6):1071-1096.

114. Fox JJ, McHarg JL, Gilmour RF, Jr. Ionic mechanism of electrical alternans. *Am J Physiol Heart Circ Physiol.* Feb 2002;282(2):H516-530.

115. Zeng J, Laurita KR, Rosenbaum DS, et al. Two components of the delayed rectifier K+ current in ventricular myocytes of the guinea pig type. Theoretical formulation and their role in repolarization. *Circ Res.* Jul 1995;77(1):140-152.

116. Viswanathan PC, Shaw RM, Rudy Y. Effects of IKr and IKs heterogeneity on action potential duration and its rate dependence: a simulation study. *Circulation.* May 11 1999;99(18):2466-2474.

117. Faber GM, Rudy Y. Action potential and contractility changes in [Na(+)](i) overloaded cardiac myocytes: a simulation study. *Biophys J.* May 2000;78(5):2392-2404.

118. Hund TJ, Kucera JP, Otani NF, et al. Ionic charge conservation and long-term steady state in the Luo-Rudy dynamic cell model. *Biophys J.* Dec 2001;81(6):3324-3331.

119. Lynch JJ, Jr., Houle MS, Stump GL, et al. Antiarrhythmic efficacy of selective blockade of the cardiac slowly activating delayed rectifier current, I(Ks), in canine models of malignant ischemic ventricular arrhythmia. *Circulation.* Nov 2 1999;100(18):1917-1922.

120. Hua F, Gilmour RF, Jr. Contribution of IKr to rate-dependent action potential dynamics in canine endocardium. *Circ Res.* Apr 2 2004;94(6):810-819.

121. Hua F, Johns DC, Gilmour RF, Jr. Suppression of electrical alternans by overexpression of HERG in canine ventricular myocytes. *Am J Physiol Heart Circ Physiol.* Jun 2004;286(6):H2342-2351.

122. Jordan PN, Christini DJ. Determining the effects of memory and action potential duration alternans on cardiac restitution using a constant-memory restitution protocol. *Physiol Meas.* Aug 2004;25(4):1013-1024.

123. Jordan PN, Christini DJ. Adaptive diastolic interval control of cardiac action potential duration alternans. *J Cardiovasc Electrophysiol.* Oct 2004;15(10):1177-1185.

124. Chialvo DR, Michaels DC, Jalife J. Supernormal excitability as a mechanism of chaotic dynamics of activation in cardiac Purkinje fibers. *Circ Res.* Feb 1990;66(2):525-545.

125. Elharrar V, Surawicz B. Cycle length effect on restitution of action potential duration in dog cardiac fibers. *Am J Physiol.* Jun 1983;244(6):H782-792.

126. Gilmour RF, Jr., Otani NF, Watanabe MA. Memory and complex dynamics in cardiac Purkinje fibers. *Am J Physiol.* Apr 1997;272(4 Pt 2):H1826-1832.

127. Vinet A, Chialvo DR, Michaels DC, et al. Nonlinear dynamics of rate-dependent activation in models of single cardiac cells. *Circ Res.* Dec 1990;67(6):1510-1524.

128. Fenton FH, Evans SJ, Hastings HM. Memory in an Excitable Medium: A Mechanism for Spiral Wave Breakup in the Low-Excitability Limit. *Phys Rev Lett.* Nov. 8, 1999 1999;83(19):3964-3967.

129. Berger RD. Electrical restitution hysteresis: good memory or delayed response? *Circ Res.* Mar 19 2004;94(5):567-569.

130. Yehia AR, Jeandupeux D, Alonso F, et al. Hysteresis and bistability in the direct transition from 1:1 to 2:1 rhythm in periodically driven single ventricular cells. *Chaos.* Dec 1999;9(4):916-931.

131. Cherry EM, Fenton FH. Suppression of alternans and conduction blocks despite steep APD restitution: electrotonic, memory, and conduction velocity restitution effects. *Am J Physiol Heart Circ Physiol.* Jun 2004;286(6):H2332-2341.

132. Saitoh H, Bailey JC, Surawicz B. Alternans of action potential duration after abrupt shortening of cycle length: differences between dog Purkinje and ventricular muscle fibers. *Circ Res.* May 1988;62(5):1027-1040.

133. Goldhaber JI, Xie LH, Duong T, et al. Action Potential Duration Restitution and Alternans in Rabbit Ventricular Myocytes. The Key Role of Intracellular Calcium Cycling. *Circ Res.* Jan 20 2005;Epub ahead of print.

134. Laurita KR. Role of action potential duration restitution in arrhythmogenesis. *J Cardiovasc Electrophysiol.* Apr 2004;15(4):464-465.

135. Koller ML, Riccio ML, Gilmour RF, Jr. Effects of [K(+)](o) on electrical restitution and activation dynamics during ventricular fibrillation. *Am J Physiol Heart Circ Physiol.* Dec 2000;279(6):H2665-2672.

136. Surawicz B. Role of potassium channels in cycle length dependent regulation of action potential duration in mammalian cardiac Purkinje and ventricular muscle fibres. *Cardiovasc Res.* Nov 1992;26(11):1021-1029.

137. Burashnikov A, Mannava S, Antzelevitch C. Transmembrane action potential heterogeneity in the canine isolated arterially perfused right atrium: effect of IKr and IKur/Ito block. *Am J Physiol Heart Circ Physiol.* Jun 2004;286(6):H2393-2400.

Vita

Runze Wu was born on January, 25th, 1974 in Beijing, China. He graduated from Beihang University with a bachelor of engineering degree in electronic engineering in 1996. After graduation, he severed as an engineer for Beijing Inside Electronics Company from 1997 to 1998. He joined biomedical engineering in Tsinghua University, and earned master's degree in 2001. He has been awarded Kentucky Opportunity Fellowship in 2003-2004 and 2004-2005.

Recent publications/presentations include:

[1] Runze Wu, Abhijit Patwardhan. "Restitution of action potential duration during sequential changes in diastolic intervals shows multi-modal behavior," *Circulation Research*, Volume 94, 634-641, Apr. 2004.

[2] Runze Wu, Abhijit Patwardhan. "Mechanism of repolarization alternans has restitution of action potential duration dependent and independent components". *Journal of Cardiovascular Electrophysiology*, 17(1):87-93, 2006

[3] Runze Wu, Abhijit Patwardhan. "Effects of rapid and slow potassium repolarization currents and calcium dynamics on hysteresis in restitution of action potential duration". *Journal of Electrocardiology*. 2006 (accepted)

[4] Runze Wu, Abhijit Patwardhan. "Restitution of Action Potential Duration is Not Necessary for Existence of Repolarization Alternans." Heart Rhythm 2005, May, 2005. (Conference abstract, poster presentation on annual conference of heart rhythm society, May 4-7, 2005, New Orleans, LA)

[5] Runze Wu, Abhijit Patwardhan. “Role of Potassium and L type Calcium Currents in Hysteresis of Restitution of APD: A Simulation Study,” Annual Conference of Biomedical Engineering Society, Oct. 2004. (Conference abstract, oral presentation on annual conference of biomedical engineering society, Oct. 13-16, 2004, Philadelphia, PA)

[6] Runze Wu, Abhijit Patwardhan. “Asymmetry in Dynamics of Action Potential Duration Transition Between Steady States: A Simulation Study,” Annual Conference of the IEEE Engineering in Medicine and Biology, Sept. 2004 (Conference paper, oral presentation annual EMBS conference, Sept. 1-5, 2004, San Francisco, CA)

[7] Runze Wu, Abhijit Patwardhan. “Restitution of action potential duration during sequential activation: A simulation study,” Annual International Conference of the IEEE Engineering in Medicine and Biology - Proceedings, v 1, 2003, p 171-174 (Conference paper)